THE AERONAUTICAL QUARTERLY

A Journal devoted to Aeronautics and the Allied Sciences

Volume XII NOVEMBER 1961 Part 4

CONTENTS

The Effects of Heat Transfer on Laminar-Boundary-Layer Separation in Supersonic Flow — *N. Curle*

The Buckling of a Reinforced Circular Plate under Uniform Radial Thrust — *I. T. Cook and H. W. Parsons*

The Non-Steady Irrotational Flow of an Inviscid, Incompressible Fluid, with Special Reference to Changes in Total Pressure Through Flow Machines — *J. H. Preston*

The Deformational Behaviour of Low Aspect Ratio Multi-Web Wings. Part I — *R. H. Gallagher and I. Rattinger*

The Static Aeroelastic Deformation of Slender Configurations. Part II — *G. J. Hancock*

The Correlation of Unstable Crack Length Data for Sheet Materials — *E. R. Welbourne*

Index to Volume XII

LONDON

ROYAL AERONAUTICAL SOCIETY

4 HAMILTON PLACE W1

15/-

THE AERONAUTICAL QUARTERLY

Editorial Board

Dr. A. M. BALLANTYNE, T.D., B.Sc., Ph.D., F.R.Ae.S., Hon.F.C.A.I., F.I.A.S. (*Chairman*)

Mr. HAYNE CONSTANT, C.B., C.B.E., M.A., F.R.S., F.R.Ae.S.

Sir HAROLD ROXBEE COX, D.Sc., D.I.C., Ph.D., F.R.Ae.S., F.I.A.S.

Sir WILLIAM FARREN, C.B., M.B.E., M.A., D.Sc., F.R.S., Hon.F.R.Ae.S., Hon.F.I.A.S.

Sir ARNOLD HALL, M.A., F.R.S., F.R.Ae.S.

Sir ALFRED PUGSLEY, O.B.E., D.Sc., F.R.S., F.R.Ae.S.

Sir GEOFFREY TAYLOR, M.A., D.Sc., F.R.S., Hon.F.R.Ae.S.

Dr. P. B. WALKER, C.B.E., M.A., F.R.Ae.S.

Editor—E. C. PIKE, M.A., A.F.R.Ae.S.

Editorial Referees

Aerodynamics

(a) *General*

Sir LEONARD BAIRSTOW
Mr. D. KEITH-LUCAS
Prof. W. A. MAIR
Mr. L. F. NICHOLSON
Dr. R. C. PANKHURST
Mr. E. F. RELF
Prof. E. J. RICHARDS
Prof. B. THWAITES
Dr. D. KÜCHEMANN

(b) *Fluid Motion*

Dr. G. K. BATCHELOR
Mr. A. FAGE
Dr. D. W. HOLDER
Prof. L. HOWARTH
Dr. W. P. JONES
Dr. J. W. MACCOLL
Prof. J. H. PRESTON
Prof. H. B. SQUIRE
Prof. G. TEMPLE
Prof. G. N. WARD
Prof. A. D. YOUNG

(c) *Stability and Control*

Mr. L. W. BRYANT
Mr. S. B. GATES
Mr. G. H. LEE
Mr. M. B. MORGAN
Mr. H. H. B. M. THOMAS

Helicopters and Propellers

Prof. J. A. J. BENNETT
Mr. P. BRETT
Mr. L. G. FAIRHURST
Mr. R. HAFNER
Dr. G. S. HISLOP
Capt. R. N. LIPTROT

Instruments and Electrical Equipment

Dr. G. E. BAIRSTO
Sir GEORGE GARDNER
Dr. C. S. HUDSON
Mr. C. N. JAQUES
Mr. F. W. MEREDITH

Aircraft Design

Mr. R. BOORMAN
Mr. R. M. CLARKSON
Mr. A. N. CLIFTON
Mr. H. H. GARDNER
Mr. H. KNOWLER
Mr. F. H. POLLICUTT
Dr. A. E. RUSSELL
Mr. R. S. STAFFORD
Mr. W. H. STEPHENS

Radio and Radar

Mr. J. F. ATHERTON
Mr. B. G. GATES
Dr. R. L. SMITH ROSE
Dr. A. M. UTTLEY
Sir ROBERT WATSON-WATT

Aviation Medicine

Dr. K. G. BERGIN
Dr. A. BUCHANAN BARBOUR

Meteorology

Sir DAVID BRUNT
Mr. J. K. HARDY
Prof. P. A. SHEPPARD

Sound

Mr. W. MAK[illegible]ON
Mr. F. B. G[illegible]ATREX
Mr. N. FLEMING

Aircraft Propulsion

Mr. A. D. BAXTER
Mr. A. V. CLEAVER
Sir A. H. ROY FEDDEN
Dr. S. HOOKER
Mr. A. R. HOWELL
Mr. W. H. LINDSEY
Mr. P. LLOYD
Prof. A. W. MORLEY
Dr. E. S. MOULT
Mr. N. S. MUIR
Mr. F. NIXON
Mr. F. M. OWNER
Mr. H. PEARSON
Mr. H. SAMMONS
Prof. O. A. SAUNDERS
Prof. A. G. SMITH

Air Transport

Mr. A. C. CAMPBELL ORDE
Mr. P. G. MASEFIELD
Mr. N. E. ROWE
Mr. B. S. SHENSTONE
Mr. W. TYE

Aircraft Accessories

Mr. A. E. BINGHAM
Mr. W. C. CLOTHIER
Mr. H. G. CONWAY
Sir GEORGE DOWTY
Mr. R. GRAHAM
Mr. C. D. HOLLAND

Performance

Mr. H. DAVIES
Mr. D. R. NEWMAN
Mr. A. H. YATES

Flight Testing

Mr. R. R. DUDDY
Mr. P. A. HUFTON
Mr. S. SCOTT HALL
Mr. H. L. STEVENS

Structures

Prof. J. H. ARGYRIS
Dr. A. J. BARRETT
Mr. A. C. BROWN
Mr. H. L. COX
Mr. D. J. FARRAR
Prof. W. S. HEMP
Prof. R. HILL
Mr. H. B. HOWARD
Col. H. T. JESSOP
Mr. E. D. KEEN
Mr. F. A. KERRY
Dr. D. M. A. LEGGETT
Mr. R. L. LICKLEY
Dr. E. H. MANSFIELD
Prof. S. C. REDSHAW
Mr. R. H. SANDIFER
Sir RICHARD SOUTHWELL

Fuels and Oils

Mr. E. L. BASS
Dr. J. W. DRINKWATER
Prof. F. H. GARNER
Prof. W. E. GARNER
Dr. K. E. W. RIDLER
Dr. C. G. WILLIAMS

Materials

Dr. L. AITCHISON
Dr. N. P. ALLEN
Mr. G. FORREST
Prof. N. F. MOTT
Mr. L. ROTHERHAM
Dr. H. SUTTON
Dr. C. SYKES

Vibration and Flutter

Mr. E. G. BROADBENT
Prof. A. R. COLLAR
Mr. H. TEMPLETON
Mr. M. O. W. WOLFE

CHAPMAN AND HALL

Published under the authority of the
Royal Aeronautical Society

AIRCRAFT HYDRAULICS

edited by **H. G. CONWAY**

Volume I—Hydraulic Systems

Size 10 in. x 6 in. 146 pages 107 illustrations

35s. net

Volume II—Component Design

Size 10 in. x 6 in. 216 pages 120 illustrations

45s. net

INSTRUMENTATION IN TESTING AIRCRAFT

by **C. N. JAQUES**

Size $8\frac{3}{4}$ in. x $5\frac{1}{2}$ in. 292 pages 117 illustrations

45s. net

LANDING GEAR DESIGN

by **H. G. CONWAY**

Size 10 in. x 6 in. 342 pages 366 illustrations

56s. net

AIRCRAFT ELECTRICAL ENGINEERING

edited by **G. G. WAKEFIELD**

Size 10 in. x 6 in. 350 pages 201 illustrations

50s. net

37 ESSEX STREET - LONDON WC2

Bristol Siddeley lift/thrust engine chosen for Fokker Republic supersonic VTOL aircraft

A Bristol Siddeley lift/thrust turbofan engine has been chosen to power the very advanced Fokker/Republic VTOL aircraft with variable wing geometry. This aircraft will have long range and high supersonic all-weather capabilities to carry out its strike/reconnaissance duties.

The engine for Fokker/Republic is an advanced version of the Pegasus lift/thrust turbofan which already powers the Hawker P 1127 and is supported by the Mutual Weapons Development Programme for NATO.

PEGASUS SUBSTANTIATES NEW LIFT/THRUST CONCEPT

The rapid development and outstanding performance of the Pegasus turbofan has proved the soundness of the Bristol Siddeley lift/thrust philosophy. This lays down that the total installed thrust of an aircraft's *main* powerplant must be available for vertical take-off and landing, hovering, as well as for forward flight.

The revolutionary propulsive system of the Pegasus realises this basic concept and at the same time provides great reserves of power in military applications. The engine is equally suitable for single or multi-engined, subsonic or supersonic aircraft. In applications which require very high payload or extreme range, Pegasus turbofans can be used in conjunction with pure lifting engines.

UNIQUE DESIGN—UNIQUE PERFORMANCE

The unique feature of the Pegasus is the use of four movable nozzles, evenly disposed around the centre of gravity, which give directional control to its total thrust. The engine's high bypass ratio results in an excellent thrust/weight ratio, a low fuel consumption and a low noise level. Installation is conventional, and operation is simple and independent of all fixed ground equipment because the movable nozzles permit the problems of ground erosion, recirculation and ingestion of debris to be reduced to a minimum.

BRISTOL SIDDELEY ENGINES LIMITED Turbojets · Turbofans · Turboprops · Piston Engines · Ramjets
Rocket Engines · Marine and Industrial Gas Turbines · Marine, Rail and Industrial Diesel Engines · Precision Engineering Products

The Effects of Heat Transfer on Laminar-Boundary-Layer Separation in Supersonic Flow

N. CURLE*, M.Sc., Ph.D.

(*Aerodynamics Division, National Physical Laboratory*)

SUMMARY: By generalising earlier work, an approximate method is derived for calculating compressible laminar boundary layers with an unfavourable pressure gradient, with the wall temperature and Prandtl number arbitrary and some allowance made for the viscosity-temperature law. The method merely requires two quadratures and uses tables of universal functions. On the basis of this method it is suggested that when the wall is at uniform temperature the viscosity-temperature law should make little difference to the results, and that, when the wall temperature varies spatially by a factor of two, the use of a linear relationship may introduce errors of order 4 per cent in the momentum thickness. It is further suggested that the effects of Prandtl number differing from unity will increase as either the Mach number is increased or the wall is cooled. These general conclusions are borne out by detailed numerical calculations in a few selected cases.

The method is used to investigate "equilibrium" laminar-boundary-layer separation which occurs well upstream of the shock or step which induces it. The equations of the basic method must be solved simultaneously with a relationship between the (unknown) pressure gradient and the thickening of the boundary layer. Subject to the physically realistic approximation that the pressure rise to separation is a short sharp one, these equations integrate very easily to yield the pressure distribution in the region of interaction. It is predicted that the pressure coefficient, C_p, at separation will equal $0{\cdot}825\,(M_0^2-1)^{-1/4}\,R^{-1/4}$, where M_0 is the upstream Mach number and R is the Reynolds number at separation, based on distance from the leading edge and conditions in the main stream. Thus C_p is independent of wall temperature. Experimental values for cases with zero heat transfer, taken from many sources, are scattered between 0 and 20 per cent above the theoretical value. It is also predicted that the pressure gradient at separation should be inversely proportional to wall temperature. The magnitude of the pressure gradient agrees satisfactorily with experimental values when there is no heat transfer; there is only limited experimental evidence concerning the magnitude of the effect of wall temperature, but this agrees reasonably with the predictions of the theory.

1. Introduction

Interactions between shock waves and laminar boundary layers often occur in aeronautical problems. In many cases of practical importance the boundary layer

*Now at the Department of Aeronautics and Astronautics, University of Southampton.

Received March 1961.

[The Aeronautical Quarterly, Vol. XII, November 1961]

will separate well upstream of the position where the shock strikes the layer. In such situations the separation is of the "equilibrium" type, in which the deflection of the external streamlines, caused by the boundary layer thickening, must lead to a pressure gradient of just the right magnitude to cause the observed thickening.

This situation can be expressed mathematically, although the resulting analysis is often complicated. In principle, any method of calculating the development of a compressible laminar boundary layer from a knowledge of the pressure distribution could be used simultaneously with the relationship between thickening and pressure rise. Gadd[1, 2] considered just this problem by extending to compressible flow the relatively simple but physically well-founded method of Stratford[3]. An interesting result of Gadd's analysis is that the predicted pressure coefficient at separation depends upon Mach number and Reynolds number, but not upon wall temperature T_w. On the other hand Gadd predicts that the extent of the region of interaction should be proportional to $T_w^{3/2}$. The accuracy of this prediction is uncertain, as it is not yet firmly established how the streamwise extent of the interaction is dependent upon wall temperature. Gadd[4] reports experiments on a flat plate in which there appears to be little effect of wall temperature. Later results, with greater heat transfer, do indicate an effect of wall temperature, and lend some quantitative support to the predictions of the theory although a measure of uncertainty remains.

An alternative theoretical approach was suggested by Crocco and Lees[5], who focused attention upon the mixing (or entrainment) which takes place at the edge of the boundary layer. Calculations of shock-wave and boundary-layer interactions by this method have been made by Bray, Gadd and Woodger[6]. This work involved a considerable amount of computation and led to the result that cooling the wall reduces the streamwise extent of the region of interaction and somewhat increases both the pressure gradient and the pressure coefficient at the separation point.

The present paper begins with the development of a method for calculating laminar boundary layers with a prescribed arbitrary adverse pressure gradient. In two earlier papers (Curle[7, 8]) such a method was presented on the assumptions that the Prandtl number σ was unity and that the viscosity μ was proportional to the absolute temperature T. These two limitations are relaxed in this paper. As in the earlier papers, an approximate integral of the thermal energy equation is assumed for the purpose of simplifying the solution of the momentum equation. The variation of μ with T is assumed to be linear in a direction normal to the wall, but arbitrary in the streamwise direction. By this means it can be arranged that the viscosity is given accurately in the crucial region near to the wall, and reasonably, even in the outer part of the boundary layer, where it is unimportant. The results take a very simple form, and the usual boundary-layer characteristics may be predicted by means of two quadratures, using tabulated universal functions.

Applications to cases with prescribed pressure distributions are given in Section 4. Some general remarks are first made. It is a consequence of the present method that, for flows past a wall at uniform temperature, the viscosity-temperature relationship is unimportant. It is implied therefore that, in a more precise calculation,

it should have little effect, a result broadly in agreement with the work of Gadd[9] and Young[10]. On the other hand, the use of a realistic viscosity-temperature law is more important for flows with non-uniform wall temperature. It is suggested that, if the wall temperature varies spatially by a factor of two, the errors introduced by a linear relationship may be of order 4 per cent as regards the momentum thickness and even more as regards the position of separation. It is clear that the linear law cannot be used when the wall temperature differs from a uniform one by more than this. The effects of Prandtl number σ being different from unity are also considered. It is indicated that, for flow with zero heat transfer, separation will occur later when $\sigma = 0{\cdot}73$, say, than when $\sigma = 1$, a result already obtained by Gadd[9]. It is further indicated that the magnitude of this effect will increase as the wall is cooled or as the Mach number is increased.

Some explicit numerical results are given for three particular problems. The first is for flow with linearly increasing pressure, the Mach number at the leading edge being 2, and the wall temperature being the free-stream temperature at the leading edge. The other two cases are each for flow with a linearly retarded external velocity, the Mach number at the leading edge being 4, and the wall temperature being (*a*) the free-stream temperature at the leading edge and (*b*) the free-stream stagnation temperature. Solutions with $\sigma = 1$ and $\mu \propto T$ were given in Ref. 7, case (*b*) having zero heat transfer when $\sigma = 1$. Since uniform wall temperatures are considered in each case, the assumption that $\mu \propto T$ is retained. Further calculations with $\sigma = 0{\cdot}73$ are made, however, and are compared with the $\sigma = 1$ results, showing changes in separation distance of order 3 per cent, 7 per cent and 0 per cent respectively due to the change in Prandtl number, with appropriate changes in the main boundary-layer characteristics. These results bear out the conclusion already mentioned that the effect becomes more marked as the Mach number increases and as the wall is cooled.

Application is then made to the shock-wave and boundary-layer interaction problem. It is found experimentally that, when the upstream Mach number M_0 and the Reynolds number at separation, $R = u_1 x / \nu_1$, are in the ranges $2 \leqslant M_0 \leqslant 4$, $10^5 \leqslant R \leqslant 10^6$, the value of u_1 at separation is only 1–2 per cent less than its upstream value. Accordingly, the assumption is made that the pressure rise to separation is a short sharp one, so that du_1/dx is non-zero but u_1 is nearly constant. With no further approximations, the equations of Refs. 7 and 8, together with an equation relating the pressure rise to the thickening of the boundary layer, are reduced to a single equation for the pressure as a function of x, and this equation is integrated very easily. The solution can be continued beyond separation, provided that the relevant universal functions in Ref. 7 are defined in this region; this is considered in Appendix III.

The method predicts, with the earlier work of Gadd, that the pressure coefficient at separation is independent of wall temperature. It also predicts that the extent of the region of interaction is directly proportional to T_w, so that the pressure gradient at separation is inversely proportional to T_w. Quantitatively, the predicted pressure coefficient at separation is $C_p = 0{\cdot}825\ (M_0^2 - 1)^{-1/4}\ R^{-1/4}$. This

agrees well with experimental results for zero heat transfer, which are scattered from 0 to 20 per cent above this value, and compares favourably with other theoretical predictions. The accuracy of the prediction concerning the pressure gradient at separation is, as implied earlier, still uncertain, although the results of the most recent experiments are encouraging in this respect.

Numerical results have been obtained in a few cases for which experimental results were available. For a case of two-dimensional flow with zero heat transfer, with $M_0 = 2$ and $R = 7 \times 10^4$, the predicted pressure distribution agrees well with experiment in the region upstream of where the shock strikes the boundary layer. Some published results were also available (Gadd[4]) for three cases with $M_0 = 3$ and $R = 4{\cdot}2 \times 10^5$. In one case there was zero heat transfer, and in the others the wall was cooled to a temperature $T_w = 0{\cdot}88\ T_z$ and heated to $T_w = 1{\cdot}25\ T_z$. The predicted pressure distribution agrees remarkably well with experiment for the case of zero heat transfer. The theory does, however, predict an effect of wall temperature which, though small, is greater than that found in the experiments. Later experiments, with $M_0 = 2{\cdot}70$ and $R = 1{\cdot}5 \times 10^5$, with zero heat transfer in one case and the wall heated to $T_w = 1{\cdot}5\ T_z$ in another, yield results which lend some support to the theory so that, although no firm conclusions can be reached as to the accuracy of the predicted effect of wall temperature, the theory is at least qualitatively correct in this respect.

Notation

x, y distances parallel and normal to the wall $y = 0$

u, v velocity components parallel to x and y axes, respectively

p pressure

ρ density

T absolute temperature

μ viscosity

ν kinematic viscosity, $= \mu/\rho$

a speed of sound

M Mach number, $= u/a$

σ Prandtl number

δ_1, δ_2 boundary layer displacement and momentum thickness, respectively

$\delta_1', \delta_2', \delta_3'$ defined in equations (25), (26), (29)

$h_1 = \delta_3'/\delta_2'$

R Reynolds number, $= u_1 x/\nu_1$

c_p specific heat at constant pressure

C_p pressure coefficient, $= \dfrac{2}{\gamma M_0^2}\left(\dfrac{p}{p_0} - 1\right)$

T_H total temperature, $= T + \dfrac{u^2}{2Jc_p}$

K defined in equation (3)

θ_0 defined in equation (5)

$\xi = 1 - u_1^2/u_0^2$

ψ stream function, $= \dfrac{1}{\rho_s} \displaystyle\int_0^y \rho u \, dy$

Y related to y as in equation (16)

χ related to ψ as in equation (17)

C a function of x, appearing in equation (19)

G defined in equation (23)

Q defined in equation (31)

$H' = \delta_1'/\delta_2'$

$l' = \dfrac{\delta_2'}{u_1}\left(\dfrac{\partial u}{\partial y}\right)_w$

$m' = -\dfrac{\delta_2^2}{C v_s}\dfrac{T_w}{T_1} u_1'$

$L' = 2m'(H' + 2) + 2l'$

$G_0 = H' - 2{\cdot}61$

c a reference length

t defined by equation (53)

F, X, Λ defined by equation (61)

Suffixes

0 conditions at edge of boundary layer upstream of interaction*

1 local conditions at edge of boundary layer

s standard reference conditions

w conditions at the wall

z conditions appropriate to zero heat transfer

2. Temperature Profile

To make it possible to perform a relatively straightforward integration of the momentum equation it is necessary first to make some assumption or approximation regarding the temperature profile. This is now considered.

It is well known that provided (*i*) the Prandtl number σ is unity, (*ii*) there is no pressure gradient, (*iii*) the wall temperature T_w is constant, then the temperature profile takes the form

$$T_H = T + \frac{u^2}{2Jc_p} = T_w + (T_z - T_w)\frac{u}{u_1} \quad . \quad . \quad . \quad (1)$$

*Except in F_0 defined by equation (65).

This will also be the profile locally at a sharp leading edge, whatever the pressure gradient and wall-temperature distribution. It is extremely difficult, except in the special case for which equation (1) is valid, to calculate the downstream development of the temperature profile, for which reason the author[7] suggested a method of choosing a quadratic in u/u_1 as an approximation to the total temperature T_H. This approximation takes the form

$$T_H = T_w + (T_s - T_w)\frac{u}{u_1} + KT_1\left(\frac{u}{u_1} - \frac{u^2}{u_1^2}\right), \quad . \quad . \quad (2)$$

where

$$KT_1 = T_w(0) - T_w + \frac{T_s - T_w(0)}{1 + \theta_0(\xi - 1)}\,\xi, \quad . \quad . \quad . \quad (3)$$

with

$$\xi = 1 - \frac{u_1^2}{u_0^2} \quad . \quad . \quad . \quad . \quad . \quad . \quad . \quad . \quad (4)$$

and

$$\theta_0 = \frac{T_w(0)/T_0 - 1 + \frac{1}{2}(\gamma - 1)M_0^2}{T_w(0)/T_0 + 1 + \frac{1}{2}(\gamma - 1)M_0^2} \quad . \quad . \quad . \quad . \quad (5)$$

Throughout this analysis it is assumed that the boundary layer starts at a sharp leading edge, at which $u_1 = u_0$. For flow past a bluff body, with the boundary layer developing from a forward stagnation point, the analysis may be applied downstream of the pressure minimum provided that the origin $x = 0$ is taken there.

The use of this profile leads to a marked improvement in calculations of the velocity boundary layer in an adverse pressure gradient, as compared with calculations assuming that the temperature profile takes the local flat-plate value (equation (1)). In typical cases the error in predicting the position of separation appears to be halved.

When the Prandtl number is not equal to unity, the position is further complicated and it is necessary to generalise equation (2) further, for which reason we require first a generalisation of the flat-plate profile (equation (1)). A major step in this direction was made by Monaghan[11], who wrote equation (1) as

$$T = T_w + (T_s - T_w)\frac{u}{u_1} - \frac{\gamma - 1}{2}M_1^2 T_1 \frac{u^2}{u_1^2}, \quad . \quad . \quad . \quad (6)$$

and showed that a similar form

$$T = T_w + (T_s - T_w)\sigma^{1/3}\frac{u}{u_1} - \frac{\gamma - 1}{2}M_1^2 T_1 \sigma \frac{u^2}{u_1^2} \quad . \quad . \quad . \quad (7)$$

yields an accurate prediction of the temperature field for values of u/u_1 up to about 0·8 when $\sigma = 0{\cdot}725$ and $\sigma = 1{\cdot}25$. To obtain a formula for T which also satisfies the correct boundary condition at the edge of the boundary layer, we shall add a term $A(x)\,u^3/u_1^3$ to the right-hand side of equation (7) and choose $A(x)$ so that $T \longrightarrow T_1$ as $u \longrightarrow u_1$. This gives the result

$$T = T_1 + (T_w - T_1)\left(1 - \frac{u^3}{u_1^3}\right) + \sigma^{1/3}(T_s - T_w)\left(\frac{u}{u_1} - \frac{u^3}{u_1^3}\right) - \\ - \frac{\gamma - 1}{2}M_1^2 T_1 \sigma \left(\frac{u^2}{u_1^2} - \frac{u^3}{u_1^3}\right) \quad (8)$$

We must now add a term, analogous to the last term in equation (2) to account for downstream variations in equation (8). In doing this it is reasonable to take this term, $KT_1\,[(u/u_1)-(u^2/u_1^2)]$, multiply the two terms in the bracket by $\sigma^{1/3}$ and σ respectively and add on a suitable multiple of u^3/u_1^3 to satisfy the external boundary condition. This procedure yields

$$T = T_1 + (T_w - T_1)\left(1 - \frac{u^3}{u_1^3}\right) + \sigma^{1/3}(T_s - T_w + KT_1)\left(\frac{u}{u_1} - \frac{u^3}{u_1^3}\right) - \\ - T_1\left(K + \frac{\gamma-1}{2}M_1^2\right)\sigma\left(\frac{u^2}{u_1^2} - \frac{u^3}{u_1^3}\right). \qquad (9)$$

Finally a minor amendment must be made in the definition of K if inconsistencies are to be avoided. From equation (9) it is seen that K must be zero when there is no heat transfer, which occurs when the wall temperature distribution is

$$T_w = T_s \simeq T_1\left\{1 + \frac{\gamma-1}{2}M_1^2\,\sigma^{1/2}\right\}. \qquad (10)$$

The definition of K given by equation (3) is easily seen to satisfy this condition only when the wall temperature for zero heat transfer is a constant, that is when $\sigma = 1$. For general values of σ we add to equation (3) a function $B(\xi, \sigma)$, such that $K = 0$ when $T_w = T_s$. This leads to the following result, accepted in all that follows, namely

$$KT_1 = T_s - T_w + \{T_w(0) - T_s(0)\}\left\{1 - \frac{\xi}{1 + \theta_0(\xi - 1)}\right\}. \qquad (11)$$

It should perhaps be remarked that the temperature profile given by equations (9) and (11) is at best empirical, and can be finally justified only by the conclusions drawn from it. In this respect the agreement with calculations by Gadd[9] and Young[10], discussed later, is encouraging.

3. Transformation of the Momentum Equation

For steady two-dimensional compressible flow the boundary-layer momentum equations and the equation of continuity take the form

$$u\frac{\partial u}{\partial x} + v\frac{\partial u}{\partial y} = -\frac{1}{\rho}\frac{\partial p}{\partial x} + \frac{1}{\rho}\frac{\partial}{\partial y}\left(\mu\frac{\partial u}{\partial y}\right), \qquad (12)$$

$$0 = \frac{\partial p}{\partial y}, \qquad (13)$$

$$\frac{\partial}{\partial x}(\rho u) + \frac{\partial}{\partial y}(\rho v) = 0. \qquad (14)$$

Equation (14) is satisfied by introduction of a stream function ψ, with

$$\rho u = \rho_s\frac{\partial \psi}{\partial y}, \qquad \rho v = -\rho_s\frac{\partial \psi}{\partial x}, \qquad (15)$$

suffix s denoting some arbitrary reference condition.

Following Howarth[12], we change from independent variables x, y to x, Y,

$$\text{where} \qquad Y = \left(\frac{p}{p_s}\right)^{1/2} \int_0^y \frac{T_s}{T}\, dy, \qquad . \quad . \quad . \quad . \quad . \quad (16)$$

and write

$$\psi(x, y) = \left(\frac{p}{p_s}\right)^{1/2} \chi(x, Y). \qquad . \quad . \quad . \quad . \quad . \quad (17)$$

Then, exactly as in Howarth's analysis, it is quite straightforward to show that

$$u\frac{\partial u}{\partial x} + v\frac{\partial u}{\partial y} = \frac{\partial^2\chi}{\partial x \partial Y}\frac{\partial \chi}{\partial Y} - \frac{\partial^2\chi}{\partial Y^2}\frac{\partial \chi}{\partial x} - \frac{1}{2p}\frac{\partial p}{\partial x}\chi\frac{\partial^2\chi}{\partial Y^2}. \quad . \quad . \quad . \quad (18)$$

To deal with the viscous term in (12), it is assumed that the viscosity is related to the temperature by the law

$$\frac{\mu(x, y)}{\mu_s} = C(x)\frac{T(x, y)}{T_s}. \qquad . \quad . \quad . \quad . \quad (19)$$

Thus, for fixed x, μ varies linearly with T across the boundary layer, but an arbitrary variation in the streamwise direction is permitted. Following the suggestion of Chapman and Rubesin[13], $C(x)$ may be fixed so that the viscosity is given either exactly at the wall or fairly accurately throughout the region near to the wall where viscosity is most important.

Accepting equation (19), and leaving $C(x)$ to be determined in one of these ways, it then follows that

$$\begin{aligned}\mu\left(\frac{\partial u}{\partial y}\right)_x &= \mu\left(\frac{p}{p_s}\right)^{1/2}\frac{T_s}{T}\frac{\partial^2\chi}{\partial Y^2} \\ &= C\left(\frac{p}{p_s}\right)^{1/2}\mu_s\frac{\partial^2\chi}{\partial Y^2}, \qquad . \quad . \quad . \quad . \quad (20)\end{aligned}$$

so that

$$\begin{aligned}\frac{1}{\rho}\left[\frac{\partial}{\partial y}\left(\mu\frac{\partial u}{\partial y}\right)\right]_x &= C\frac{p}{p_s}\frac{\mu_s T_s}{\rho T}\frac{\partial^3\chi}{\partial Y^3} \\ &= C\nu_s\frac{\partial^3\chi}{\partial Y^3}. \qquad . \quad . \quad . \quad . \quad (21)\end{aligned}$$

Then, substituting from equations (18) and (21) into equation (12), we obtain

$$\begin{aligned}\frac{\partial^2\chi}{\partial x \partial Y}\frac{\partial \chi}{\partial Y} - \frac{\partial^2\chi}{\partial Y^2}\frac{\partial \chi}{\partial x} &= \frac{1}{2p}\frac{\partial p}{\partial x}\chi\frac{\partial^2\chi}{\partial Y^2} - \frac{1}{\rho}\frac{\partial p}{\partial x} + C\nu_s\frac{\partial^3\chi}{\partial Y^3}, \\ &= Gu_1\frac{du_1}{dx} + C\nu_s\frac{\partial^3\chi}{\partial Y^3}, \qquad . \quad . \quad . \quad . \quad (22)\end{aligned}$$

following Howarth, with $G = \dfrac{T}{T_1} - \dfrac{\gamma}{2a_1^2}\chi\dfrac{\partial^2\chi}{\partial Y^2}$. $\qquad . \quad . \quad . \quad . \quad (23)$

We now integrate across the boundary layer, from $Y=0$ to $Y=\infty$. Upon defining

$$\delta_1' = \int_0^\infty \left(1-\frac{u}{u_1}\right) dY \quad . \quad . \quad . \quad . \quad (24)$$

and $$\delta_2' = \int_0^\infty \frac{u}{u_1}\left(1-\frac{u}{u_1}\right) dY, \quad . \quad . \quad . \quad . \quad (25)$$

this yields

$$u_1^2 \frac{d\delta_2'}{dx} + u_1 \frac{du_1}{dx}(\delta_1' + 2\delta_2') = C\nu_s \left(\frac{\partial u}{\partial Y}\right)_w - u_1 \frac{du_1}{dx}\int_0^\infty (G-1)\, dY. \quad . \quad (26)$$

From equation (23) we deduce that

$$\int_0^\infty (G-1)\, dY = \int_0^\infty \left(\frac{T}{T_1}-1\right) dY - \tfrac{1}{2}\gamma M_1^2 \delta_2', \quad . \quad . \quad . \quad (27)$$

and, upon substituting from equation (9) for T, this yields

$$\int_0^\infty (G-1)\, dY = \left(\frac{T_w}{T_1}-1\right)(\delta_1' + \delta_3') + \sigma^{1/3}\frac{T_s - T_w + KT_1}{T_1}\delta_3' -$$
$$- \left(K + \frac{\gamma-1}{2}M_1^2\right)\sigma(\delta_3' - \delta_2') - \tfrac{1}{2}\gamma M_1^2 \delta_2', \quad . \quad (28)$$

where $$\delta_3' = \int_0^\infty \frac{u}{u_1}\left(1-\frac{u^2}{u_1^2}\right) dY. \quad . \quad . \quad . \quad . \quad (29)$$

By substituting from equation (28) into (26), and writing h_1 for the ratio δ_3'/δ_2', we find that

$$u_1^2 \frac{d\delta_2'}{dx} + u_1 \frac{du_1}{dx}\left\{\frac{T_w}{T_1}\delta_1' + Q\delta_2'\right\} = C\nu_s \left(\frac{\partial u}{\partial Y}\right)_w, \quad . \quad . \quad (30)$$

where $$Q = 2 - \tfrac{1}{2}M_1^2 + \left(\frac{T_1}{T_w}-1\right) h_1(1-\sigma^{1/3}) + K\{h_1\sigma^{1/3} - (h_1-1)\sigma\} +$$
$$+ \frac{\gamma-1}{2} M_1^2 \{h_1\sigma^{5/6} - (h_1-1)\sigma - 1\}. \quad . \quad (31)$$

It is noted that Q takes the form of the sum of a constant plus multiples of M_1^2, $[(T_w/T_1)-1]$ and K, the multiples being respectively $-\frac{1}{2}$, 0, 1, when σ is unity. When σ takes other values it is necessary to know h_1 before Q can be tabulated. It was pointed out by the author[6], following Truckenbrodt[14], that h_1 is almost constant, and that a reasonable mean value is 1·58. It is worth noting that, with this value of h_1, the coefficient of K in (31) becomes $1{\cdot}58\,\sigma^{1/3} - 0{\cdot}58\,\sigma$, which lies

TABLE I

THE FUNCTIONS $H'(m')$ AND $l'(m')$

m'	H'	l'	m'	H'	l'	m'	H'	l'
−0·25	2·00	0·500	0·060	2·99	0·113	0·075	4·65	−0·112
−0·20	2·07	0·463	0·064	3·04	0·104	0·070	4·84	−0·116
−0·14	2·18	0·404	0·068	3·09	0·095	0·065	5·05	−0·118
−0·12	2·23	0·382	0·072	3·15	0·085	0·060	5·30	−0·117
−0·10	2·28	0·359	0·076	3·22	0·072	0·055	5·60	−0·115
−0·080	2·34	0·333	0·080	3·30	0·056	0·050	5·96	−0·112
−0·064	2·39	0·313	0·084	3·39	0·038	0·045	6·41	−0·108
−0·048	2·44	0·291	0·086	3·44	0·027	0·040	7·00	−0·103
−0·032	2·49	0·268	0·088	3·49	0·015	0·035	7·74	−0·097
−0·016	2·55	0·244	0·090	3·55	0	0·030	8·64	−0·089
0	2·61	0·220	0·090	3·55	0	0·025	9·67	−0·081
0·016	2·67	0·195	0·088	3·92	−0·050	0·020	10·92	−0·072
0·032	2·75	0·168	0·086	4·12	−0·070	0·015	12·61	−0·062
0·040	2·81	0·153	0·084	4·26	−0·084	0·010	15·26	−0·050
0·048	2·87	0·138	0·082	4·38	−0·094	0·005	21·05	−0·034
0·056	2·94	0·122	0·080	4·48	−0·102	0	∞	0

between 0·990 and 1·004 for values of σ in the range $0{\cdot}636 \leqq \sigma \leqq 1{\cdot}135$, and equals 0·999 when $\sigma = 0{\cdot}73$, close to the value for air. For this reason it would appear worthwhile simply to replace the coefficient of K in (31) by unity throughout this range of σ.

We now define $$H' = \frac{\delta_1'}{\delta_2'} , \qquad (32)$$

$$l' = \frac{\delta_2'}{u_1}\left(\frac{\partial u}{\partial Y}\right)_w , \qquad (33)$$

and $$m' = -\frac{\delta_2'^2}{C\nu_s}\frac{du_1}{dx}\frac{T_w}{T_1} , \qquad (34)$$

so that equation (30) may be written as

$$\frac{u_1}{C}\frac{d}{dx}\left(\frac{\delta_2'^2}{\nu_s}\right) = 2m'\left(H' + Q\frac{T_1}{T_w}\right) + 2l'$$

$$= L' - 4m' + 2m'Q\frac{T_1}{T_w} , \qquad (35)$$

where $$L' = 2m'(H' + 2) + 2l' . \qquad (36)$$

It remains to prescribe values for the functions l', H', L', in terms of m' and such other variables as may be relevant, and then to transform from the artificially introduced δ_1', δ_2', Y, to the physically more important δ_1, δ_2, y. As the analysis is rather similar to that for the case $\sigma = 1$, $\mu \propto T$, given in Ref. 7, these results are derived in Appendices I and II and the results are now used.

It is indicated in Appendix I that H', l' and L' depend primarily upon m', being functionally independent of wall temperature, Mach number and Prandtl number.

It follows that, in general, the best results should be given by using Thwaites's values, which are quoted for convenience in Table I, as modified by Curle and Skan[15].

Now Thwaites showed that L' is given, to a very good approximation, as

$$L' = 0{\cdot}45 + 6m', \qquad (37)$$

so that equation (35) becomes

$$\frac{u_1}{C}\frac{d}{dx}\left(\frac{\delta_2'^2}{\nu_s}\right) = 0{\cdot}45 + 2m'\left(1 + Q\frac{T_1}{T_w}\right), \qquad (38)$$

which may be written as

$$\frac{d}{dx}\left(\frac{\delta_2'^2}{\nu_s}\right) + \frac{2u_1'}{u_1}\left(\frac{T_w}{T_1} + Q\right)\frac{\delta_2'^2}{\nu_s} = \frac{0{\cdot}45C}{u_1}. \qquad (39)$$

The integrating factor for this equation is

$$G_3 = \exp\left\{2\int_0^x \frac{u_1'}{u_1}\left(\frac{T_w}{T_1} + Q\right)dx\right\}, \qquad (40)$$

whereupon

$$\delta_2'^2 = \frac{0{\cdot}45\nu_s}{G_3}\int_0^x \frac{G_3 C}{u_1}\,dx. \qquad (41)$$

In Appendix II it is shown that

$$\delta_2^2 = \frac{C\nu_s}{\nu_1}\delta_2'^2, \qquad (42)$$

so equation (41) may be written

$$\delta_2^2 = \frac{0{\cdot}45\nu_1}{G_3 C}\int_0^x \frac{G_3 C}{u_1}\,dx. \qquad (43)$$

It follows similarly from equations (34) and (42) that

$$m' = -\frac{\delta_2^2}{\nu_1}u_1'\frac{T_w}{T_1}. \qquad (44)$$

It is also shown in Appendix II that

$$\delta_1 = \delta_2\left\{\frac{T_w}{T_1}H' + \left(\frac{T_w}{T_1} - 1\right)(1-\sigma^{1/3})h_1 + K + \frac{\gamma-1}{2}M_1^2\left[h_1\sigma^{5/6} - (h_1-1)\sigma\right]\right\}, \qquad (45)$$

the coefficient of K being almost exactly unity when $0{\cdot}636 \leqslant \sigma \leqslant 1{\cdot}135$.

Finally,

$$\left(\frac{\partial u}{\partial y}\right)_w = \left(\frac{\partial u}{\partial Y}\right)_w\left(\frac{\partial Y}{\partial y}\right)_w = \frac{u_1}{\delta_2'}I'\left(\frac{p}{p_s}\right)^{1/2}\frac{T_s}{T_w}. \qquad (46)$$

After some algebra equation (46) may be reduced to

$$\left(\frac{\partial u}{\partial y}\right)_w = \frac{u_1}{\nu_w^{1/2}} \frac{\nu_1^{1/2}}{\delta_2} I' \left(\frac{\mu_w T_e}{C \mu_e T_w}\right)^{1/2} \quad . \quad . \quad . \quad (47)$$

where the last bracket will be unity if C is chosen to give the viscosity exactly at the wall.

The solution of the compressible laminar-boundary-layer equations is then given by equations (43), (44), (45) and (47), with equations (11), (31) and (40) being used to determine the function G_3. It will be noted that, even with the added generalisations of this paper, the method requires only two simple quadratures and the use of tabulated universal functions.

4. Applications to Some Flows with Prescribed Pressure Gradient

We begin with some general observations as to the effects of Prandtl number and viscosity-temperature relationship on the predicted laminar-boundary-layer development.

Consider first the effects of the viscosity-temperature relationship, which enters through the function $C(x)$, σ being assumed to equal unity. It seems reasonable to suppose, following Chapman and Rubesin's remarks, that it is most important to ensure that viscosity is accurately represented in the region close to the wall. If we go all the way and determine $C(x)$ by the condition that viscosity is given exactly at the wall itself, then we find

$$C(x) = \frac{\mu_w(x)}{T_w(x)} \frac{T_e}{\mu_e} \quad . \quad . \quad . \quad . \quad . \quad (48)$$

It follows immediately that, when the wall temperature is uniform, C is a constant, and the results obtained by the present method will be identical with those for $\mu \propto T$. We conclude that in a more precise calculation the viscosity-temperature relationship will have little effect for flows past a wall at uniform temperature.

This conclusion agrees well with some results of Gadd[9], who considers flow past an insulated wall with a uniform adverse external velocity gradient, and assumes $\mu \propto T^{\omega}$. He finds that the distance to separation when $\omega = 8/9$ is 2 per cent greater than when $\omega = 1$, the Mach number being $M_0 = 4$. Similarly, when $M_0 = 10$ the separation distance is 6 per cent greater when $\omega = 8/9$. The corresponding results given by the method of Young[10] are also quoted by Gadd, and are 2 per cent and 3 per cent respectively. The effect of changing ω is small, even at high Mach number, which lends some support to the use of the approximate viscosity-temperature relationship of this paper.

The position is somewhat more complicated when the wall temperature is a function of position, but a rough idea as to the errors introduced in taking $\mu \propto T$ may be obtained as follows. With $\mu \propto T^{\omega}$ equation (48) may be written

$$C(x) \propto T_w^{\omega - 1} \quad . \quad . \quad . \quad . \quad . \quad (49)$$

Hence, comparing the cases $\omega = 1$, $\omega = 8/9$, and remembering that the integrand in equation (43) is always positive, we note that there is an additional factor $T_w^{-1/9}$ in the integrand when $\omega = 8/9$, associated with a factor $T_w^{1/9}$ outside the integral. If $T_w(x)$ increases with x, the integral will be multiplied by a factor lying between $\{T_w(0)\}^{-1/9}$ and $\{T_w(x)\}^{-1/9}$, so the value of δ_2^2 (and hence of m') is multiplied by a factor lying between unity and $\{T_w(x)/T_w(0)\}^{1/9}$. Since separation occurs at a prescribed value of m', the distance to separation will be decreased, by a factor of order $\{T_w(x)/T_w(0)\}^{-1/9}$ at most. Accordingly, when the wall temperature doubles or halves itself, the use of a linear viscosity-temperature law may affect the predicted momentum thickness by about 4 per cent, and the separation position by up to 8 per cent, with correspondingly smaller differences in the upstream characteristics of the boundary layer.

Consider now the effects of Prandtl number, assuming $\mu \propto T$. These effects enter through the function $Q(x)$ used in the preliminary quadrature, and defined in equation (31). For values of σ near to unity it is easy to expand $Q(x)$ in the form

$$Q(x) = Q_0(x) + (1-\sigma)\,Q_1(x) + O(1-\sigma)^2, \quad . \quad . \quad . \quad . \quad (50)$$

where

$$Q_1(x) = 0{\cdot}53\left(\frac{T_w}{T_1} - 1\right) - 0{\cdot}74\,\frac{\gamma-1}{2}\,M_1^2$$

$$= 0{\cdot}53\,\frac{T_w - T_z}{T_1} - 0{\cdot}21\,\frac{\gamma-1}{2}\,M_1^2. \quad . \quad . \quad . \quad . \quad (51)$$

Unless T_w is greater than T_z by a factor which increases from unity at low Mach numbers to 1·4 at high Mach numbers, it follows that Q_1 will be negative. Unless T_w is sufficiently great, G_3 will thus be larger when $\sigma = 0{\cdot}73$ than when $\sigma = 1$, since retarded flow with $u_1' < 0$ is being considered. It is deduced from equations (43) and (44) that $m'(x)$ is usually smaller when $\sigma = 0{\cdot}73$, since the increase in G_3 will change the integral proportionately less than the maximum change in G_3. It follows that separation is delayed. We deduce that the effect should be considerably greater for a cooled wall and at higher Mach numbers.

These general tendencies agree with the predictions of Gadd. At $M_0 = 4$, for the linearly retarded external velocity and no heat transfer, the distance to separation in the case $\sigma = 0{\cdot}73$ is increased (relative to the case $\sigma = 1$) by about 7 per cent, according to both Gadd's method and that of Young. At $M_0 = 10$ the effect is increased to 11 per cent according to Young's method or 24 per cent according to Gadd's method.

Numerical results for three cases, obtained by the present method, are now considered. The first case is of flow with a linearly increasing pressure

$$p = p_0\left(1 + \frac{x}{c}\right) . \quad . \quad . \quad . \quad . \quad . \quad . \quad (52)$$

the Mach number at the leading edge being 2, and the wall being cooled to the temperature T_0 of the main stream at the leading edge. Results of calculations with

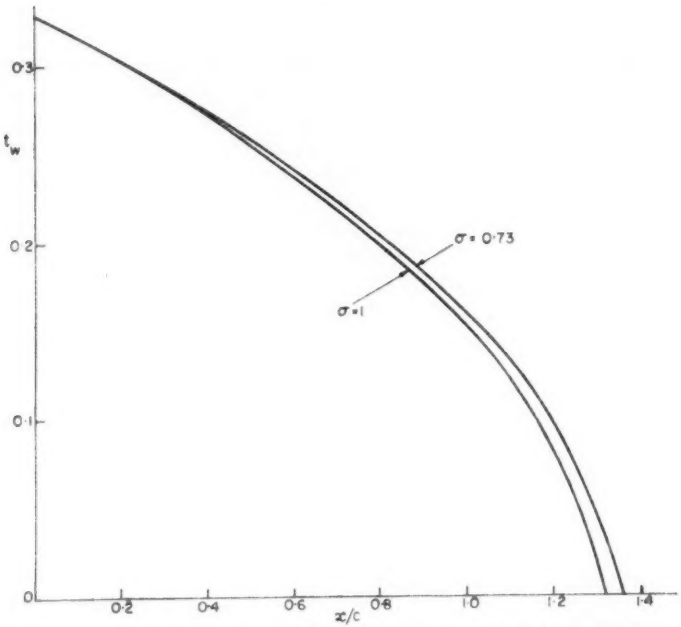

FIGURE 1. Skin friction for the case $T_w = T_0$, $p = p_0\,(1 + x/c)$ at Mach number 2.

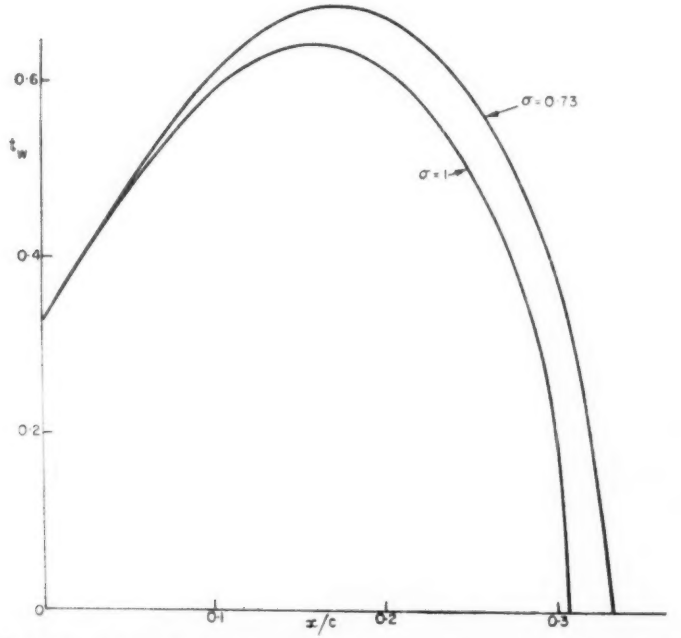

FIGURE 2. Skin friction for the case $T_w = T_0$, $u_1 = u_0\,(1 - x/c)$ at Mach number 4.

TABLE II

SOLUTION FOR

$T_w = T_0$, $p = p_0(1 + x/c)$, $M_0 = 2$

x/c	t_w	
	$\sigma = 1$	$\sigma = 0{\cdot}73$
0	0·328	0·328
0·1	0·316	0·316
0·2	0·302	0·303
0·3	0·288	0·289
0·4	0·272	0·274
0·5	0·255	0·258
0·6	0·237	0·241
0·7	0·218	0·222
0·8	0·198	0·203
0·9	0·175	0·182
1·0	0·150	0·158
1·1	0·122	0·132
1·2	0·079	0·095
1·3	0·018	0·044
1·32	0	—
1·36	—	0

TABLE III

SOLUTION FOR

$T_w = T_0$, $u_1 = u_0(1 - x/c)$, $M_0 = 4$

x/c	t_w	
	$\sigma = 1$	$\sigma = 0{\cdot}73$
0	0·328	0·328
0·025	0·404	0·407
0·05	0·475	0·483
0·075	0·538	0·551
0·1	0·588	0·608
0·125	0·622	0·651
0·15	0·639	0·677
0·175	0·636	0·684
0·2	0·613	0·671
0·225	0·569	0·638
0·25	0·493	0·582
0·275	0·389	0·495
0·3	0·180	0·368
0·311	0	—
0·325	—	0·117
0·331	—	0

$\sigma = 1$ and $\sigma = 0{\cdot}73$ are given in Table II and shown in Fig. 1, in terms of a skin-friction coefficient t_w, defined as

$$t_w = \frac{\tau_w}{\mu_0 u_0} \left(\frac{\nu_0 x}{u_0} \right)^{1/2} . \quad . \quad . \quad . \quad . \quad . \quad (53)$$

It is noted that $t_w(x)$ is only slightly affected by the change in σ, so that the position of separation changes from $x = 1{\cdot}32c$ when $\sigma = 1$ to $x = 1{\cdot}36c$ when $\sigma = 0{\cdot}73$, an increase of 3 per cent. If separation positions are calculated by the empirically improved criterion indicated in Ref. 7, so that the value of m' at separation is a function of M_0, then the respective positions are $x = 1{\cdot}24c$ and $x = 1{\cdot}28c$, again 3 per cent greater.

In the second case the external velocity decreases linearly with distance,

$$u_1 = u_0 \left(1 - \frac{x}{c} \right) . \quad . \quad . \quad . \quad . \quad . \quad (54)$$

the wall temperature again being $T_w = T_0$, but at a Mach number of 4. The results are given in Table III and Fig. 2. The change of Prandtl number produces, in this case, a change in separation position from $x = 0{\cdot}311c$ to $x = 0{\cdot}331c$ or (with the empirical correction) from $x = 0{\cdot}248c$ to $0{\cdot}266c$, an increase of about 7 per cent. The detailed distribution of skin friction is changed appropriately.

In the third case the external velocity is as in the second case, namely equation (54), with a leading edge Mach number of 4, but the wall is at the free-stream stagnation temperature. It follows that there is zero heat transfer when $\sigma = 1$, the wall being slightly heated when $\sigma = 0{\cdot}73$. It can be seen from Table IV that the distribution of skin friction and the position of separation are virtually unaffected

TABLE IV

SOLUTION FOR $T_w = T_0\left(1+\frac{\gamma-1}{2}M_0^2\right)$, $u_1 = u_0\left(1-\frac{x}{c}\right)$, $M_0 = 4$

x/c	t_w	
	$\sigma=1$	$\sigma=0{\cdot}73$
0	0·328*	0·328
0·01	0·318	0·318
0·02	0·301	0·302
0·03	0·277	0·278
0·04	0·244	0·244
0·05	0·200	0·199
0·06	0·112*	0·111
0·0670	—	0
0·0671	0	—

*These two values were incorrectly given in Ref. 7.

by the change in σ. The reason for this is that a reduction in σ would tend to cause a reduced momentum thickness and a later separation if there were zero heat transfer throughout. On the other hand, though there is zero heat transfer when $\sigma=1$, the wall is slightly heated above the zero heat transfer value when $\sigma<1$. This causes an opposite effect, and the two appear to balance.

A comparison of the results obtained in these three cases bears out the general conclusions already mentioned, that according to the present method the effects of change of Prandtl number become more marked as the Mach number is increased, or as the wall is cooled below the zero-heat-transfer value.

5. Application to Interactions between Shock Waves and Boundary Layers

The type of situation to be considered here is that illustrated in Figs. 3 and 4, in which laminar-boundary-layer separation in supersonic flow is provoked by an oblique shock wave, a wedge on the wall, or some similar mechanism. In such a flow separation will usually occur well upstream of the agency which produces it, and will be of the "equilibrium" type, in which the deflection of the external streamlines due to the thickening of the boundary layer produces a pressure gradient which must be just sufficient to cause the requisite amount of thickening.

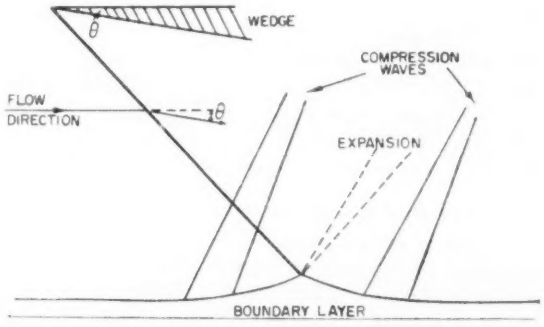

FIGURE 3. Boundary layer and externally generated shock.

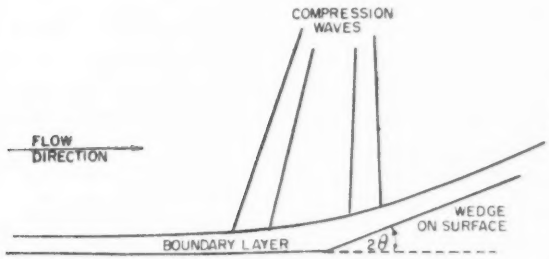

FIGURE 4. Shock generated from within boundary layer by wedge on surface.

Mathematically there are two relationships between the thickening of the boundary layer and the pressure distribution, which must be such that these relationships are consistent. On the one hand, if the pressure $p(x)$ or the free-stream velocity $u_1(x)$ were known, then the usual boundary-layer characteristics could be calculated by the theory of Section 3, in particular $\delta_1(x)$, the displacement thickness. On the other hand the pressure rise is related to the angle through which the external streamlines are deflected, that is to

$$\frac{d}{dx}\left\{\delta_1(x)-\delta_{10}(x)\right\}+2\varepsilon\theta, \quad . \quad . \quad . \quad . \quad . \quad (55)$$

where $\delta_{10}(x)$ is the displacement thickness when there is no pressure gradient and the temperature boundary conditions are unaltered, and $\varepsilon=0$ upstream of the shock or wedge apex and $\varepsilon=1$ downstream thereof. This relationship, expressed mathematically, is

$$\frac{p}{p_0}-1=\frac{\gamma M_0^2}{(M_0^2-1)^{1/2}}\left[\frac{d}{dx}\left\{\delta_1-\delta_1\right\}+2\varepsilon\theta\right],$$

or, upon integration,

$$\delta_1(x)-\delta_{10}(x)+2\varepsilon\theta(x-x_1)=\frac{(M_0^2-1)^{1/2}}{\gamma M_0^2}\int_0^x\left(\frac{p}{p_0}-1\right)dx, \quad . \quad . \quad (56)$$

where $x=x_1$ is the shock or wedge apex. Simultaneous solution of (56) and the various equations of Section 3 is, in general, a matter for high-speed computing machines. With suitable restrictions, however, an analytic solution can be obtained, as follows.

Consider flows in which the pressure rise to separation is a sharp one, occurring over only a short distance. In such circumstances it is permissible to regard quantities such as the pressure, external velocity and temperature, and wall temperature, as being sensibly constant, although their gradients may not be set equal to zero. From a practical point of view this approximation seems good, for if the Mach number M_0 and the Reynolds number at separation R are in the ranges $2\leqslant M_0\leqslant 4$, $10^5\leqslant R\leqslant 10^6$, the value of u_1 at separation differs by only 1 or 2 per cent from its upstream value, and in a typical case might decrease by only a further 1 or 2 per cent between separation and the point where the shock strikes the boundary layer. Accordingly the value at separation is a good mean value to take.

With this approximation it is found that the relevant equations for the development of the boundary layer simplify as follows. In the region upstream of the interaction, u_1' is zero and hence, by (40), G_3 is unity. In the region of interaction, $(T_w/T_1)+Q$ remains sensibly constant (provided that T_w does not vary too rapidly with x), so that G_3 becomes equal to a power of u_1/u_0, and therefore remains close to unity. If, following the arguments advanced in Section 4, C is taken to be constant, then it can be deduced from (43) that δ_2^2 is almost constant through the interaction and may be taken as

$$\delta_2^2 = 0{\cdot}45 \left(\frac{\nu_1 x}{u_1}\right)_{sep} \quad . \quad . \quad . \quad . \quad . \quad . \quad (57)$$

It then follows from (44) that

$$m'(x) = -0{\cdot}45 \left(\frac{x}{u_1}\frac{T_w}{T_1}\right)_{sep} u_1'(x), \quad . \quad . \quad . \quad . \quad (58)$$

and then, from (45),

$$\delta_1 = \left\{0{\cdot}45 \frac{\nu_1 x}{u_1}\right\}^{1/2} \left\{\frac{T_w}{T_1} H' + \left(\frac{T_w}{T_1} - 1\right)(1-\sigma^{1/3}) + K + \frac{\gamma-1}{2} M_1^2 [h_1 \sigma^{5/6} - (h_1 - 1)\sigma]\right\}, \quad . \quad . \quad . \quad (59)$$

where all values except H' are to be taken at separation. In the same way we may deduce that the displacement thickness δ_{10}, in the absence of a pressure gradient, is given by the same expression with $H'(m')$ replaced by $H'(0)$. Accordingly it follows that (56) becomes

$$\frac{(M_0^2-1)^{1/2}}{\gamma M_0^2} \int_0^x \left(\frac{p}{p} - 1\right) dx = \left\{\left(0{\cdot}45 \frac{\nu_1 x}{u_1}\right)^{1/2} \frac{T_w}{T_1}\right\}_{sep} \{H'(m') - 2{\cdot}61\} + 2\varepsilon\theta (x - x_1). \quad . \quad . \quad . \quad (60)$$

It is worth noting that this relationship is independent of σ, the Prandtl number. The reason for this is that, although (59) shows that the displacement thickness δ_1 is dependent on σ, the increment in δ_1 due to the pressure gradient is independent of it.

We may simplify (60), and isolate the relevant parameters, by writing

$$\left.\begin{aligned} F &= 0{\cdot}4096 (M_0^2-1)^{1/4} R^{1/4} \left\{1 - \frac{u_1^2(x)}{u_0^2}\right\} \\ X &= 1{\cdot}820 \ (M_0^2-1)^{1/4} R^{1/4} \left(\frac{T_w}{T_1}\right)_{sep}^{-1} \left(\frac{x}{x_{sep}} - 1\right) \\ \Lambda &= 1{\cdot}638 \theta R^{1/4} (M_0^2-1)^{-1/4} \end{aligned}\right\} \quad . \quad . \quad . \quad (61)$$

where R is the Reynolds number, $u_1 x/\nu_1$, at separation. Then equations (60) and (61) become

$$\int_X^X F \, dX = H'(m') - 2{\cdot}61 + \Lambda\varepsilon (X - X_1), \quad . \quad . \quad . \quad (62)$$

In equation (62) $$m' = dF/dX, \quad . \quad . \quad . \quad . \quad . \quad . \quad (63)$$

and X_1 is the value of X where $x = x_1$. The lower limit of integration represents the leading edge $x = 0$, and, according to the assumptions made, is many times the interaction length away, and may be taken as minus infinity. So if we define $G_0 = H' - 2{\cdot}61$, and, if F' denotes derivatives with respect to X, then (63) becomes

$$\int_{-\infty}^{X} F\,dX = G_0(F') + \Lambda(X - X_1). \quad . \quad . \quad . \quad . \quad (64)$$

A solution of this equation may be obtained by writing

$$F(X) = F_0(X) + \Lambda\varepsilon, \quad . \quad . \quad . \quad . \quad . \quad (65)$$

whence F_0 satisfies $$\int_{-\infty}^{X} F_0\,dX = G_0(F_0'). \quad . \quad . \quad . \quad . \quad (66)$$

Upon multiplying by F_0'', and integrating from $X = -\infty$ to X, we find

$$\int_0^{F_0'} G_0(z)\,dz = \int_{X}^{-\infty} F_0'' \left\{ \int_{X}^{-\infty} F_0\,dX \right\} dX = \left[F_0' \int_{-\infty}^{X} F_0\,dX \right] - \int_{-\infty}^{X} F_0 F_0'\,dX$$

$$= F_0' \int_{-\infty}^{X} F_0\,dX - \tfrac{1}{2}F_0^2. \quad . \quad . \quad . \quad . \quad (67)$$

Substitution for $\int_{-\infty}^{X} F_0\,dX$ from equation (66) gives

$$F_0^2 = 2F_0' G_0(F_0') - 2\int_0^{F_0'} G_0(z)\,dz = P(F_0'). \quad . \quad . \quad (68)$$

or $$F_0 = \pm\{P(F_0')\}^{1/2}. \quad . \quad . \quad . \quad . \quad . \quad . \quad (69)$$

For each of these two solutions it is a simple matter to derive F_0' in terms of F_0 by interpolation, and then to relate F_0 and X by

$$X = \int_{F_{0\,\mathrm{sep}}}^{F_0} \frac{dF_0}{F_0'} \quad . \quad . \quad . \quad . \quad . \quad . \quad (70)$$

In proceeding beyond separation it is necessary to define the function $H'(m')$ for such a region. Details of the best choice are given in Appendix III and Table I. Accepting these values, the integration of (70) leads to the results given in Table V.

TABLE V

THE FUNCTION $F(X)$ OCCURRING IN SHOCK-WAVE AND BOUNDARY-LAYER INTERACTIONS

X	$F(X)$	$F'(X)$	X	$F(X)$	$F'(X)$
−7·03	0·02	0·0103	0·70	0·40	0·0885
−5·12	0·05	0·0237	1·86	0·50	0·0828
−4·09	0·08	0·0351	3·21	0·60	0·0645
−3·14	0·12	0·0479	5·03	0·70	0·0465
−2·21	0·17	0·0612	7·61	0·80	0·0323
−1·32	0·23	0·0736	11·75	0·90	0·0174
−0·55	0·29	0·0832	15·52	0·95	0·0101
0	0·338	0·0900	23·33	1·00	0·0042
			∞	1·03	0

Since the pressure rises to separation it follows that F must be positive. Upstream of separation, where $\varepsilon = 0$, it follows that $F = F_0$, so the positive sign in (69) must be taken. Thus, at separation, where $F'(X) = 0{\cdot}090$, the value of F is

$$F_{sep} = 0{\cdot}338. \quad . \quad . \quad . \quad . \quad . \quad . \quad (71)$$

It follows from (61), remembering that $C_p \simeq 1 - (u_1^2/u_0^2)$, that

$$C_p (M_0^2 - 1)^{1/4} R^{1/4} = 0{\cdot}338/0{\cdot}4096 = 0{\cdot}825. \quad . \quad . \quad . \quad (72)$$

so that the pressure rise to separation depends upon Mach number and Reynolds number, but not upon wall temperature.

At the position where the shock strikes the boundary layer or at the wedge apex, the pressure is continuous, so F is continuous. Hence, since $\Lambda\varepsilon$ is discontinuous at this point, it follows that the opposite sign in (69) must be taken for F_0 downstream of separation. This can only be so if F_0 changes from $+\frac{1}{2}\Lambda$ to $-\frac{1}{2}\Lambda$. It follows that the pressure is symmetrical about $x = x_1$, and that the pressure rise to this point is one half of the final value.

The predicted pressure coefficient at separation, equation (72), may be compared with experiment. Chapman, Kuehn and Larson[16] have correlated a considerable number of experimental results at zero heat transfer over a range of Mach numbers $1{\cdot}1 < M_0 < 3{\cdot}6$ and Reynolds numbers $10^4 < R < 10^8$, and find that $C_p (M_0^2 - 1)^{1/4} R^{1/4}$ has a mean value at separation of about 0·93, the scatter being of order 10 per cent. Some of the theoretical values known to the author are 1·05 and 1·15 (Hakkinen *et al.*[17]), 1·03 (Gadd[1]), 1·13 (Gadd[2]) and 0·94 (Bray *et al.*[6]).

On the other hand the scale in the x-direction, which determines the upstream influence, is predicted by (61) to be directly proportional to T_w, so that the pressure gradient at separation is inversely proportional to T_w. Now some experimental results of Gadd[4] suggest that the pressure distribution is dependent upon wall temperature to a remarkably small degree. On the other hand, later experiments (as yet unpublished) have shown that there is some dependence provided that heat transfer rates are sufficiently high.

Direct comparisons with detailed experimental pressure distributions have been made for a few cases. Firstly we consider some unpublished results of Gadd for flow along a flat plate with an upstream Mach number $M_0=2$, and with zero heat transfer at the wall. By matching the theoretical and experimental pressures at the theoretical separation point, it is found that separation occurs 0·78 in. from the leading edge, with $R=6{\cdot}93\times10^4$. It then follows from (61) that

$$\left.\begin{aligned} p/p_0 &= 1+0{\cdot}320F \\ x &= 0{\cdot}78\,(1+0{\cdot}0463X) \end{aligned}\right\}, \qquad (73)$$

with x measured in inches, whence Table V yields the pressure distribution. The results are given in Fig. 5. The agreement is good as far as the position where the shock strikes the boundary layer. Downstream of this position the agreement is less good, the experimental pressure distribution having a more pronounced foot.

We now consider some results of Gadd[4], indicating the effects of heat transfer. These experiments were carried out on a flat plate with $M_0=3$ and $R=4{\cdot}2\times10^5$, with zero heat transfer in one case and the wall heated to a temperature $T_w=1{\cdot}25\,T_z$ and cooled to $T_w=0{\cdot}88\,T_z$ in the other cases. Using the same matching technique as before, the theoretical pressure distributions were predicted and are shown in Fig. 6 with the experimental values. The agreement is excellent for zero heat transfer. The predicted effects of heat transfer are small, but are rather greater than given by experiment.

The amount by which the wall temperature differed from the zero-heat-transfer value was quite small in the cases just considered. Accordingly, comparison has also been made between the theory and some later results (as of Gadd and Attridge[18]). These relate to flow with an upstream Mach number $M'=2{\cdot}70$ and with $R=1{\cdot}5\times10^5$, the wall temperature being $T_w=T_z$ in one case and $T_w=1{\cdot}5\,T_z$ in the other. The results are given in Fig. 7, theory and experiment being matched

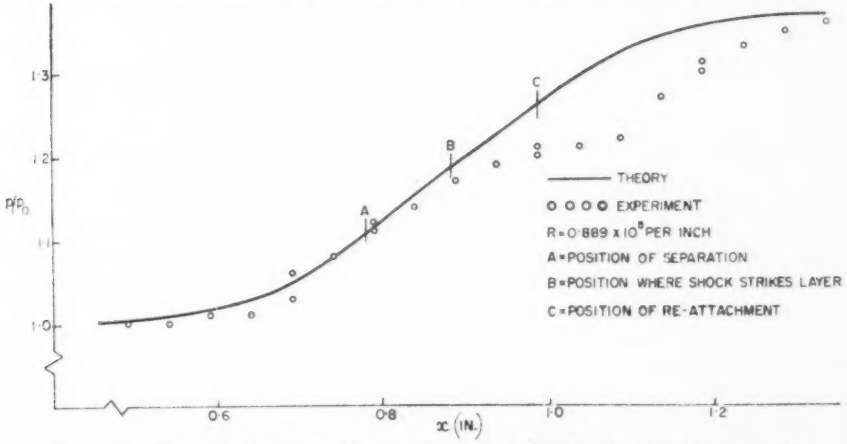

FIGURE 5. Theoretical and experimental pressure distribution for $M_0=2$, $R=7\times10^4$.

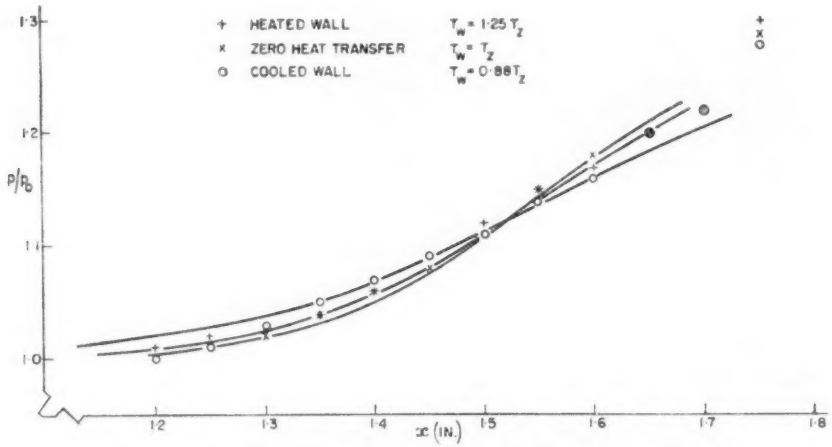

FIGURE 6. Experimental and theoretical results for $M_0 = 3$, $R = 4{\cdot}2 \times 10^5$.

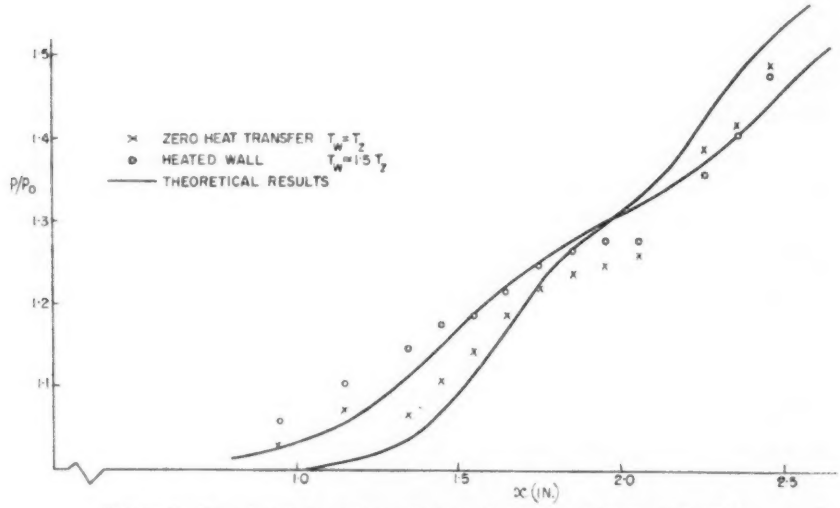

FIGURE 7. Experimental and theoretical results for $M_0 = 2{\cdot}7$, $R = 1{\cdot}5 \times 10^5$.

at the apex of the wedge which provoked separation. We note that the agreement is reasonable in that the upstream influence is greater when the wall is hotter, and this lends valuable support to the theory; although a detailed comparison of the experimental and theoretical pressure distributions is a little disappointing, it should be remembered that, on the one hand the accuracy of the experimental pressures is probably not high and, on the other hand, the overall pressure rise of 60 per cent is rather large. Further experiments with a lower pressure rise and more accurate measurements would be desirable.

ACKNOWLEDGMENTS

The work described in this paper was carried out in the Aerodynamics Division of the National Physical Laboratory. The paper is published by permission of the Director, and on the recommendation of the Aeronautical Research Council.

Appendix I

FUNCTIONAL RELATIONSHIPS

It was pointed out by the author that, when $\sigma=1$ and $\mu \propto T$, the functions H', l' and L' depend mainly on m', and are essentially independent of wall temperature and Mach number. It is the purpose here to examine whether a similar result holds for arbitrary fixed σ and general viscosity-temperature law.

It is assumed that the velocity profile may be approximated by a suitable function of the (transformed) normal co-ordinate Y. Thus

$$\frac{u}{u_1}=f(\eta), \quad \eta=\frac{Y}{\Delta}. \qquad (74)$$

where the edge of the boundary layer is taken at $\eta=1$ if a method analogous to that of Pohlhausen[19] is used, and at $\eta=\infty$ if a method analogous to that of Timman[20] is used. Upon choosing f to satisfy certain of the boundary conditions relevant to (22), we find that at the edge of the boundary layer

$$f\longrightarrow 1; \quad f', f'', f''', \ldots \longrightarrow 0. \qquad (75)$$

At the wall, the primary boundary condition, $u=0$, yields

$$f(0)=0, \qquad (76)$$

while, upon putting $Y=0$ in (22), we obtain

$$f''(0)=-\frac{T_w}{T_1}\frac{du_1}{dx}\frac{\Delta^2}{C\nu_s}=\left(\frac{\Delta}{\delta_2'}\right)^2 m'=\Lambda'. \qquad (77)$$

The next boundary condition at the wall is obtained by differentiating (22) with respect to Y and then putting $Y=0$. This yields

$$C\nu_s\left(\frac{\partial^4\lambda}{\partial Y^4}\right)_w=-u_1\frac{du_1}{dx}\left(\frac{\partial G}{\partial Y}\right)_w=\frac{1}{T_1}\frac{du_1}{dx}\sigma^{1/3}(T_s-T_w+KT_1)\left(\frac{\partial u}{\partial y}\right)_w$$

by (23) and (9), and this may be written

$$f'''(0)=\Lambda'\frac{T_s-T_w+KT_1}{T_w}f'(0)\sigma^{1/3}. \qquad (78)$$

As in Ref. 7, it is argued that the right-hand side of (78) is zero at a sharp leading edge ($\Lambda'=0$), at separation ($f'=0$) and when there is zero heat transfer. Accordingly (78) is approximated by the simpler relationship

$$f'''(0)=0. \qquad (79)$$

The equations (75), (76), (77), (79) are formally the same as for incompressible flow, so that $H'(m')$, $l'(m')$ and $L'(m')$ are functionally independent of Mach number, wall temperature, Prandtl number and viscosity law, the effects of these quantities appearing only implicitly in the transformation of the normal co-ordinate and in the definitions of the functions, H', l' and L'.

Appendix II

The True Boundary-Layer Thicknesses

By definition

$$\delta_2 = \int_0^\infty \frac{\rho u}{\rho_1 u_1}\left(1-\frac{u}{u_1}\right) dy. \qquad (80)$$

By equation (16),

$$\frac{\rho}{\rho_1} dy = \frac{\rho}{\rho_1}\left(\frac{p_s}{p}\right)^{1/2} \frac{T}{T_s} dY$$

$$= \left(\frac{\nu_1}{C\nu_s}\right)^{1/2} dY, \qquad (81)$$

so that (80) yields

$$\delta_2 = \left(\frac{\nu_1}{C\nu_s}\right)^{1/2} \delta_2'. \qquad (82)$$

Similarly

$$\delta_1 = \int_0^\infty \left(1-\frac{\rho u}{\rho_1 u_1}\right) dy$$

$$= \left(\frac{\nu_1}{C\nu_s}\right)^{1/2} \int_0^\infty \left(\frac{\rho_1}{\rho}-\frac{u}{u_1}\right) dY$$

$$= \left(\frac{\nu_1}{C\nu_s}\right)^{1/2} \left\{\delta_1' + \int_0^\infty \left(\frac{T}{T_1}-1\right) dY\right\}. \qquad (83)$$

By substituting from equation (9), and carrying out the relevant integrations, this may be easily shown to lead to

$$\delta_1 = \left(\frac{\nu_1}{C\nu_s}\right)^{1/2} \left\{\frac{T_w}{T_1}\delta_1' + \left[\left(\frac{T_1}{T_w}-1\right)(1-\sigma^{1/3})\, h_1 + \frac{\gamma-1}{2} M_1^2 (\sigma^{5/6}h_1 - \sigma h_1 + \sigma) + \right.\right.$$

$$\left.\left. + K(\sigma^{1/3}h_1 - \sigma h_1 + \sigma)\right]\delta_1'\right\}$$

$$= \delta_2 \left\{\frac{T_w}{T_1}H' + \left(\frac{T_w}{T_1}-1\right)(1-\sigma^{1/3})\, h_1 + \frac{\gamma-1}{2} M_1^2 (\sigma^{5/6}h_1 - \sigma[h_1-1]) + K\right\}, \qquad (84)$$

using the fact that the coefficient of K is almost exactly unity when $0{\cdot}636 \leqslant \sigma \leqslant 1{\cdot}135$.

Appendix III

Flow Downstream of Separation

The universal functions used in Thwaites's method were obtained from a considered analysis of all the exact and approximate solutions of the laminar-boundary-layer equations then known. To extend these functions into the region downstream of the separation point requires a similar analysis of the relevant solutions.

As far as the approximate solutions are concerned, it is a fairly straightforward matter to calculate the consequences of formally applying them downstream of separation, and the functions $l(m)$, $H(m)$, $L(m)$, are given in Figs. 8 to 10 for the methods of Pohlhausen[19] and Timman[20], and for the exact similarity solutions given originally for the upstream flow by Falkner and Skan[21] and extended to flow beyond separation by Stewartson[22].

In spite of the wide divergences between the solutions, there are points of similarity.

(*i*) In each case the value of m increases to a maximum, and then decreases to zero far downstream of separation, corresponding physically to a considerable "dead-air" region.

(*ii*) For the exact "similarity" solutions the maximum of m occurs at separation, where there is a cusp in the curve of L against m. For the fairly accurate approximate method of Timman, the maximum of m occurs slightly beyond separation, near which there is a fairly tight loop in the (L, m) curve. For the less accurate approximate method of Pohlhausen, the maximum of m occurs further beyond separation, and the loop in the (L, m) curve is a loose one.

The near appearance of a cusp in the (L, m) curve for Timman's method, and its actual appearance for the similarity solutions, suggests that it may be realistic to include it in the functions to be defined and, accordingly, to have the maximum value of m at separation. The functions $H(m)$ and $l(m)$ are chosen to satisfy these requirements

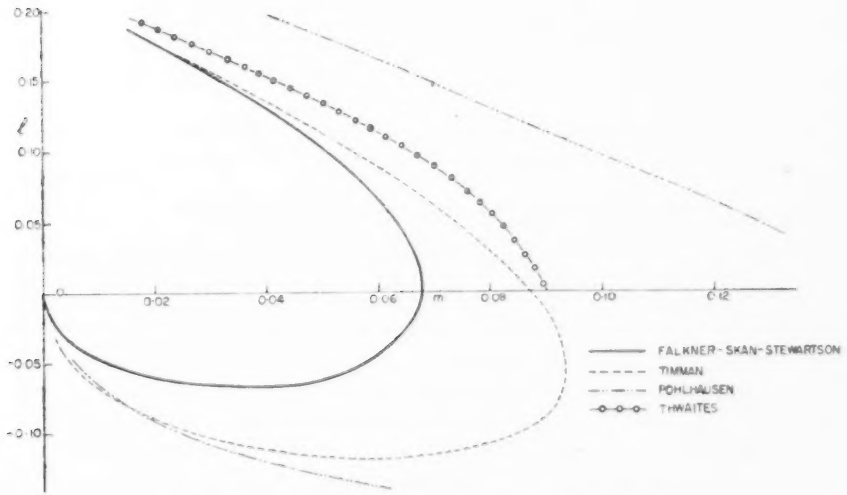

Figure 8. The function $l(m)$ according to several methods.

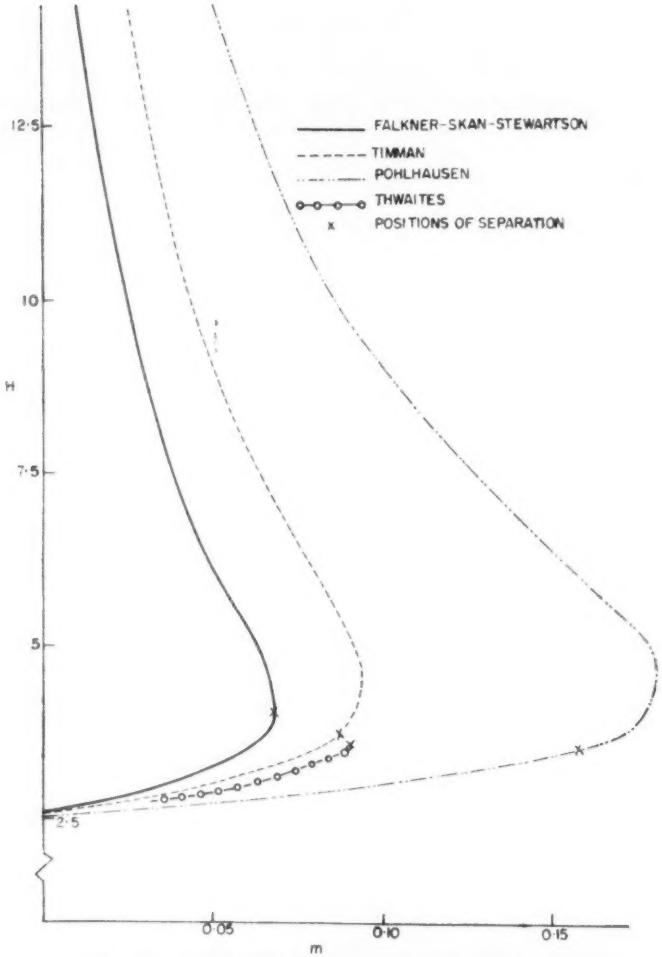

FIGURE 9. The function $H(m)$ according to several methods.

and to join as smoothly as possible onto the values given by Thwaites (and amended by Curle and Skan) at separation. In the region downstream of separation, they are chosen to tend to the values for the similarity solutions as $m \longrightarrow 0$. The function $L(m)$ is chosen to be continuous with the amended Thwaites value, but with a cusp as described.

The functions $l(m)$, $H(m)$, are given in Table I, while $L(m)$, given approximately by $L=0{\cdot}45+6m$ upstream of separation, may be adequately approximated in the downstream region by

$$\left.\begin{aligned} L&=0{\cdot}45+6m, \qquad 0{\cdot}0900 \geqslant m \geqslant 0{\cdot}0625 \\ L&=1{\cdot}8m^{1/2}+6m, \qquad 0{\cdot}0625 \geqslant m \geqslant 0 \end{aligned}\right\} \quad . \quad . \quad . \quad . \quad (85)$$

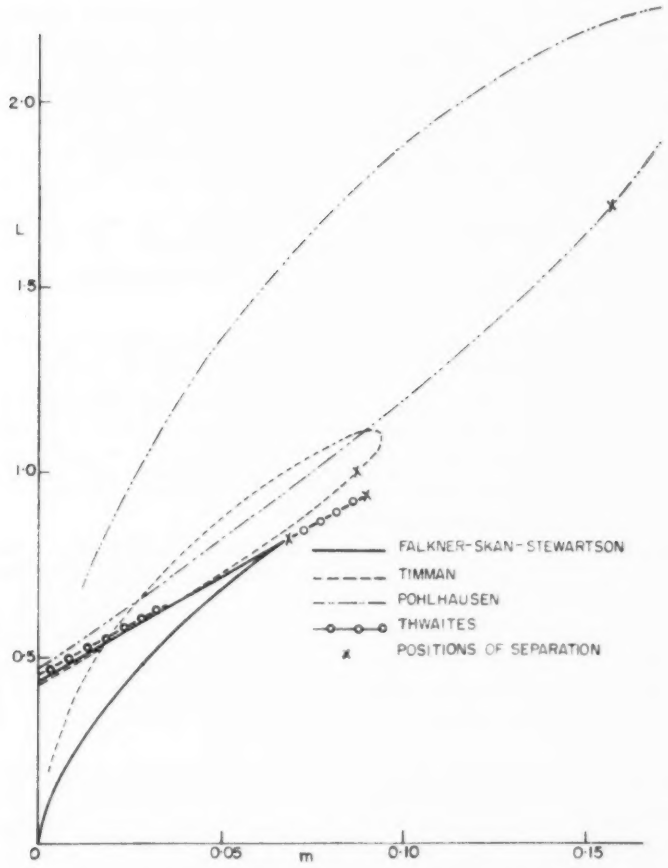

FIGURE 10. **The function $L(m)$ according to several methods.**

REFERENCES

1. GADD, G. E. Interactions between Wholly Laminar or Wholly Turbulent Boundary Layers and Shock Waves Strong Enough to Cause Separation. *Journal of the Aeronautical Sciences*, Vol. 20, p. 729, 1953.

2. GADD, G. E. A Theoretical Investigation of Laminar Separation in Supersonic Flow. *Journal of the Aeronautical Sciences*, Vol. 24, p. 759, 1957.

3. STRATFORD, B. S. Flow in the Laminar Boundary Layer near Separation. R. & M. 3002, 1954.

4. GADD, G. E. An Experimental Investigation of Heat Transfer Effects on Boundary-Layer Separation in Supersonic Flow. *Journal of Fluid Mechanics*, Vol. 2, p. 105, 1957.

5. CROCCO, L. and LEES, L. A Mixing Theory for the Interaction between Dissipative Flows and Nearly Isentropic Streams. *Journal of the Aeronautical Sciences*, Vol. 19, p. 649, 1952.

6. BRAY, K. N. C., GADD, G. E. and WOODGER, M. Some Calculations by the Crocco-Lees and Other Methods of Interactions between Shock Waves and Laminar Boundary Layers, including Effects of Heat Transfer and Suction. A.R.C. Current Paper 556, 1960.

7. CURLE, N. The Steady Compressible Laminar Boundary Layer, with Arbitrary Pressure Gradient and Uniform Wall Temperature. *Proc. Roy. Soc.* A. 249, p. 206, 1958.

8. CURLE, N. Heat Transfer and Laminar Boundary-Layer Separation in Steady Compressible Flow Past a Wall with Non-Uniform Temperature. R. & M. 3179, 1958.

9. GADD, G. E. Some Aspects of Laminar Boundary Layer Separation in Compressible Flow with No Heat Transfer to the Wall. *Aeronautical Quarterly*, Vol. IV, p. 123, 1953.

10. YOUNG, A. D. Skin Friction in Compressible Flow. *Aeronautical Quarterly*, Vol. I, p. 137, 1949.

11. MONAGHAN, R. J. An Approximate Solution of the Compressible Laminar Boundary Layer on a Flat Plate. R. & M. 2760, 1949.

12. HOWARTH, L. Concerning the Effect of Compressibility on Laminar Boundary Layers and Their Separation. *Proc. Roy. Soc.* A. 194, p. 16, 1948.

13. CHAPMAN, D. R. and RUBESIN, M. W. Temperature and Velocity Profiles in the Compressible Laminar Boundary Layer with Arbitrary Distribution of Surface Temperature. *Journal of the Aeronautical Sciences*, Vol. 16, p. 547, 1949.

14. TRUCKENBRODT, E. Ein Quadraturrerfahren zur Berechnung der laminaren und turbulenten Reibungsschichten bei ebener und rotationssymmetrischer Strömung. *Ingenieur-Archiv*, Vol. 20, p. 211, 1952.

15. CURLE, N. and SKAN, S. W. Approximate Methods for Predicting Separation Properties of Laminar Boundary Layers. *Aeronautical Quarterly*, Vol. VIII, p. 257, 1957.

16. CHAPMAN, D. R., KUEHN, D. M. and LARSON, H. K. Investigation of Separated Flows in Supersonic and Subsonic Streams with Emphasis on the Effect of Transition. N.A.C.A. Report 1356, 1958.

17. HAKKINEN, R. J., GREBER, I., TRILLING, L. and ABARBANEL, S. S. The Interaction of an Oblique Shock Wave with a Laminar Boundary Layer. N.A.S.A. Memo. 2-18-59W, 1959.

18. GADD, G. E. and ATTRIDGE, J. L. A Note on the Effects of Heat Transfer on the Separation of a Laminar Boundary Layer. A.R.C. Current Paper 569, 1961.

19. POHLHAUSEN, K. Zur Integration der Differential-gleichung der laminaren Grenschicht. *Zeitschrift für Angewandte Mathematik und Mechanik*, Vol. 1, p. 252, 1921.

20. TIMMAN, R. A One Parameter Method for the Calculation of Laminar Boundary Layers. N.L.L. (Amsterdam) Report F. 35, 1949.

21. FALKNER, V. M. and SKAN, S. W. Some Approximate Solutions of the Boundary-Layer Equations. R. & M. 1314, 1930.

22. STEWARTSON, K. Further Solutions of the Falkner-Skan Equation. *Proceedings of the Cambridge Philosophical Society*, Vol. 50, p. 454, 1954.

The Buckling of a Reinforced Circular Plate under Uniform Radial Thrust

I. T. COOK and H. W. PARSONS

(Department of Mathematics, The University, Hull)

SUMMARY: An exact solution for the symmetrical buckling under uniform radial thrust is obtained for a thin circular plate having a particular type of thickness function for the cases in which the edge of the plate is either clamped or simply-supported. In both cases it is found that the critical thrust necessary to produce buckling can be increased from its value for the uniform circular plate of the same material and volume by concentrating material in the central region of the plate. For the clamped plate the increase is about 18 per cent and for the simply-supported plate about 29 per cent.

1. Introduction

The initial symmetrical buckling of a uniform thin circular plate under uniform radial thrust applied round its edge has been discussed by a number of authors including Bryan[1] and Timoshenko[2]. Meissner[3] discusses the problem of a uniform annulus and Olsson[4] the problem of an annulus with quadratically varying stiffness.

In the present paper an exact solution is obtained for a thin circular plate of radius a having a simple thickness variation, buckling similarly under the same type of loading. Following Capey[5], the plate has a "step" thickness function (Fig. 1) so that it consists of an inner circular portion of constant thickness h_0 surrounded by an annular portion of constant thickness h_1, the change-over radius from h_0 to h_1 being at.

By varying h_0/h_1 and t, the optimum distribution of a given volume of material in the form of a circular plate of given radius and having the thickness variation described can be determined for the loading and buckling pattern assumed.

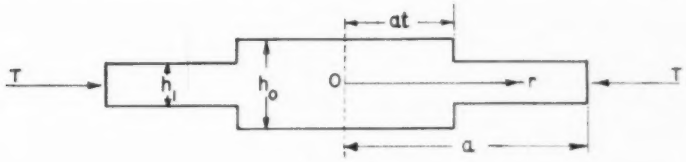

FIGURE 1.

Received March 1961.

NOTATION

a radius of plate

h thickness of plate, $\left.\begin{matrix} =h_0, & 0 \leqslant r < at \\ =h_1, & at < r \leqslant a \end{matrix}\right\}$

$p = h_0/h_1$

$\bar{h}$ average thickness of plate, $= h_1(1 - t^2 + pt^2)$

σ Poisson's ratio (taken as 0·333)

D flexural rigidity of plate, $= \dfrac{Eh^3}{12(1-\sigma^2)}$

S parameter in the definition of T_{cr}

T applied radial thrust per unit length at circumference $r = a$

T_{cr} critical value of T for buckling, $= \dfrac{SE\bar{h}^3}{12(1-\sigma^2)a^2}$

S_{max} maximum value of S for variable t and p

r, θ polar co-ordinates

$w = w(r)$, deflection of plate

$\phi = dw/dr$

$\left.\begin{matrix} N_r = B + A/r^2 \\ N_\theta = B - A/r^2 \\ N_{r\theta} = C/r^2 \end{matrix}\right\}$ resultant stress components (A, B, C are constants)

$\left.\begin{matrix} M_r = D\left(\dfrac{d\phi}{dr} + \dfrac{\sigma\phi}{r}\right) \\ Q = D\left(\dfrac{d^2\phi}{dr^2} + \dfrac{1}{r}\dfrac{d\phi}{dr} - \dfrac{\phi}{r^2}\right) \end{matrix}\right\}$ bending moment and shear stress

$k^2 = B/D$

$q = 1 - A/D$

$n^2 = 1 - A_1/D_1 = -m^2$

D, A, B, C, k, q take suffix 0 or 1 according as $0 \leqslant r < at$ or $at < r \leqslant a$ respectively.

2. Equilibrium Equations for the Plate

The stress resultants in the plane of the plate are determined by the boundary conditions at $r = 0$, at and a and by the continuity of the radial displacement at $r = at$. It is found that $N_r = N_\theta = B_0$, $N_{r\theta} = 0$ for $0 \leqslant r \leqslant at$ and $N_r = B_1 + A_1/r^2$, $N_\theta = B_1 - A_1/r^2$, $N_{r\theta} = 0$ for $at \leqslant r \leqslant a$, where

$$\frac{B_0}{2p} = \frac{B_1}{2p-(1-\sigma)(p-1)} = \frac{A_1}{a^2t^2(1-\sigma)(p-1)} = \frac{T}{2p-(1-\sigma)(p-1)(1-t^2)} \qquad (1)$$

Assuming that when the plate buckles it does so symmetrically, so that $w=w(r)$, the equilibrium of a circular portion of the plate with centre O and radius r gives

$$Q+N_r\phi=0. \qquad . \quad . \quad . \quad (2)$$

Substitution for Q and N_r then gives the Bessel equation in ϕ, namely

$$\frac{d^2\phi}{dr^2}+\frac{1}{r}\frac{d\phi}{dr}+\phi\left(k^2-\frac{q}{r^2}\right)=0. \qquad . \quad . \quad . \quad . \quad (3)$$

When $0\leqslant r\leqslant at$, $q=1$, and $\phi=0$ when $r=0$, so that solution of equation (3) gives

$$\phi=E_0J_1(k_0r) \qquad 0\leqslant r\leqslant at,$$

where E_0 is a constant.

When $at\leqslant r\leqslant a$, $q=q_1$ and (3) gives

$$\phi=E_1U(k_1r)+F_1V(k_1r)\ ,$$

where E_1, F_1 are constants and $U(k_1r)$, $V(k_1r)$ are independent solutions of equation (3).

If $q_1=n^2>0$, then $U(k_1r)$ and $V(k_1r)$ can be replaced by the Bessel functions $J_n(k_1r)$ and $J_{-n}(k_1r)$. It is to be noted that, in general, n is not an integer and the functions may be evaluated by the series expansion

$$J_n(k_1r)=\frac{(k_1r/2)^n}{\Gamma(n+1)}\left[1-\frac{(k_1r/2)^2}{1!\,(n+1)}+\frac{(k_1r/2)^4}{2!\,(n+1)(n+2)}-\ldots\right].$$

The gamma functions involved may be absorbed in the arbitrary constants E_1 and F_1.

If $q_1=-m^2<0$,

$$U(k_1r)=\sum_{s=0}^{\infty}\left[\alpha_s\cos(m\log k_1r)+\beta_s\sin(m\log k_1r)\right](k_1r/2)^{2s}$$

$$V(k_1r)=\sum_{s=0}^{\infty}\left[\gamma_s\cos(m\log k_1r)+\delta_s\sin(m\log k_1r)\right](k_1r/2)^{2s},$$

where $\alpha_0=1,\quad \beta_0=0,\quad \alpha_s=\dfrac{m\beta_{s-1}-s\alpha_{s-1}}{s(m^2+s^2)}\ ,\quad \beta_s=\dfrac{-m\alpha_{s-1}-s\beta_{s-1}}{s(m^2+s^2)}$

$$\gamma_0=0,\quad \delta_0=1,\quad \gamma_s=\frac{m\delta_{s-1}-s\gamma_{s-1}}{s(m^2+s^2)}\ ,\quad \delta_s=\frac{-m\gamma_{s-1}-s\delta_{s-1}}{s(m^2+s^2)}\ .$$

3. Determination of the Buckling Thrust

E_0, E_1 and F_1 must be chosen to satisfy the boundary conditions at $r=at$, namely, ϕ, M_r and Q are continuous. Since, however, N_r is continuous at $r=at$,

equation (2) shows that there are only two independent boundary conditions. The condition that ϕ is continuous at $r=at$ gives

$$E_0 J_1(k_0 at) = E_1 U(k_1 at) + F_1 V(k_1 at) \quad . \quad . \quad . \quad . \quad (4)$$

and the condition that M_r is continuous at $r=at$ gives

$$D_0 E_0 \left[k_0 J_1'(k_0 at) + \frac{\sigma}{at} J_1(k_0 at) \right] = D_1 \left[E_1 \left\{ k_1 U'(k_1 at) + \frac{\sigma}{at} U(k_1 at) \right\} + F_1 \left\{ k_1 V'(k_1 at) + \frac{\sigma}{at} V(k_1 at) \right\} \right], \quad (5)$$

primes (′) denoting differentiation.

Using equation (4), equation (5) may be written

$$E_0 \left[k_0 p^3 J_1'(k_0 at) + \frac{\sigma}{at}(p^3 - 1) J_1(k_0 at) \right] = E_1 k_1 U'(k_1 at) + F_1 k_1 V'(k_1 at). \quad (6)$$

The boundary condition satisfied at $r=a$ is that $\phi=0$ or $M_r=0$, according as the plate is clamped or simply-supported.

$$i.e. \quad E_1 U(k_1 a) + F_1 V(k_1 a) = 0 \quad \text{(plate clamped)} \quad . \quad . \quad . \quad (7)$$

or

$$E_1 \left[k_1 U'(k_1 a) + \frac{\sigma}{a} U(k_1 a) \right] + F_1 \left[k_1 V'(k_1 a) + \frac{\sigma}{a} V(k_1 a) \right] = 0 \text{ (plate simply-supported).} \quad . \quad . \quad . \quad (8)$$

Eliminating E_0, E_1, F_1 between equations (4), (6) and (7) or (8) gives the equation

$$\begin{vmatrix} J_1(k_0 at) & U(k_1 at) & V(k_1 at) \\ k_0 at p^3 J_1'(k_0 at) + \sigma(p^3 - 1) J_1(k_0 at) & k_1 at U'(k_1 at) & k_1 V'(k_1 at) \\ 0 & \mu k_1 a U'(k_1 a) + \sigma U(k_1 a) & \mu k_1 a V'(k_1 a) + \sigma V(k_1 a) \end{vmatrix} = 0 \quad (9)$$

where $\mu=0$ or 1 according as the plate is clamped or simply-supported and k_0, k_1 and q_1 are determined by equation (1), namely,

$$\frac{p^2 k_0^2}{2} = \frac{k_1^2}{2p - (1-\sigma)(p-1)} = \frac{(1-q_1)}{a^2 t^2 (1-\sigma)(p-1)} = \frac{T}{D_1 [2p - (1-\sigma)(p-1)(1-t^2)]}.$$

The least positive root of equation (9) is T_{cr}, the critical value of T for buckling.

Now the critical buckling thrust $\overline{T}$ for a uniform plate of radius a and thickness h, is

$$\frac{\lambda E h^3}{12(1-\sigma^2) a^2},$$

where $\lambda = 14{\cdot}68$ or $4{\cdot}28$ according as the plate is clamped or simply-supported.

TABLE I

VALUES OF S FOR CLAMPED PLATE (FOR A UNIFORM PLATE, $S=14{\cdot}68$)

	$t=0{\cdot}03$	0·1	0·2	0·3	0·4	0·45	0·5	0·55	0·6	0·7	0·8	0·9	0·97
$p=0{\cdot}3$	14·58	13·71	12·04		5·47				3·82		4·65	6·88	11·05
0·4					9·14								
0·5	14·59	13·84	12·42	11·69	11·27		10·36		9·48		9·61	11·12	13·28
0·6					12·07							12·60	13·89
0·7	14·64	14·21	13·24		12·63				13·21		13·25	13·66	
0·9	14·66	14·56	14·25		13·94				14·35	14·57	14·66	14·66	
1·1	14·68	14·77	15·00		15·39	15·37		15·16	15·00		14·43	14·45	
1·3					16·49	16·55	16·45	16·16	15·71			13·53	
1·4						16·94	16·88	16·58	16·06			12·96	
1·5	14·70	14·91	15·49		16·94	17·15	17·16	16·91	16·38		12·99	12·39	
1·6					16·93	17·19	17·28	17·12	16·60				
1·7					16·79	17·07	17·24	17·16					
1·8					16·54	16·83	17·04	17·05	16·72				
1·9					16·23		16·70	16·79					
2·0	14·69	14·83	15·13		15·85	16·07	16·27	16·40	16·32	14·85	12·03	10·09	11·32
3·0	14·66	14·45	13·73		11·58		10·80		10·62	11·22	11·11	8·26	7·87

TABLE II

VALUES OF S FOR SIMPLY-SUPPORTED PLATE (FOR A UNIFORM PLATE, $S=4{\cdot}28$)

	$t=0{\cdot}03$	0·2	0·4	0·6	0·7	0·75	0·8	0·85	0·9	0·97
$p=0{\cdot}3$	4·27	3·71	3·05	2·72			3·13			
0·5	4·27	3·78	3·14	2·96			3·27			4·08
0·7	4·28	3·99	3·53	3·34			3·55		3·84	4·13
0·8									3·98	
0·9							4·03			
1·1	4·29	4·34	4·47	4·58	4·58		4·53		4·42	
1·3				5·01	5·07		4·96		4·67	4·40
1·5	4·29	4·39	4·70	5·17	5·35	5·36	5·29		4·88	4·47
1·6				5·15	5·41		5·41			
1·7				5·07	5·40	5·50	5·49	5·33		4·52
1·8				4·95	5·34	5·49	5·53	5·40		
1·9				4·79			5·54			
2·0	4·28	4·26	4·25	4·61	5·07	5·33	5·52	5·49	5·21	4·57
2·2								5·49		
2·5				3·60	4·01		4·89	5·33	5·33	
3·0	4·27	3·86	3·07	2·74	2·98		3·85	4·64	5·22	4·69

For comparison with $\overline{T}$ it is convenient to write

$$T_{cr} = \frac{SEh^3}{12(1-\sigma^2)a^2} \text{ and evaluate } S.$$

For given values of t and p, equation (9) can be solved by trial and error. The value of t lies between 0 and 1, the extreme values of t corresponding to a uniform plate for all values of p. The main features of the variation of S with t and p can be seen by considering values of p in the range $0 < p \leqslant 3$. Tables I and II show the results of the calculations for selected values of t and p.

In Tables I and II, the heavy line separates the calculations for which the Bessel function expansions are used (above the line) from the calculations requiring the other expansions (below the line). From the tables, $S_{max} = 17{\cdot}28$ occurring for $t = 0{\cdot}5$ and $p = 1{\cdot}6$ (clamped plate) and $S_{max} = 5{\cdot}54$ occurring for $t = 0{\cdot}8$ and $p = 1{\cdot}9$ (simply-supported plate), so that resistance to buckling by redistribution of the material forming a uniform plate can be increased by about 18 per cent or 29 per cent, according as the plate is clamped or simply-supported.

ACKNOWLEDGMENTS

The authors are glad to take the opportunity of expressing their gratitude to Imperial Chemical Industries Limited for computing facilities made available on the Mercury computer at Wilton, and to Dr. G. E. Thomas, the manager of the computer section there. The authors are also very grateful to Mr. P. T. Daniel and Mr. R. C. Williams for assistance in running programmes.

REFERENCES

1. BRYAN, G. H. On the Stability of a Plane Plate under Thrusts in its own Plane, with Applications to the Buckling of the Sides of a Ship. *Proceedings of the London Mathematical Society*, Vol. XXII, 1890-91.

2. TIMOSHENKO, S. *Theory of Elastic Stability*. McGraw-Hill, New York, 1936.

3. MEISSNER, E. Uber das Knicken Kreisringförmingen Scheiben. *Schweizerische Bauzeitung*, Band 101, 1933.

4. OLSSON, R. G. Knickung der Kreisringplatte von quadratisch veränderlicher Steifigkeit. *Ingenieur Archiv*, Band IX, p. 205, 1938.

5. CAPEY, E. C. The Buckling under Longitudinal Compression of a Simply Supported Panel that Changes in Thickness across the Width. A.R.C. Current Paper 235, 1956.

The Non-steady Irrotational Flow of an Inviscid, Incompressible Fluid, with Special Reference to Changes in Total Pressure through Flow Machines

J. H. PRESTON

(Department of Fluid Mechanics, University of Liverpool)

SUMMARY: In this paper the way in which an inviscid incompressible fluid changes its total pressure is discussed. The basic equations are set out and it is shown that changes in total pressure are essentially associated with time variable flows. Simple examples are worked to illustrate this and finally application is made to single-stage flow machines, using a simple vortex representation.

1. Introduction

Dean[1] has demonstrated that the frictionless flow through a flow machine, doing work or having work done on it by the fluid, must be unsteady. A little consideration shows that almost all practically useful flow machines exhibit this characteristic. As an example, consider a single-stage axial-flow machine such as a fan. The forces on the blades forming the fan do work on the fluid as it passes through the fan; this appears as a rise in total pressure of the fluid. The forces on the blades give rise to pressure differences on the two surfaces of the blades and in the spaces between the blades, and consequently there are associated variations in velocity. To an observer situated on the blade, the motion would appear to be steady; but to an observer at rest and near to the fan disc, the motion would appear to be unsteady and periodic, with variations in total and static pressure and in velocity and its direction. A simplified equivalent of the fan is the two-dimensional, infinite, moving row of aerofoils. If the whole system is given an equal, but opposite, velocity to that of the moving row, then the row is reduced to rest, becoming a fixed cascade of aerofoils, and the motion is steady. This is the basis of cascade testing and of calculating the forces and pressure distributions on the aerofoils. Since the aerofoils are at rest, they do no work and the total pressure is constant throughout the field of flow. If, at a fixed point near a moving cascade, information about the fluctuations in total pressure, velocity, and so on is required, then further investigation is necessary. So far as the author is aware this has not been previously attempted and in the past has been deliberately avoided by use of the concept of an actuator disc.

Received May 1961.

In this paper the basic equations for the unsteady irrotational motion of an inviscid incompressible fluid are set out. Simple, illustrative applications of these are made (*a*) to the problem of the flow along a long pipe connected to a large reservoir when a valve is suddenly opened and (*b*) to the fluctuations in total pressure at a point when a vortex or a doublet are in uniform motion past this point. The calculations are then extended to an infinite moving row of bound vortices and the variation of total pressure with time at a fixed point is obtained. This gives a simplified picture of the total pressure changes through an axial flow fan. The problem of a single-stage radial-flow machine is similarly approximated by a rotating ring of equally spaced bound vortices and the solution for the infinite straight row of vortices can be extended to this problem by a simple conformal transformation. Calculations have also been made for a moving row of doublets to indicate the effect of aerofoil thickness. The actuator disc concept is examined on the basis of the total pressure fluctuations. Also, interaction of the fixed and moving stages in a compressor is briefly discussed. A short discussion is also given of the significance of the results in relation to the design and calibration of instruments for measuring total pressure, static pressure, velocity and flow direction in tests on flow machines.

NOTATION

q resultant velocity

s distance measured along a streamline

D/Dt differentiation following a fluid element

t time

p static pressure

P total pressure

ρ density (constant)

g acceleration due to gravity

z height above some datum

ϕ velocity potential

P_0 datum value of P in time-variable flows

H height of fluid in reservoir

L length of pipe

U velocity of flow in pipe (in Section 3.1 only)

p_0 atmospheric pressure

P_E total pressure at pipe exit

W potential function

$z = x + iy$, complex co-ordinate

Γ strength of bound vortex (circulation)

u, v velocity components

$2\pi\nu$ strength of doublet

U velocity in x-direction of moving vortex or doublet

V velocity in y-direction at infinity

L_x x-component of force on bound vortex

L_y y-component of force on bound vortex

h pitch of vortices or doublets in a row

n number of vortices

P_1 total pressure at $y=-\infty$

P_2 total pressure at $y=+\infty$

U_1 x-velocity component at $y=-\infty$

U_2 x-velocity component at $y=+\infty$

$\Delta P=P_2-P_1$

Ω angular velocity of rotating ring of vortices

a radius of ring

L_θ force component in circumferential (θ) direction

m source strength

v_a radial component of velocity at radius a

$\left.\begin{aligned}\zeta&=\xi+i\eta\\&=\mu+i\theta\\&=a\end{aligned}\right\}$ complex co-ordinate in plane of ring of vortices

$2X$ length on real axis of z-plane representing perimeter of circle radius a in ζ-plane.

— bar, denoting time average over a cycle

2. Basic Theory

Consider the motion of a fluid element along a streamline. Denote differentiations following the fluid element by D/Dt; then, if q is the velocity and s is measured along the streamline,

$$\frac{D}{Dt}=\frac{\partial}{\partial t}+q\frac{\partial}{\partial s}. \quad . \quad . \quad . \quad . \quad . \quad . \quad (1)$$

Denote the total pressure by P, then

$$P=p+\tfrac{1}{2}\rho q^2+\rho gz, \quad . \quad . \quad . \quad . \quad . \quad (2)$$

where p is the static pressure, ρ is the density and z is the height of the element above some datum.

The equation of motion along the streamline is

$$\frac{\partial q}{\partial t}+\frac{1}{\rho}\frac{\partial P}{\partial s}=0. \qquad (3)$$

This will form the basis of the subsequent calculations. The change of total pressure of a fluid element is

$$\frac{DP}{Dt}=\frac{\partial P}{\partial t}+q\frac{\partial P}{\partial s}$$
$$=\frac{\partial}{\partial t}(p+\rho gz)+\rho q\left(\frac{\partial q}{\partial t}+\frac{1}{\rho}\frac{\partial P}{\partial s}\right).$$

The second bracket term is zero, from (3).

$$\text{Hence}\quad \frac{DP}{Dt}=\frac{\partial}{\partial t}(p+\rho gz)$$
$$=\frac{\partial p}{\partial t} \qquad (4)$$

Hence the total pressure P of a fluid element only varies with the time if the static pressure at a fixed point varies with the time. Since the purpose of a flow machine is to give or abstract total pressure to or from the fluid, the motion relative to a fixed point must be unsteady.

The result in equation (4) is contained in a similar result for stagnation enthalpy derived by Dean[1] and it is apparently given in a book by Eck[2].

Returning to equation (3), since the motion is irrotational a velocity potential ϕ exists and

$$q=\frac{\partial \phi}{\partial s}, \qquad (5)$$

whence, integrating (3) along a streamline,

$$\frac{\partial \phi}{\partial t}+\frac{P}{\rho}=f(t). \qquad (6)$$

This equation is given in Lamb's *Hydrodynamics*[3] (paragraph 20).

3. Applications of the Theory

3.1. Long Uniform Pipe Connected to a Large Reservoir. Sudden Opening of Valve at End of Pipe

This is a textbook example but it is given here to show the part which acceleration plays in determining the total pressure.

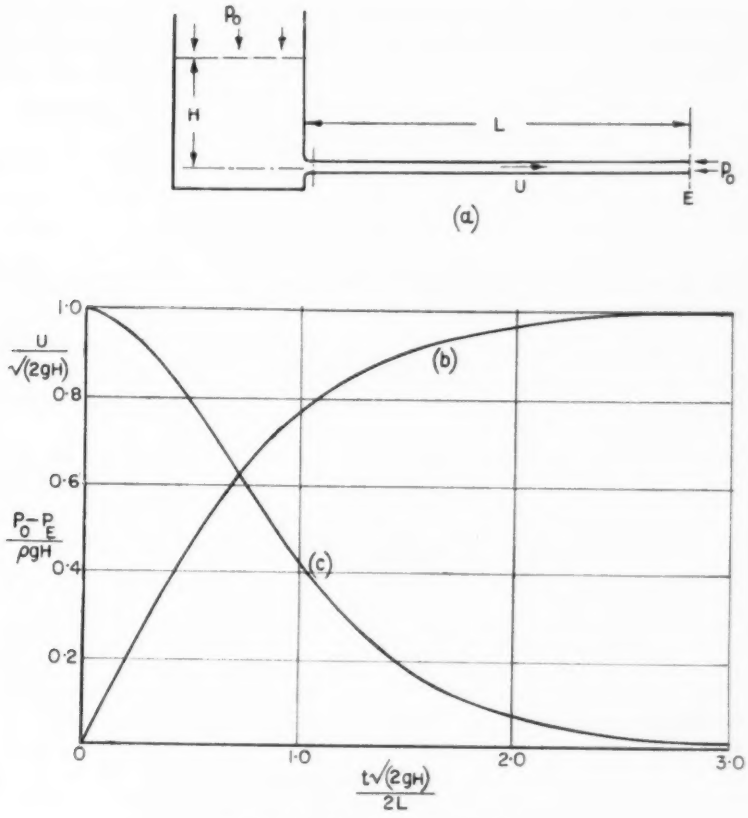

FIGURE 1. Flow from a reservoir.
(*a*) Notation.
(*b*) Velocity against time (equation (10)).
(*c*) Loss of total pressure against time (equation (11)).

The level of the liquid in the reservoir above the axis of the pipe is denoted by H and is assumed to remain constant (*see* Fig. 1(*a*)).

Equation (6) therefore becomes

$$\frac{\partial \phi}{\partial t} + \frac{P}{\rho} = \text{constant} = \frac{P_0}{\rho}, \qquad (7)$$

which holds throughout the fluid, since the motion is irrotational and the fluid is at rest in the reservoir. Denote the length of pipe by L, the velocity in the pipe by U and atmospheric pressure by p_0, which is applied at the reservoir surface and at the pipe exit after the valve opens. Contributions to ϕ in the neighbourhood of the

pipe entry are neglected and the value of ϕ there is taken to be zero. Applying (7) to stations at the entry and exit of the pipe, we have, if p_1 is the pressure just inside the entry,

$$p_1 + \tfrac{1}{2}\rho U^2 = p_0 + \tfrac{1}{2}\rho U^2 + \rho \frac{\partial}{\partial t}\int_0^L U\,dx,$$

giving

$$p_1 - p_0 = \rho L \frac{dU}{dt}, \qquad (8)$$

which is the equation of motion for the fluid in the pipe. Between the pipe entry and the reservoir surface, ϕ, and hence $\partial\phi/\partial t$, is negligible and so

$$p_1 + \tfrac{1}{2}\rho U^2 = p_0 + \rho g H, \qquad (9)$$

whence (8) becomes

$$\rho g H - \tfrac{1}{2}\rho U^2 = \rho L \frac{dU}{dt}$$

$$\text{or} \quad dt = 2L \frac{dU}{2gH - U^2}$$

$$\text{and} \quad t = \frac{2L}{\sqrt{(2gH)}} \tanh^{-1} \frac{U}{\sqrt{(2gH)}} + C.$$

The condition $t=0$, $U=0$ gives $C=0$

$$\text{and} \quad \frac{U}{\sqrt{(2gH)}} = \tanh\left(\frac{t\sqrt{(2gH)}}{2L}\right) \qquad (10)$$

This is shown plotted in Fig. 1(*b*), where it is seen that U rises from $U=0$, $t=0$ to $U=\sqrt{(2gH)}$, $t=\infty$.

Denote the total pressure at the reservoir surface by P_0 and at the pipe exit by P_E then

$$P_0 - P_E = p_1 - p_0 = \rho g H - \rho \frac{U^2}{2}$$

$$\text{or} \quad \frac{P_0 - P_E}{\rho g H} = 1 - \frac{U^2}{2gH} = \operatorname{sech}^2\left(\frac{t\sqrt{(2gH)}}{2L}\right). \qquad (11)$$

This is shown plotted on Fig. 1(*c*). It will be noted that, at $t=0$, $U=0$, $P_0 - P_E = \rho g H$, so that the available head H is used in accelerating the fluid in the pipe from rest. At $t=\infty$, $U=\sqrt{(2gH)}$ and $(P_0 - P_E)=0$, since the motion has now become steady.

If the level of the reservoir falls perceptibly or is controlled in some way as a function of the time, then the "constant" of equation (7) must be replaced by the appropriate function of the time.

One further point is worthy of note:—

$$p_1 - p_0 = \rho L \frac{dU}{dt}. \quad . \quad . \quad . \quad . \quad . \quad (8)$$

Hence

$$\int_0^t (p_1 - p_0)\, dt = \rho L\, U(t). \quad . \quad . \quad . \quad . \quad . \quad (12)$$

Hence the "pressure-time" integral will yield the velocity or mass flow. Practical use is made of this in the Gibson method of determining the mass flow through the penstock of a hydraulic turbine installation.

4. Vortex Moving Past a Fixed Point

$$\left.\begin{aligned} W = \phi + i\psi &= \frac{-i\Gamma}{2\pi} \log z, \\ z &= x + iy, \end{aligned}\right\} \quad . \quad . \quad . \quad . \quad (13)$$

gives the potential for a stationary vortex at the origin.

$$\left.\begin{aligned} \phi &= \frac{\Gamma}{2\pi}\,\theta \\ \theta &= \tan^{-1}(y/x) \end{aligned}\right\} \quad . \quad . \quad . \quad . \quad . \quad . \quad (14)$$

Suppose the vortex is in steady motion with velocity $-U$ parallel to the x-axis. Then the co-ordinates of a fixed point relative to the vortex are $x = Ut$ and y,

and

$$\frac{\partial \phi}{\partial t} = U \frac{\partial \phi}{\partial x} = Uu. \quad . \quad . \quad . \quad . \quad . \quad (15)$$

Now

$$u - iv = \frac{dW}{dz},$$

whence, with $x = Ut$,

$$u = -\frac{\Gamma}{2\pi} \frac{y}{(Ut)^2 + y^2}, \quad . \quad . \quad . \quad . \quad . \quad (16)$$

$$v = \frac{\Gamma}{2\pi} \frac{x}{(Ut)^2 + y^2}. \quad . \quad . \quad . \quad . \quad . \quad (17)$$

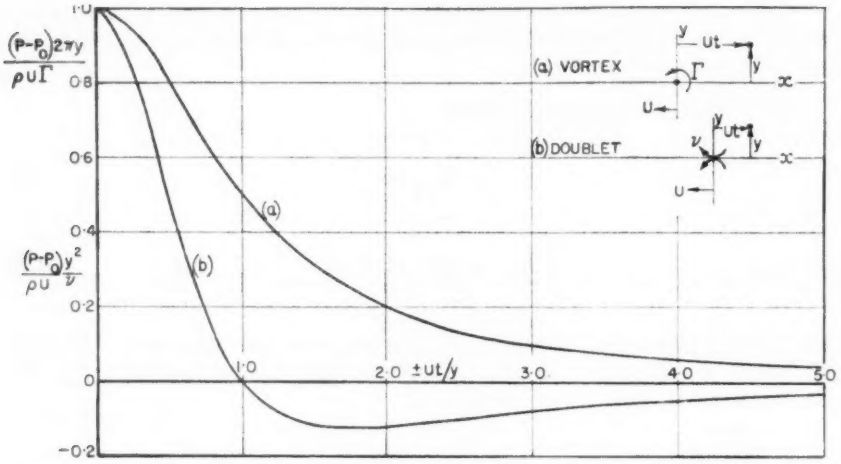

FIGURE 2. Uniform motion of vortex and doublet pass a fixed point. Change of total pressure with time.
(*a*) Vortex (equation (19)).
(*b*) Doublet (equation (23)).

Equation (6) may be written

$$\rho \frac{\partial \phi}{\partial t} + P = \text{constant} = P_0, \quad . \quad . \quad . \quad . \quad . \quad (18)$$

since the motion is irrotational and at rest at infinity. Hence, using (15) and (16),

$$P_0 - P = -\frac{\rho U \Gamma}{2\pi} \frac{y}{(Ut)^2 + y^2}$$

or

$$\frac{(P - P_0)}{\rho U \Gamma} 2\pi y = \frac{1}{1 + (Ut/y)^2} \quad . \quad . \quad . \quad . \quad . \quad (19)$$

This is shown plotted in Fig. 2(*a*). The velocities are given by (16) and (17), so that the direction of the velocity vector and the static pressure can be found as functions of the time.

5. Doublet Moving Past a Fixed Point

For a stationary doublet of strength $2\pi\nu$ with its axis parallel to the x-axis

$$W = \phi + i\psi = \frac{\nu}{z} \; ; \quad . \quad . \quad . \quad . \quad . \quad (20)$$

$$\text{also} \qquad u = -\nu \frac{(x^2-y^2)}{(x^2+y^2)^2} \quad . \quad . \quad . \quad . \quad . \quad (21)$$

$$v = -\nu \frac{2xy}{(x^2+y^2)^2} \quad . \quad . \quad . \quad . \quad . \quad (22)$$

For a doublet of strength $2\pi\nu$ moving with a velocity $-U$ parallel to the x-axis (which is the same as a circular cylinder of radius $\sqrt{(\nu/U)}$ moving with this velocity),

$$x = Ut$$

and, from equations (15), (18) and (21),

$$P - P_0 = -\rho \frac{\partial \phi}{\partial t} = \frac{\rho U \nu}{y^2} \frac{(Ut/y)^2 - 1}{\{(Ut/y)^2+1\}^2}$$

or

$$\frac{(P-P_0)}{\rho U} \frac{y^2}{\nu} = \frac{(Ut/y)^2-1}{\{(Ut/y)^2+1\}^2} \quad . \quad . \quad . \quad . \quad (23)$$

This is shown plotted on Fig. 2(*b*).

6. Moving Row of Bound Vortices

Consider first the flow arising from a fixed row of vortices (Fig. 3(*a*)). Let the vortices lie along the x-axis with a spacing h and a circulation Γ in the anticlockwise direction.

The velocity potential W (Lamb[3] paragraph 156, or by use of the transformation (37)) for the vortices only is

$$W = -\frac{i\Gamma}{2\pi} \log \sin\left(\frac{\pi z}{h}\right) \quad . \quad . \quad . \quad . \quad . \quad (24)$$

and the velocity components are

$$u = \frac{-\Gamma}{2h} \frac{\sinh(2\pi y/h)}{\cosh(2\pi y/h) - \cos(2\pi x/h)} \quad . \quad . \quad . \quad (25)$$

$$\text{and} \quad v = \frac{\Gamma}{2h} \frac{\sin(2\pi x/h)}{\cosh(2\pi y/h) - \cos(2\pi x/h)} \quad . \quad . \quad (26)$$

Consider now conditions at a *fixed* point when the row is in motion. Then, relative to instantaneous axes moving with the row, the fixed point has co-ordinates

$$x = Ut \quad \text{and} \quad y,$$

which, inserted in equations (25) and (26), give u and v at the point.

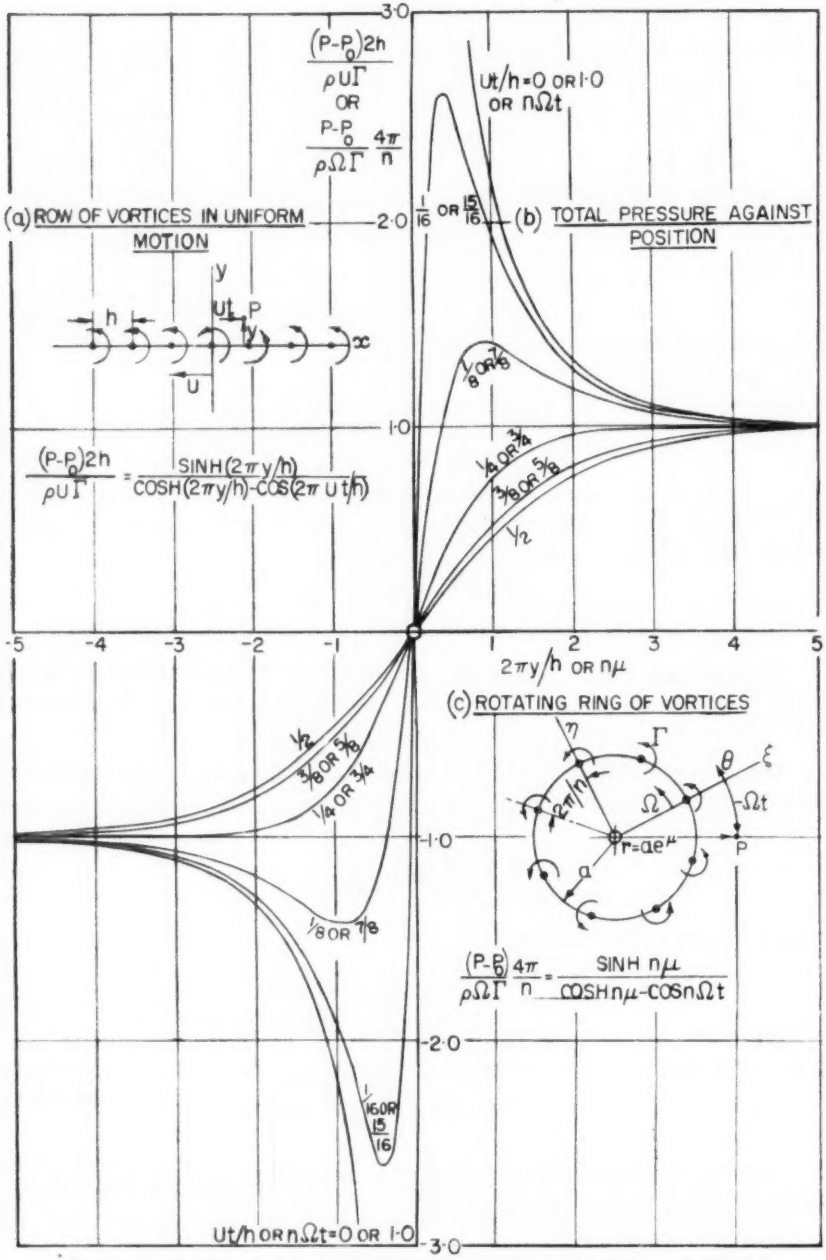
(P-P0)2h / ρUΓ OR P-P0 / ρΩΓ 4π/n
Ut/h=0 OR 1·0 OR nΩt
(a) ROW OF VORTICES IN UNIFORM MOTION
(b) TOTAL PRESSURE AGAINST POSITION
1/16 OR 15/16
1/8 OR 7/8
1/4 OR 3/4
3/8 OR 5/8
1/2
(P-P0)2h / ρUΓ = SINH(2πy/h) / COSH(2πy/h)-COS(2πUt/h)
2πy/h OR nμ
(c) ROTATING RING OF VORTICES
r=ae^μ
(P-P0) 4π/n / ρΩΓ = SINH nμ / COSH nμ-COS nΩt
Ut/h OR nΩt=0 OR 1·0

FIGURE 3. Vortex row or vortex ring in uniform motion. Total pressure changes.
(*a*) Row of vortices in uniform motion.
(*b*) Total pressure against position.
(*c*) Rotating ring of vortices.

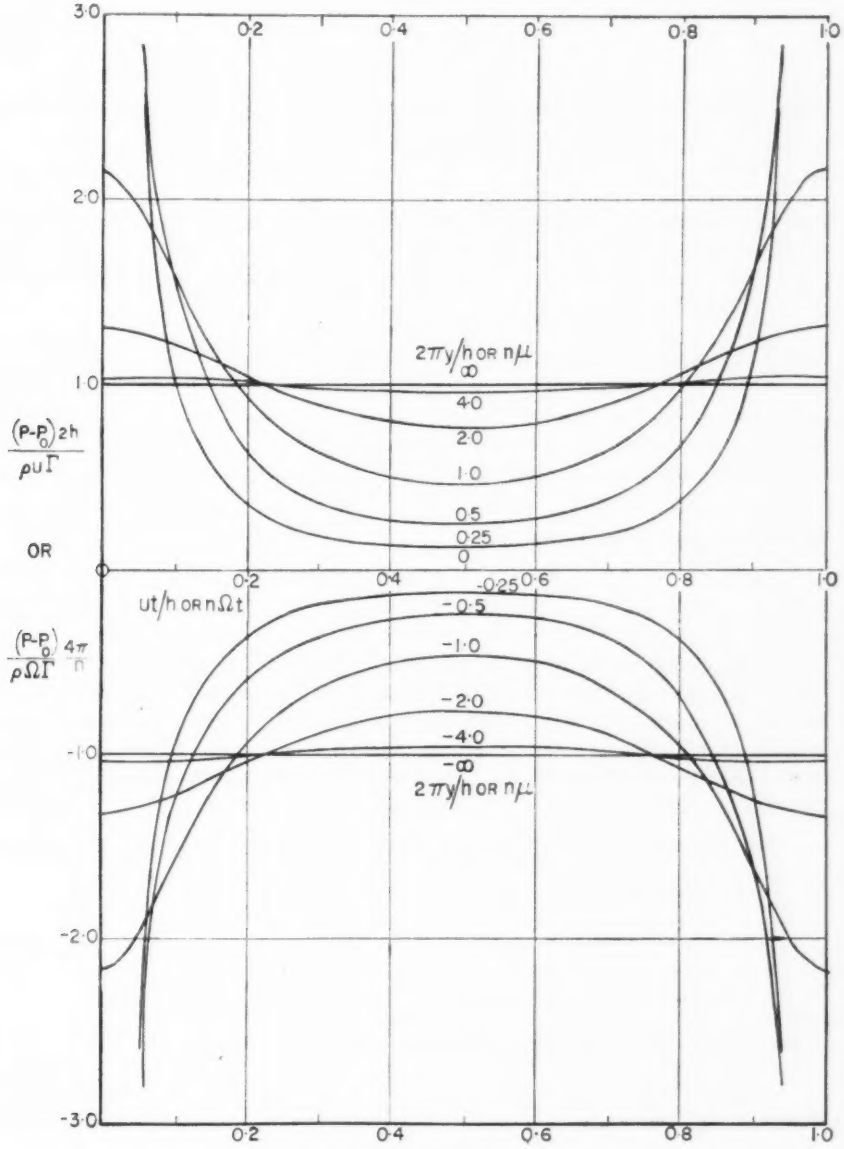

FIGURE 3(*d*). Total pressure against time.

To calculate the changes in total pressure, we use equation (6) in the form

$$\rho \frac{\partial \phi}{\partial t} + P = \text{constant} = P_0, \quad . \quad . \quad . \quad . \quad . \quad . \quad (27)$$

since the motion is irrotational and steady at $y = \pm\infty$.

With $x = Ut$ and using equation (25),

$$P_0 - P = \rho \frac{\partial \phi}{\partial t} = \rho U u$$

$$= \frac{-\rho U \Gamma}{2h} \frac{\sinh(2\pi y/h)}{\cosh(2\pi y/h) - \cos(2\pi Ut/h)} \quad . \quad (28)$$

For $y = -\infty$ and $y = +\infty$ respectively the total pressures are

$$\left.\begin{aligned} P = P_1 &= P_0 - \frac{\rho U \Gamma}{2h} \\ P = P_2 &= P_0 + \frac{\rho U \Gamma}{2h} \end{aligned}\right\}, \quad . \quad . \quad . \quad . \quad . \quad (29)$$

so that the gain in total pressure is

$$\Delta P = P_2 - P_1 = \frac{\rho U \Gamma}{h} \quad . \quad . \quad . \quad . \quad . \quad (30)$$

From equation (28), the variation in total pressure is given in Fig. 3(*b*), where $2h(P - P_0)/\rho U\Gamma$ has been plotted as a function of $2\pi y/h$ for a range of values of Ut/h. It may be noted that the fluctuations in total pressure have practically vanished at $y/h = 1{\cdot}0$ and amount to 10 per cent of the total pressure change through the row at $y/h = \frac{1}{2}$. A cross-plotting in Fig. 3(*d*) shows the variation through the cycle $0 < Ut/h < 1{\cdot}0$ at constant values of $2\pi y/h$.

The average value of $(P - P_0)$ over a cycle $(0 < Ut/h < 1{\cdot}0)$ can be computed.

From equation (27)

$$-\frac{\overline{(P - P_0)}}{\rho} = \overline{\frac{\partial \phi}{\partial t}} = \frac{1}{T} \int_0^T \frac{\partial \phi}{\partial t}\, dt,$$

where the bar denotes the mean value over a time $T = h/U$.

Hence $$-\frac{\overline{(P - P_0)}}{\rho} = \frac{\phi_T - \phi_0}{T} = \frac{(\phi)_{Ut/h=1} - (\phi)_{Ut/h=0}}{h/U} \quad . \quad . \quad . \quad (31)$$

From equation (24) it is readily found that

$$\phi = \frac{\Gamma}{2\pi} \tan^{-1}[(\cot(\pi Ut/h) \tanh(\pi y/h)]. \quad . \quad . \quad . \quad (32)$$

Hence, for y positive,

$$\left.\begin{aligned}\frac{(\overline{P-P_0})}{\rho} &= \frac{\Gamma U}{2h}\\ \text{and for } y \text{ negative,}\qquad \frac{(\overline{P-P_0})}{\rho} &= -\frac{\Gamma U}{2h}\end{aligned}\right\} \quad . \quad . \quad . \quad . \quad . \quad . \quad (33)$$

So that the average value of $(P-P_0)$ is independent of y on either side of the vortex row, but it changes discontinuously through the row by $\Gamma U/h$, thus substantiating the actuator disc hypothesis.

7. Rotating Ring of Bound Vortices

n bound vortices of strength Γ are disposed at equal angular intervals at a radius a and rotate with angular velocity Ω (*see* Fig. 3(*c*)). There is a radial flow through the rotor which can be represented by a source of strength m at the origin.

The rate of doing work by the rotor is

$$\Omega \times \text{opposing torque} = \Omega \times -n L_\theta a,$$

where L_θ is the force on the vortex in the direction of θ positive,

$$L_\theta = -\rho \frac{m}{2\pi a} \Gamma = -\rho v_a \Gamma, \quad . \quad . \quad . \quad . \quad . \quad (34)$$

where v_a is the radial component of velocity at $r=a$. Hence the rate of doing work equals

$$\Omega \times n \left(\frac{\rho m \Gamma}{2\pi}\right).$$

This must equal the rate at which the fluid gains total pressure (ΔP), *i.e.* $\Delta P m$.

$$\text{Hence} \quad \Delta P = \frac{n\rho\Omega\Gamma}{2\pi} \quad . \quad . \quad . \quad . \quad . \quad (35)$$

From equation (31),

$$P - P_0 = -\rho \frac{\partial \phi}{\partial t} \quad . \quad . \quad . \quad . \quad . \quad (36)$$

so that it is necessary to determine ϕ for a stationary ring of vortices.

This is done by transforming conformally the ring of vortices into an infinite row of vortices.

$$\text{Take} \quad \zeta = a\, e^{i\pi z}/X \qquad . \quad . \quad . \quad . \quad . \quad (37)$$

where $\zeta = \xi + i\eta$ is the plane of the ring and $z = x + iy$ is the plane of the row.

$$\text{Putting} \quad \zeta = a\, e^{\mu + i\theta}, \qquad . \quad . \quad . \quad . \quad . \quad (38)$$

$$\text{so that} \quad r = \sqrt{(\xi^2 + \eta^2)} = a\, e^{\mu},$$

$$\left.\begin{aligned} \text{then} \quad \mu &= -\pi y/X \\ \theta &= \pi x/X \end{aligned}\right\} \qquad . \quad . \quad . \quad . \quad . \quad (39)$$

A strip of width $2X$, stretching from $y = -\infty$ in the z-plane, maps into the whole of the ζ-plane and, in particular, the portion of the x-axis $0 < x < 2X$ corresponds to the full circle radius a and $0 < \theta < 2\pi$. Also, the vortices which are disposed at equal intervals of $\theta = 2\pi/n$ on the circle $r = a$ ($\mu = 0$) in the ζ-plane correspond to equally spaced vortices (pitch h) on the x-axis in the z-plane.

$$\text{Using equation (39),} \quad \frac{2\pi}{n} = \frac{\pi h}{X},$$

$$\text{so that} \quad \frac{h}{2X} = \frac{1}{n} \; . \qquad . \quad . \quad . \quad . \quad . \quad (40)$$

Since successive strips of width $2X$ in the z-plane map into similar successive sheets in the ζ-plane, we have therefore transformed a ring of vortices in the ζ-plane into an infinite row of vortices on the x-axis in the z-plane for which, from (24),

$$W = \phi + i\psi = -\frac{i\Gamma}{2\pi} \log \sin \frac{\pi z}{h} \; .$$

It therefore follows that the values of ϕ are the same at corresponding points in the two planes.

When the ring of vortices rotates with angular velocity Ω, then, for a fixed point on the ξ-axis, the co-ordinates relative to the rotating system are μ and $\theta = -\Omega t$; but, from (39),

$$\mu = -\pi y/X$$
$$\theta = \pi x/X$$

and, with $x = Ut$,

$$\Omega = -\pi \frac{U}{X} \; . \qquad . \quad . \quad . \quad . \quad . \quad (41)$$

Using relations (39), (40), and (41), the value of $\partial\phi/\partial t$ (which is the same at corresponding points) can be found from equation (25) for the moving row of vortices and thus

$$P - P_0 = -\frac{\rho\partial\phi}{\partial t}$$

$$= \frac{n\rho\Gamma\Omega}{4\pi}\,\frac{\sinh n\mu}{\cosh n\mu - \cos n\Omega t},$$

$$\text{or} \qquad \frac{(P-P_0)\,4\pi}{\rho\Gamma\Omega\ n} = \frac{\sinh n\mu}{\cosh n\mu - \cos n\Omega t}, \qquad (42)$$

which has the same form as equation (25) and so the Figs. 3(*b*) and 3(*d*) still apply with appropriate change of variables. The change in total pressure from ($\mu=\infty$, $r=0$) to ($\mu=+\infty$, $r=\infty$) is

$$\Delta P = \frac{n}{2\pi}\,\rho\Gamma\Omega,$$

which is identical with equation (35).

8. Moving Row of Doublets

To complete the picture the calculations are now made for a moving row of doublets which give a first approximation to the effects of thickness. Since there is no force on the doublets they do no work and so there is no net gain of total pressure across the row.

The velocity potential W for a row of doublets of strength ν and pitch h situated on the x-axis with their axes parallel to the x-axis can be obtained by differentiating equation (24) or using the transformation (37) to transform a doublet and its image in the half ζ-plane into an infinite row in the z-plane.

$$W = \frac{\pi\nu}{h}\cot(\pi z/h). \qquad (43)$$

This yields

$$\phi = \frac{\pi\nu}{h}\,\frac{\sin(2\pi x/h)}{[\cosh(2\pi y/h) - \cos(2\pi x/h)]}, \qquad (44)$$

$$u = -2\nu\left(\frac{\pi}{h}\right)^2 \frac{[1-\cos(2\pi x/h)\cosh(2\pi y/h)]}{[\cosh(2\pi y/h) - \cos(2\pi x/h)]^2}, \qquad (45)$$

$$v = -2\nu\left(\frac{\pi}{h}\right)^2 \frac{\sin(2\pi x/h)\sinh(2\pi y/h)}{[\cosh(2\pi y/h) - \cos(2\pi x/h)]^2}. \qquad (46)$$

The variation in total pressure for a moving row is found as before by putting $x=Ut$. Then

$$P-P_0=-\rho\frac{\partial\phi}{\partial t}=-\rho Uu$$

which, using equation (45), yields

$$\frac{P-P_0}{\rho U^2}\frac{1}{2\pi^2}\frac{Uh^2}{\nu}=\frac{[1-\cos(2\pi Ut/h)\cosh(2\pi y/h)]}{[\cosh(2\pi y/h)-\cos(2\pi Ut/h)]^2} \quad . \quad . \quad (47)$$

This is shown plotted in Fig. 4.

Over a cycle $0<Ut/h<1{\cdot}0$, the average value of $\partial\phi/\partial t$ is, for the period $T=h/U$,

$$\overline{\frac{\partial\phi}{\partial t}}=[(\phi)_{Ut/h=1}-(\phi)_{Ut/h=0}]\frac{U}{h}$$

whence, using equation (44),

$$\overline{\frac{\partial\phi}{\partial t}}=0 \quad . \quad . \quad . \quad . \quad . \quad . \quad . \quad . \quad . \quad (48)$$

and the average value of the total pressure is P_0.

9. Concluding Remarks

The first example (Section 3.1) shows that, in the accelerating flow from a reservoir, the total pressure is not constant. The assumption of an incompressible fluid means that, on the opening of the valve, the pressure adjusts itself instantaneously along the pipe for a constant value of $(p_0+\rho gH)$ to a value varying linearly from $(p_0+\rho gH)$ at the inlet to p_0 at exit. In a real fluid the adjustment will take place over a finite time with a pressure wave travelling up the pipe at the speed of sound and with possible reflections at each end. The use of a pressure-time integral to obtain the mass flow may be noted. The time delay which occurs before steady mass flow conditions are reached after the sudden opening of a valve may have an application to the fuel control of aircraft engines. The set-up might possibly be used to check the response of instruments designed to measure total or static pressure.

The motions of a vortex and of a doublet (given in Sections 4 and 5) relative to a fixed point set up time variations in total pressure, static pressure and velocity at a fixed point. In combination they could be used to represent the effects of the passage of a lifting aerofoil of finite thickness as experienced by a distant point. Again, it is possible that the solutions might be of use in an experimental check of the response of measuring instruments.

Sections 6 and 7 are concerned with effects experienced at a fixed point caused by a moving row of bound vortices and a rotating ring of bound vortices. They

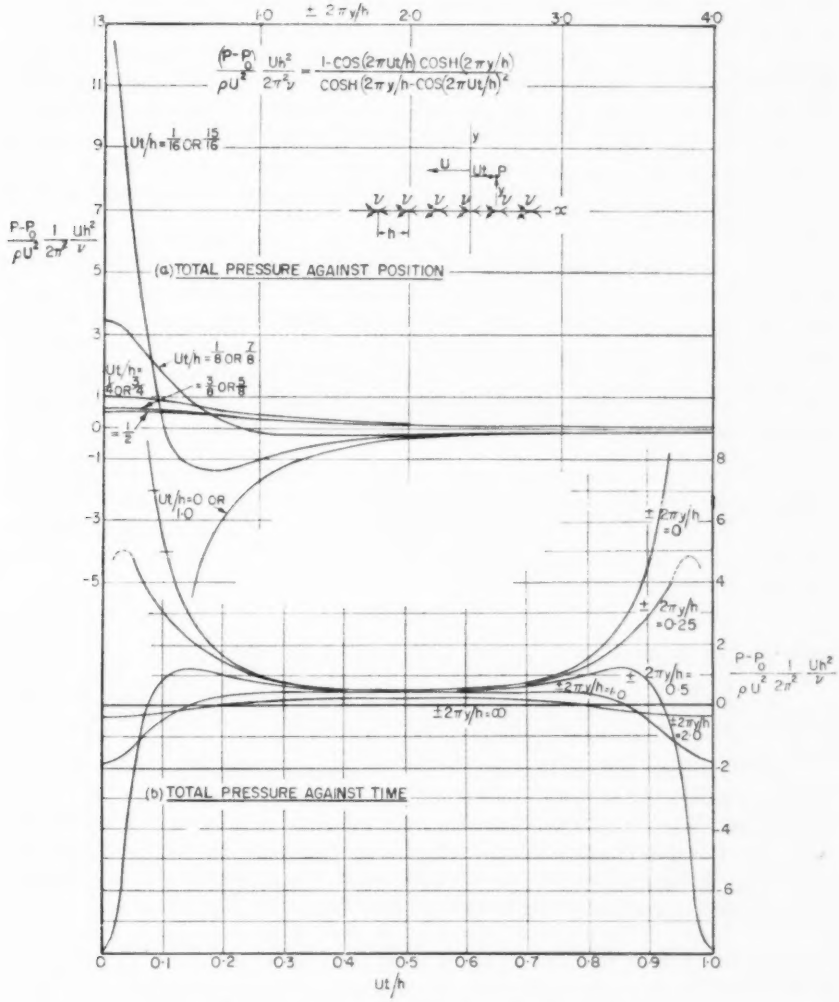

FIGURE 4. Row of doublets in uniform motion.
(*a*) Total pressure against position.
(*b*) Total pressure against time.

give a first approximation to the effects of the blades of single-stage, axial flow or radial flow machines. In both case the time variations in total pressure at a fixed point are entirely similar. The variation is periodic and is anti-symmetrical for equidistant points on either side of the moving row. The variations of total pressure close to the row are large, but fall away to steady values at large distances. At a distance about equal to the pitch of the vortices the fluctuation in total pressure is

less than 1 per cent of the total pressure rise through the row, and at half the pitch it is about 10 per cent. Since, in practice, the distance between the rotors and stators of an axial flow compressor is about half the pitch, instruments for measuring total pressure, and so on, will be situated at about a quarter of the pitch from the moving row. They will thus be subject, on the basis of the present theory, to considerable fluctuations, which may cause errors in the mean readings. It may be noted that the time average of the total pressure is constant on either side of the vortex row, but it changes discontinuously through the row, thus agreeing with the actuator disc concept.

If we consider a stator in front of or behind a rotor, then it will be subject to fluctuations in magnitude and direction of the velocity. Consequently the forces on the stator blades will change with time and free vortices will be shed downstream and thus the blades of the rotor will find themselves passing through a fluctuating flow field. A complex interaction will be set up between the stator and rotor, giving rise to fluctuating loads on both the stator and rotor blades, which may be of significance in relation to fatigue and flutter.

The present calculations could easily be extended to cover continuous distributions of vorticity and doublet strength along the aerofoil chords and also if, for aerofoils in a fixed cascade, the velocity field is calculable, then the time variations in total pressure, and so on, at a fixed point in relation to a moving cascade, are also calculable.

10. Conclusions

A basic theory exists for the calculation of the total pressure changes at a fixed point in the non-steady, irrotational motion of an inviscid, incompressible fluid.

This has been applied to a number of problems, in particular to the calculation of total pressure changes with time at a fixed point in relation to the flow through a simplified single-stage flow machine. The periodic variation of total pressure with time varies in magnitude and form with the position of the fixed point and it is found that fluctuations in total pressure are less than 1 per cent of the total pressure rise through the stage at distances greater than the pitch of the vortices.

References

1. Dean, R. C., Jr. On the Necessity of Unsteady Flow in Fluid Machines. *Journal of Basic Engineering, Transactions of the American Society of Mechanical Engineers*, Series D, p. 24-28, March 1959.

2. Eck, B. *Technische Stromungslehre*. Springer, Berlin, p. 50, 1957.

3. Lamb, H. *Hydrodynamics*, 6th edition. Cambridge University Press, 1932.

The Deformational Behaviour of Low Aspect Ratio Multi-Web Wings*

PART I: Experimental Data

R. H. GALLAGHER† and I. RATTINGER‡

SUMMARY: Results of a study of the accuracy attainable from various approaches to low aspect ratio wing deformational analyses are described. Seven model multi-web wings, representing a restricted range of sweep angles, aspect ratios and other geometric factors, were tested for deflection influence coefficients. Methods of matrix structural analysis and other techniques, involving numerous idealisations, were then applied in the prediction of the test data. This paper presents the experimental data. Subsequent papers will describe the analytical methods, the level of test-theory correspondence, and the merits and shortcomings of the theories studied.

1. Introduction

In the period following the Second World War aerodynamic efficiency considerations dictated a change from wings of essentially rectangular and high aspect ratio plan form to swept, low aspect ratio plan forms. Continued progress in design resulted in still other types of plan forms (*e.g.* the delta wing) as well as a trend towards wings of high solidity. Analysts responsible for the prediction of the elastic characteristics of proposed supersonic wing designs recognised the need to use more sophisticated concepts of structural behaviour than those encompassed by elementary beam and torsion theory. Both indeterminate structural analysis procedures and approaches based on classical plate theory found favour. Whatever approach was taken, however, the analyses involved the solution of higher order simultaneous equations than could be solved by hand computation. Fortunately, a concurrent development of automatic computational devices, both analogue and digital, occurred during the post-war period. The devices made feasible the solution of problems phrased in terms of many unknowns and, in addition, it has become economical to formulate automatically the equations to be solved. A major

---

*The contents of this paper formed a part of a presentation to a meeting of the Structures and Materials Panel, Advisory Group for Aeronautical Research and Development, N.A.T.O., in Athens, 28th September 1960.

†Aerospace Department, Bell Aerosystems Company.

‡Aerospace Corporation.

Received January 1961.

remaining problem lies in the selection, from the many proposed theoretical approaches, of that one which will accurately and efficiently predict the elastic characteristics of a given wing. The efforts of the study described in this paper were specifically directed towards answering questions of accuracy.

Two primary factors upon which accuracy depends are the analytical representation of the structure and the number of analytical degrees of freedom employed. Although it should be apparent that greater accuracy will be obtained when more realistic analytical representations of the structure are used, this factor has often been obscured. Questions concerning the relationship between attainable accuracy and the number of analytical degrees of freedom have not been considered to a significant extent in the literature. To evaluate the relationship between these factors, deflection influence coefficient tests were performed on seven realistic, yet simplified, low aspect ratio wing models and the results were compared with analytically predicted values. Each of the wings was of full span but was tested only for symmetrical loadings. The models were chosen so as to introduce, in a controlled manner, those problem variables that could be studied within the limited number decided upon for the programme.

2. Experimental Programme

Deflection influence coefficient tests were performed on seven model wings designed specifically for the purpose of delineating the effects of sweep angle, aspect ratio, relative skin thickness, and internal member configuration. Other significant factors such as plan-form taper and variations in the type of internal structure and support conditions were represented in the three additional wings not discussed in

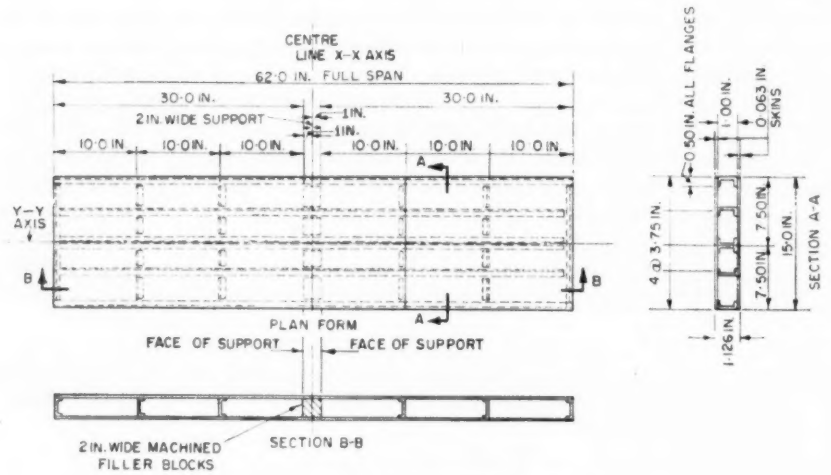

FIGURE 1. Model 1. Geometry and details.
Model material: 6061-T6 aluminium. All internal members formed of 0·040 in. sheet.

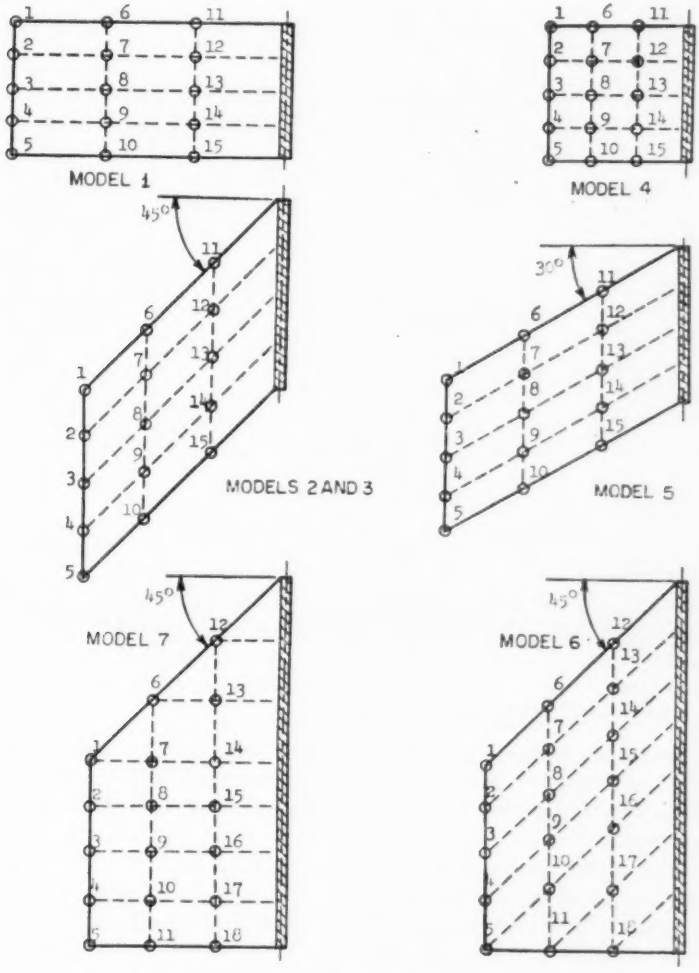

FIGURE 2. Geometry and node point locations. Model wings.
All models are clamped along centre support. O denotes a node point.

this paper. Data relating to these three wings, as well as more detailed information on the tests to be described, are given in Ref. 1.

Parametric variations of the foregoing factors essentially have their basis in the rectangular plan form, aspect ratio 4·0 wing (Model 1) shown in Fig. 1. This and all other models were fabricated from 6061-T6 aluminium alloy sheet. All internal members were formed channels, 0·040 in. thick, while the skins were single sheets, 0·063 in. thick. The spars were 30 in. long for each semi-span and

continuous from tip to tip, being joined to the rib segments with clip angles. The skins were joined to the internal members with $\frac{1}{8}$ in. diameter rivets, spaced $\frac{3}{4}$ in. on centre.

During test the model was clamped in a 2 in. wide support along the X-X axis (*see* Fig. 1). Severe clamping effects were precluded by means of a set of solid internal blocks in the support area. Load application points were defined by the spar-rib intersections, numbered as shown in Fig. 2. The remaining six model wings were of the same basic construction, with the exceptions noted in the following descriptions (*see* Fig. 2).

Models 2 and 3 were swept 45°; the root-to-tip spar lengths of Model 1 were retained. Model 3 had a skin thickness of 0·125 in., and was the only model in the series to differ in this regard. Model 4 was unswept and of half the span of Model 1. Model 5 was swept 30°, and semi-span spar lengths of 30 in. were again retained. Models 6 and 7 were delta wings, the former representing the 45° swept wing (Model 2) with structure added to form an unswept trailing edge. Model 7 typified the rectangular plan form wing (Model 1) with an added 45° swept leading edge area. Note however, that the tip chords and spans of these models differ in length from those of Model 1.

The manner in which an ordered variation in the chosen parameters was effected is now discussed (*see* Fig. 2). Models 1 and 4 attempt to highlight the effects of aspect ratio, chordwise bending, proximity of load to the support and shear lag. Sweep angle effects were delineated by Models 1, 2, and 5, where there is consistency of skin thickness, depth of section and internal member configuration. Models 2 and 3 assess the effects of skin thickness, while internal structural configuration effects were defined in Models 6 and 7.

Typical test arrangements are pictured in Fig. 3, which shows Model 6 positioned in the support frame. To ensure symmetric behaviour about the X-X axis, loads were applied to corresponding points on both semi-spans through rods with hemispherical ends. The loading apparatus was supported independently of the model support fixture. Load variations were accomplished by a turnbuckle arrangement. Load magnitudes were measured by a 1000 lb. Baldwin load cell placed in series with the rods and deflections were measured directly from dial gauges that could be read to an accuracy of 0·001 in. at points near the support and 0·01 in. at outboard points.

Before testing, a number of preliminary operations were conducted in order to minimise experimental error. All points were cyclically loaded to remove initial slippage, to define the extent of hysteresis and to aid in determining the load range and intervals to be used during test. It should be noted that hysteresis effects proved to be insignificant for all models.

The actual test sequence started by recording all zero-load dial gauge readings. Then, the load was increased to one interval above the maximum value desired and, as the load was removed in decrements, deflection measurements were made at each level. Complete unloading was comprised of six equal decrements. Upon com-

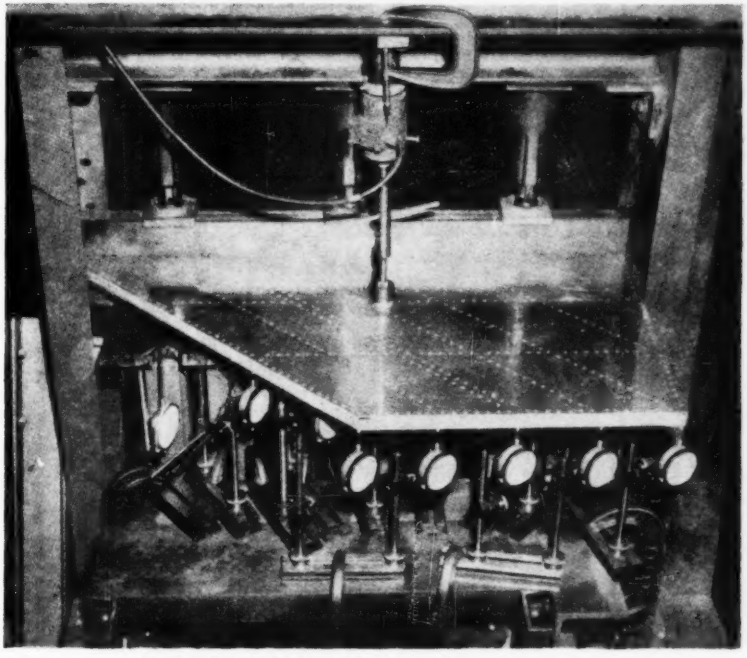

FIGURE 3. Typical model wing testing arrangement.

pleting this sequence the initial and final zero-load dial gauge readings were compared. Re-testing was undertaken if variations in the deflection differences between successive load decrements or deflectional dis-symmetry about the X-X axis were greater than 10 per cent, or if there were indications of permanent set as given by zero-load gauge reading comparisons.

Once a satisfactory set of readings had been acquired, deflection influence coefficients were obtained from the slope of a least-square straight line fitted through the load deflection points. Slopes were calculated on the basis of not only all load intervals but also all intervals except the lowest, since any existing hysteresis effects were most pronounced near zero load. A careful study of the measurements was made to determine the most representative value and this was the last step in reducing the test data.

3. Results

Due to the stringency of the criteria for the suitability of recorded data the cross-coefficients in each complete set of displacement influence coefficients ($[\delta]$) were closely in accord with the reciprocity condition. This condition requires that $\delta_{ij}=\delta_{ji}$, where δ_{ij} symbolises the displacement at point i due to a load at point j and δ_{ji} is the displacement at j due to a load at i. (All loads and displacements discussed

TABLE 1

TEST DEFLECTION INFLUENCE COEFFICIENTS. MODELS 1 AND 2
(Values shown are displacements in inches, due to 100 lb. loads)

MODEL 1 / MODEL 2	Points on Model 1														
Load application points (both models)	1	2	3	4	5	6	7	8	9	10	11	12	13	14	15
1	0·0854	0·1746	0·1621	0·1510	0·1415	0·1296	0·0987	0·0902	0·0827	0·0750	0·0660	0·0312	0·0285	0·0252	0·0216	0·0175
2	0·0863	0·0999	0·1631	0·1554	0·1494	0·1428	0·0914	0·0880	0·0846	0·0802	0·0747	0·0280	0·0279	0·0257	0·0238	0·0212
3	0·0897	0·1117	0·1360	0·1572	0·1566	0·1546	0·0832	0·0836	0·0854	0·0844	0·0823	0·0244	0·0257	0·0254	0·0255	0·0242
4	0·0917	0·1207	0·1541	0·1923	0·1645	0·1664	0·0772	0·0804	0·0854	0·0895	0·0914	0·0216	0·0248	0·0264	0·0276	0·0284
5	0·0968	0·1319	0·1715	0·2215	0·2776	0·1804	0·0706	0·0766	0·0847	0·0930	0·1014	0·0184	0·0234	0·0262	0·0292	0·0318
6	0·0423	0·0374	0·0353	0·0332	0·0323	0·0339	0·0687	0·0591	0·0502	0·0444	0·0379	0·0250	0·0216	0·0173	0·0136	0·0106
7	0·0475	0·0505	0·0527	0·0548	0·0582	0·0288	0·0354	0·0573	0·0512	0·0468	0·0426	0·0208	0·0178	0·0173	0·0151	0·0130
8	0·0502	0·0582	0·0674	0·0760	0·0839	0·0232	0·0328	0·0422	0·0540	0·0515	0·0492	0·0168	0·0174	0·0180	0·0172	0·0165
9	0·0532	0·0676	0·0835	0·0994	0·1139	0·0215	0·0337	0·0462	0·0627	0·0580	0·0583	0·0139	0·0158	0·0178	0·0196	0·0209
10	0·0575	0·0781	0·0997	0·1254	0·1514	0·0209	0·0359	0·0519	0·0744	0·1007	0·0714	0·0105	0·0142	0·0170	0·0205	0·0250
11	0·0128	0·0090	0·0066	0·0044	0·0022	0·0147	0·0100	0·0055	0·0039	0·0018	0·0177	0·0174	0·0124	0·0071	0·0048	0·0028
12	0·0156	0·0135	0·0135	0·0130	0·0123	0·0129	0·0126	0·0096	0·0088	0·0083	0·0096	0·0117	0·0137	0·0082	0·0064	0·0052
13	0·0172	0·0189	0·0209	0·0230	0·0235	0·0108	0·0135	0·0151	0·0154	0·0160	0·0046	0·0071	0·0108	0·0105	0·0081	0·0073
14	0·0190	0·0231	0·0272	0·0319	0·0355	0·0093	0·0139	0·0175	0·0218	0·0248	0·0025	0·0049	0·0085	0·0137	0·0125	0·0118
15	0·0215	0·0294	0·0377	0·0479	0·0565	0·0082	0·0153	0·0222	0·0318	0·0409	0·0008	0·0040	0·0081	0·0143	0·0257	0·0169
	1	2	3	4	5	6	7	8	9	10	11	12	13	14	15
	Points on Model 2														

TABLE II

TEST DEFLECTION INFLUENCE COEFFICIENTS. MODELS 3 AND 4
(Values shown are displacements in inches, due to 100 lb. loads)

MODEL 3 / MODEL 4	*Points on Model* 3														
Load application points (both models)	1	2	3	4	5	6	7	8	9	10	11	12	13	14	15
1	0·0407	0·0461	0·0463	0·0472	0·0489	0·0527	0·0231	0·0251	0·0272	0·0295	0·0317	0·0078	0·0095	0·0104	0·0109	0·0124
2	0·0327	0·0309	0·0543	0·0588	0·0640	0·0712	0·0208	0·0272	0·0326	0·0363	0·0424	0·0065	0·0093	0·0115	0·0132	0·0165
3	0·0246	0·0270	0·0274	0·0726	0·0812	0·0900	0·0202	0·0285	0·0376	0·0458	0·0544	0·0052	0·0090	0·0128	0·0166	0·0216
4	0·0170	0·0208	0·0252	0·0294	0·0988	0·1150	0·0197	0·0308	0·0421	0·0531	0·0681	0·0043	0·0089	0·0138	0·0192	0·0267
5	0·0116	0·0168	0·0229	0·0308	0·0387	0·1475	0·0191	0·0350	0·0448	0·0601	0·0844	0·0031	0·0080	0·0147	0·0218	0·0296
6	0·0256	0·0188	0·0141	0·0097	0·0065	0·0202	0·0187	0·0156	0·0135	0·0126	0·0120	0·0084	0·0076	0·0067	0·0057	0·0053
7	0·0191	0·0194	0·0150	0·0119	0·0092	0·0152	0·0155	0·0189	0·0190	0·0191	0·0206	0·0058	0·0072	0·0081	0·0080	0·0085
8	0·0144	0·0157	0·0162	0·0146	0·0132	0·0087	0·0098	0·0122	0·0235	0·0259	0·0288	0·0040	0·0065	0·0090	0·0108	0·0129
9	0·0093	0·0116	0·0139	0·0176	0·0180	0·0054	0·0068	0·0095	0·0133	0·0340	0·0405	0·0032	0·0060	0·0094	0·0131	0·0183
10	0·0061	0·0092	0·0128	0·0180	0·0240	0·0030	0·0054	0·0085	0·0133	0·0182	0·0571	0·0025	0·0056	0·0101	0·0150	0·0240
11	0·0110	0·0080	0·0049	0·0028	0·0014	0·0104	0·0064	0·0034	0·0016	0·0008	0·0092	0·0089	0·0053	0·0030	0·0018	0·0011
12	0·0086	0·0074	0·0054	0·0040	0·0030	0·0068	0·0066	0·0040	0·0026	0·0019	0·0048	0·0060	0·0069	0·0045	0·0032	0·0028
13	0·0050	0·0052	0·0056	0·0050	0·0046	0·0033	0·0039	0·0046	0·0035	0·0032	0·0016	0·0023	0·0036	0·0064	0·0053	0·0050
14	0·0032	0·0043	0·0052	0·0066	0·0075	0·0020	0·0028	0·0041	0·0059	0·0063	0·0006	0·0013	0·0022	0·0056	0·0088	0·0092
15	0·0010	0·0028	0·0045	0·0070	0·0100	0·0004	0·0014	0·0034	0·0060	0·0092	0·0002	0·0006	0·0014	0·0046	0·0081	0·0154
	1	2	3	4	5	6	7	8	9	10	11	12	13	14	15	
	Points on Model 4															

TABLE III

TEST DEFLECTION INFLUENCE COEFFICIENTS. MODELS 6 AND 7
(Values shown are displacements, in inches, due to 100 lb. loads)

MODEL 6 / MODEL 7	*Points on Model 6*																	
Load application points (both models)	1	2	3	4	5	6	7	8	9	10	11	12	13	14	15	16	17	18
1	0·0422	0·0604	0·0552	0·0480	0·0410	0·0328	0·0342	0·0351	0·0336	0·0288	0·0246	0·0183	0·0112	0·0144	0·0148	0·0144	0·0113	0·0076	0·0060
2	0·0353	0·0419	0·0610	0·0580	0·0512	0·0430	0·0286	0·0344	0·0367	0·0332	0·0284	0·0240	0·0089	0·0126	0·0152	0·0154	0·0130	0·0096	0·0084
3	0·0292	0·0372	0·0492	0·0644	0·0620	0·0543	0·0228	0·0298	0·0364	0·0360	0·0324	0·0299	0·0061	0·0102	0·0138	0·0154	0·0136	0·0114	0·0109
4	0·0238	0·0324	0·0440	0·0560	0·0713	0·0688	0·0176	0·0252	0·0330	0·0382	0·0371	0·0379	0·0038	0·0077	0·0115	0·0141	0·0143	0·0138	0·0142
5	0·0196	0·0290	0·0428	0·0606	0·0742	0·0811	0·0137	0·0204	0·0272	0·0342	0·0398	0·0478	0·0025	0·0060	0·0088	0·0118	0·0134	0·0152	0·0180
6	0·0214	0·0146	0·0104	0·0078	0·0056	0·0207	0·0349	0·0276	0·0194	0·0152	0·0108	0·0074	0·0148	0·0144	0·0107	0·0096	0·0071	0·0038	0·0022
7	0·0223	0·0192	0·0156	0·0132	0·0108	0·0140	0·0187	0·0328	0·0266	0·0204	0·0158	0·0118	0·0106	0·0148	0·0140	0·0120	0·0088	0·0056	0·0040
8	0·0195	0·0218	0·0203	0·0186	0·0172	0·0092	0·0138	0·0183	0·0328	0·0265	0·0202	0·0164	0·0070	0·0114	0·0154	0·0144	0·0109	0·0074	0·0062
9	0·0160	0·0206	0·0247	0·0260	0·0258	0·0062	0·0098	0·0134	0·0196	0·0349	0·0276	0·0216	0·0043	0·0080	0·0120	0·0158	0·0144	0·0098	0·0083
10	0·0132	0·0179	0·0243	0·0318	0·0380	0·0046	0·0079	0·0112	0·0173	0·0265	0·0341	0·0284	0·0028	0·0055	0·0078	0·0120	0·0146	0·0122	0·0122
11	0·0103	0·0162	0·0244	0·0344	0·0448	0·0025	0·0062	0·0103	0·0165	0·0264	0·0389	0·0387	0·0010	0·0031	0·0051	0·0076	0·0100	0·0128	0·0164
12	0·0050	0·0032	0·0020	0·0008	0·0001	0·0080	0·0038	0·0022	0·0010	0·0006	0·0002	0·0113	0·0161	0·0108	0·0053	0·0040	0·0023	0·0010	0·0004
13	0·0066	0·0050	0·0036	0·0026	0·0016	0·0074	0·0054	0·0037	0·0024	0·0017	0·0006	0·0040	0·0082	0·0140	0·0091	0·0065	0·0042	0·0021	0·0012
14	0·0080	0·0073	0·0060	0·0051	0·0042	0·0059	0·0072	0·0060	0·0043	0·0031	0·0024	0·0020	0·0037	0·0074	0·0133	0·0097	0·0052	0·0029	0·0020
15	0·0072	0·0081	0·0076	0·0070	0·0065	0·0042	0·0060	0·0072	0·0062	0·0049	0·0040	0·0011	0·0020	0·0042	0·0073	0·0188	0·0124	0·0054	0·0034
16	0·0060	0·0077	0·0088	0·0094	0·0098	0·0026	0·0042	0·0058	0·0074	0·0072	0·0074	0·0006	0·0012	0·0021	0·0035	0·0064	0·0183	0·0082	0·0051
17	0·0048	0·0068	0·0096	0·0127	0·0142	0·0014	0·0030	0·0049	0·0076	0·0114	0·0123	0·0002	0·0007	0·0014	0·0026	0·0048	0·0108	0·0133	0·0084
18	0·0032	0·0056	0·0086	0·0125	0·0167	0·0002	0·0018	0·0039	0·0067	0·0110	0·0162	0·0003	0·0001	0·0010	0·0018	0·0040	0·0096	0·0189	0·0128
	1	2	3	4	5	6	7	8	9	10	11	12	13	14	15	16	17	18	
	Points on Model 7																		

TABLE IV

TEST DEFLECTION INFLUENCE COEFFICIENTS. MODEL 5

(Values shown are displacements, in inches, due to 100 lb. loads)

Load application point	*Points*														
	1	2	3	4	5	6	7	8	9	10	11	12	13	14	15
1	0·1499	0·1555	0·1586	0·1533	0·1554	0·0891	0·0927	0·0884	0·0914	0·0914	0·0284	0·0368	0·0349	0·0342	0·0389
2		0·1742	0·1852	0·1884	0·1976	0·0881	0·1009	0·1033	0·1130	0·1184	0·0262	0·0416	0·0416	0·0442	0·0507
3			0·2071	0·2184	0·2290	0·0839	0·1046	0·1118	0·1270	0·1345	0·0240	0·0414	0·0446	0·0486	0·0568
4				0·2511	0·2802	0·0804	0·1062	0·1170	0·1445	0·1620	0·0209	0·0414	0·0488	0·0569	0·0718
5					0·3330	0·0810	0·1106	0·1226	0·1584	0·1882	0·0198	0·0424	0·0517	0·0622	0·0840
6						0·0680	0·0642	0·0545	0·0518	0·0494	0·0279	0·0304	0·0248	0·0218	0·0222
7							0·0712	0·0672	0·0680	0·0696	0·0219	0·0336	0·0310	0·0288	0·0328
8								0·0729	0·0744	0·0748	0·0159	0·0293	0·0335	0·0314	0·0364
9									0·1005	0·0992	0·0136	0·0291	0·0354	0·0397	0·0496
10										0·1267	0·0118	0·0288	0·0364	0·0427	0·0604
11											0·0226	0·0171	0·0094	0·0066	0·0054
12												0·0269	0·0190	0·0148	0·0151
13													0·0253	0·0200	0·0206
14														0·0253	0·0282
15															0·0407

TABLE V

TEST DEFLECTIONS. UNIFORM LOAD CONDITION

Model Number	*Deflections at Point*																	
	1	2	3	4	5	6	7	8	9	10	11	12	13	14	15	16	17	18
1	1·295	1·318	1·319	1·331	1·329	0·770	0·760	0·765	0·769	0·762	0·255	0·263	0·258	0·257	0·253	—	—	—
2	0·787	0·936	1·108	1·289	1·469	0·365	0·496	0·602	0·738	0·888	0·106	0·157	0·213	0·268	0·364	—	—	—
3	0·429	0·511	0·602	0·695	0·797	0·209	0·277	0·338	0·407	0·497	0·071	0·100	0·131	0·163	0·209	—	—	—
4	0·230	0·231	0·225	0·220	0·218	0·150	0·148	0·142	0·138	0·140	0·067	0·065	0·055	0·062	0·060	—	—	—
5	1·399	1·629	1·776	1·941	2·116	0·838	1·003	1·033	1·196	1·294	0·272	0·448	0·477	0·505	0·614	—	—	—
6	0·492	0·537	0·555	0·563	0·539	0·295	0·350	0·382	0·389	0·366	0·338	0·113	0·156	0·177	0·203	0·187	0·151	0·140
7	0·295	0·330	0·363	0·399	0·421	0·147	0·183	0·207	0·232	0·259	0·274	0·045	0·061	0·081	0·091	0·099	0·119	0·122

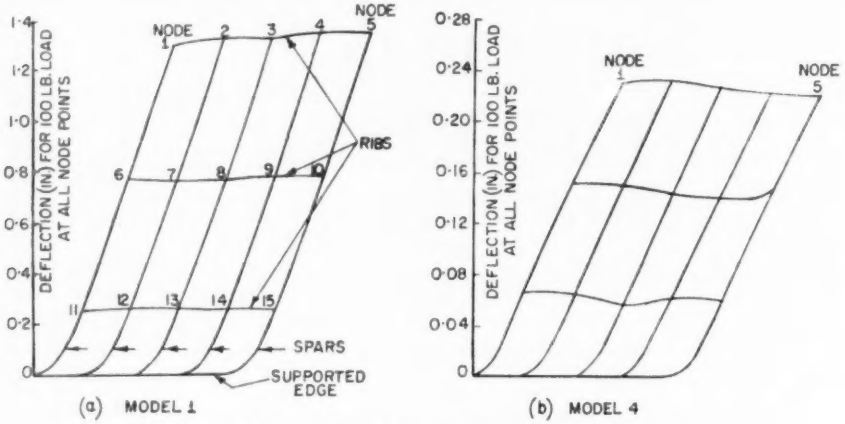

FIGURE 4. Deflected surface shape. Uniform load. Models 1 and 4.

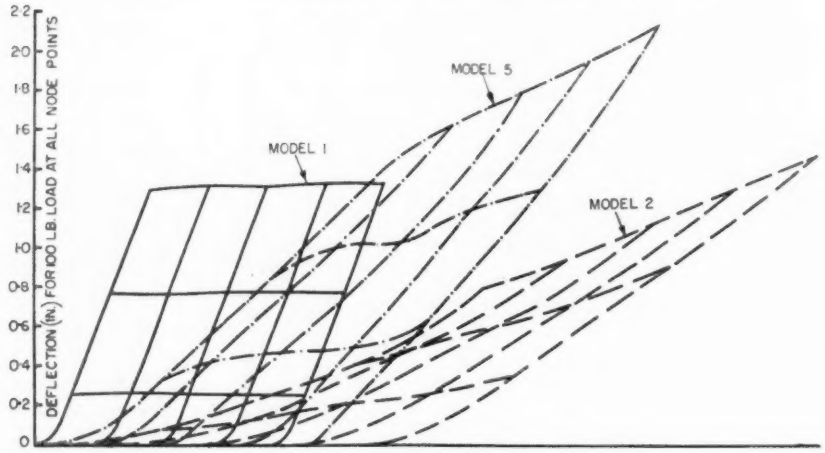

FIGURE 5. Deflected surface shape. Uniform load. Models 1, 2 and 5.

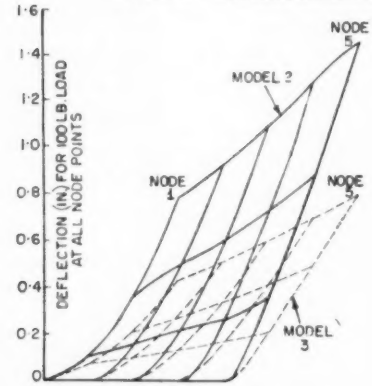

FIGURE 6. Deflected surface shape. Uniform load. Models 2 and 3.

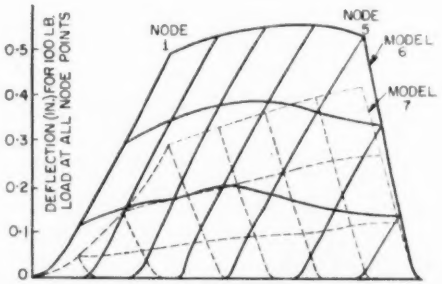

FIGURE 7. Deflected surface shape. Uniform load. Models 6 and 7.

here are understood to be directed normal to the wing mid-plane.) To allow for an efficient presentation of data, and since the analytical methods to be evaluated necessarily produce a symmetric set of displacement influence coefficients, the experimentally derived cross-coefficients have been averaged to yield a symmetric set. The results are shown in Tables I-IV as displacements in inches, due to 100 lb. loads. For economy in presentation the results for Models 1 and 2, 3 and 4, and 6 and 7 have been paired. In each case, advantage has been taken of symmetry by tabulating only the values on and to one side of the main diagonal.

Further operations on the test data are useful in the interests of providing concise parameters for the test-theory comparisons. There are numerous such parameters that can be obtained from the complete set of displacement influence coefficients and which represent certain basic properties of the elastic system. One is the fundamental wing vibrational frequency; another is the deformed shape under distributed loads. Since this study had an ultimate concern with static aeroelasticity, the latter parameter was selected.

In particular, the chosen distributed loading case involved the simultaneous application of 100 lb. loads at all spar-rib intersection points. The displacement at each reference point on each wing for this loading case, henceforth referred to as the uniform load condition, is listed in Table V. Graphical representations are also shown (Figs. 4-7) in the form of carpet plots of the deflected surface shape. Each plot typifies a geometric characteristic.

Figure 4 illustrates the results for Models 1 and 4, the rectangular plan form wings. Results for the family of swept wings, Models 1, 2 and 5 (0°, 45°, and 30° sweep, respectively) are shown on Fig. 5. A comparison between Models 2 and 3, where the skin thickness is doubled, is given in Fig. 6, and Fig. 7 compares the delta plan forms, Models 6 and 7. It is noteworthy that the deformed shapes of Models 6 and 7 differ significantly in consequence of the difference between internal member orientation. Not all of the node point locations on Models 6 and 7 exactly correspond, but this factor should not heavily influence the level of agreement in the uniform load comparisons.

Acknowledgments

The work described in the paper was performed under the sponsorship of the Aeromechanics Branch, Flight Control Laboratory, Wright Air Development Division, U.S.A.F. Mr. H. M. Davis acted as Air Force Project Officer. The authors are indebted to their many colleagues who assisted in this study during the past four years.

References

1. Rattinger, I. and Gallagher, R. H. Supersonic Aeroelastic Effects on Static Stability and Control. Part II—Structures. Wright Air Development Center, T.R. 58-95, April 1960

The Static Aeroelastic Deformation of Slender Configurations*

PART II: Some Calculations on Slender Plate Aircraft, Including Non-Linear Aerodynamics

G. J. HANCOCK

(Department of Aeronautical Engineering, Queen Mary College, University of London)

SUMMARY: Calculations have been applied to a series of flexible plates (delta, gothic and ogee) to estimate their static aeroelastic behaviour. Assuming linear aerodynamics, the general tendencies of Part I are particularised. Assuming non-linear aerodynamics, it is shown that in general two positions of equilibrium are apparently possible at each speed. The stability of the models is not considered.

1. Introduction

In Part I[1] a qualitative idea of the primary type of aeroelastic deformation of a slender configuration under linear aerodynamic loading, involving a lengthwise deformation only, is given for the trimmed cruising condition in level flight at various forward speeds. It is shown that the aeroelastic deformation may become very large at a finite speed when the elevator control force to trim the aircraft also becomes very large. In this note some detailed calculations are carried out to supplement these statements with quantitative results, and to extend these ideas to cover configurations under non-linear aerodynamic loadings (*i.e.* including leading-edge vortices).

The procedure followed here is now indicated.

(*i*) The equation for the lengthwise deformation is derived for general distributions of weight and stiffness, including expressions to represent the non-linear aerodynamic loadings associated with slender configurations, based on the assumption that the whole airframe can be treated as a free-free beam. This assumption may not be a severe one for a slender configuration, which will comprise a centre body fuselage supported by wings of a slender plan form. The main difficulty is introduced by the present lack of knowledge regarding the non-linear aerodynamic loading on streamwise cambered slender wings. A linear theory[2] is

*A summary of part of this work was read at the meeting of the AGARD Stability and Control Panel in Brussels, April 1961.

Received January 1961.

available for this case, but this theory is only applicable when the leading-edge vortices are absent. Non-linear theories have been established for delta wings[3], without camber, to illustrate the effects of these leading-edge vortices. In this paper, the non-linear form of the loading is retained in general form (in the derivation of the fundamental deformation equation), so that, as more aerodynamic information becomes available, substitution of more exact theories may be easily accomplished, being of an arithmetical nature, without altering the approach to the problem. However, for the purposes of calculation here an intuitive representation for the non-linear aerodynamic loading for general shapes with camber is made, based on the existing information referred to so that, although the quantitative results derived in this paper are dependent on this assumption, it is hoped that these results reflect the general aeroelastic behaviour of slender configurations.

(*ii*) The general equation derived in (*i*) is solved exactly for the case of a trimmed delta plate of constant thickness with both the linear and non-linear aerodynamic loading, for both its deformation and control force characteristics.

(*iii*) A simple numerical technique for an approximate solution to the general equation derived in (*i*) is suggested, and is applied to the trimmed delta plate solution derived in (*ii*) to check the accuracy of the method.

(*iv*) The numerical technique, introduced in (*iii*), is applied to the cases of gothic and ogee trimmed plates with linear aerodynamic loading.

(*v*) The gothic trimmed plate with non-linear aerodynamic loading (*i.e.* in the presence of leading-edge vortices) is investigated.

It is seen that the actual calculations are restricted to plates of different plan forms with constant thickness. Although it may be argued that this is not representative of a typical slender configuration in regard to either weight distribution or stiffness distribution, at least the important parameters are inherent to these simple cases, which are consistent in their relation between weight and stiffness distributions, particularly in the respect of the effects of change of plan form. In any case the numerical method, mentioned in (*iii*), is applicable to the more general configuration.

Finally, at this stage it is worth noting some of the implications of the applications of linear and non-linear aerodynamic theories. In the interests of efficiency the slender aircraft may cruise without any appreciable leading-edge vorticity, and this can be achieved by a design incorporating a spanwise camber[4]. So the application of linear aerodynamic theory at cruising speeds for such shapes will be valid. It will still be essential to investigate the deformation characteristics below the cruise condition when the leading-edge vortices will play an increasingly important role. However, this aspect is not covered directly here, since we shall consider a given plate without any spanwise camber so that the leading-edge vorticity will always be present when lift is generated.

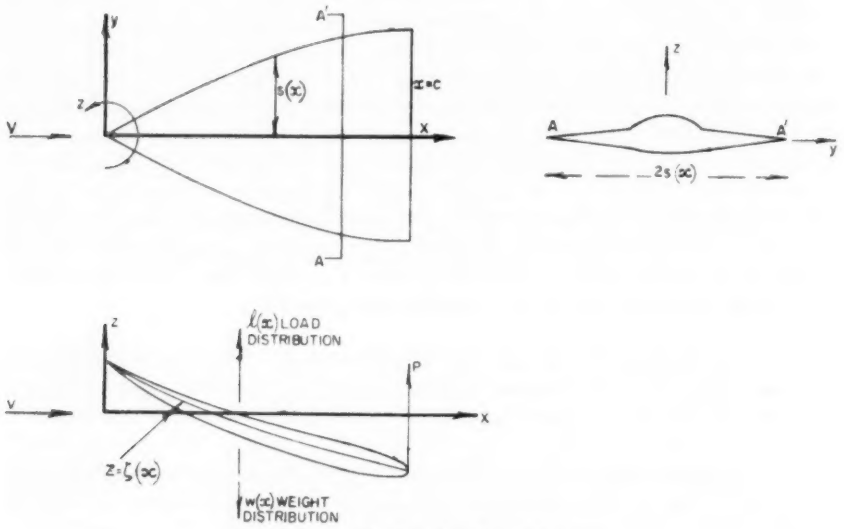

FIGURE 1. Slender aircraft notation.

NOTATION

$y \leqq |s(x)|$, $0 \leqq x \leqq c$ } wing plan form

$l(x)$ load distribution

$l_1(x), l_2(x)$ generalised functions in the load distribution (equation (8))

$K = \tan\gamma$

P trailing edge control force

$w(x)$ weight distribution

W all-up weight

V relative free stream velocity

V_c maximum trim speed

$z = \zeta(x)$, wing camber shape

$\xi = x/c$

$\alpha(x) = -\zeta'(x)$, incidence distribution

Λ speed parameter (equation (30))

Λ_1 weight parameter (equation (31))

σ weight distribution (equation (31))

γ semi-apex angle of the plate

ν Poisson's ratio

2. The General Deformation Equation

The slender configuration is shown in Fig. 1. The origin of a right-handed Cartesian set of co-ordinates is taken as the apex of the wing in the zero-lift position. The x-axis is in the relative stream direction and the y-axis denotes the spanwise direction. The relative free stream velocity is denoted as V. The plan form of the wing on the plane $z=0$ is given by

$$y = \pm s(x) \quad \text{for } 0 \leqslant x \leqslant c. \qquad (1)$$

It is assumed that $s'(x) \geqslant 0$ for all the plan forms considered. The attitude of the wing to the free stream is denoted by

$$z = \zeta(x), \qquad (2)$$

which is assumed to be a function of x only, since in this paper interest is restricted to the longitudinal bending of the aircraft. The weight distribution is denoted by $\sigma(x, y)$ lb./ft.^{2}, so that

$$w(x) = \frac{\text{weight}}{\text{unit length}} = \int_{-s(x)}^{+s(x)} \sigma(x, y)\, dy, \qquad (3)$$

$$\text{and so} \quad W = \text{total weight} = \int_0^c w(x)\, dx. \qquad (4)$$

The effective longitudinal bending stiffness distribution may be represented as $EI(x)$, which can be calculated for any given structure.

The aerodynamic loading is now considered. The primary interest is the lift distribution along the chord. According to linear slender-wing theory[2], assuming that the configuration is sufficiently thin for the theory to be applied, the lift distribution $l(x)$ lb./ft. along the chord is given by

$$l(x) = -\rho V^2 \pi \frac{d}{dx}\left[s^2(x)\,\zeta'(x)\right]. \qquad (5)$$

It is seen that, on integration of equation (5), the total lift is given by the conditions at the trailing edge only. In the presence of leading-edge vortices, equation (5) is seriously inaccurate, as demonstrated on a delta flat plate (*i.e.* symmetrical sharp edged section) wing[3]. The formula

$$l(x) = -\rho V^2 \left[2\pi s(x)\, s'(x)\, \zeta'(x) + 4s(x)\, \zeta'(x)\, |\zeta'(x)|\right] \qquad (6)$$

is reasonably accurate for this type of wing, *i.e.* when $s'(x)$ and $\zeta'(x)$ are constant,

on the basis of both theoretical and experimental evidence. No definite information is available at present to cover cases where $s'(x)$ is not constant (*i.e.* curved leading edges) or where $\zeta'(x)$ is not constant (*i.e.* chordwise cambered wings) so that some assumptions must be made in order to proceed with the general distortion problem.

Now equation (5) is completely general, with regard to $s'(x)$ and $\zeta'(x)$, but is limited by its linearity. Equation (6) is a reasonable non-linear equation when $s'(x)$ and $\zeta'(x)$ are constant, and the first term (or the linear term) of equation (6) is then identical to equation (5). Therefore it is suggested that an approximation for the general non-linear case could be written

$$l(x) = -\rho V^2 \frac{d}{dx}\left[\pi s^2(x)\,\zeta'(x) + 4\zeta'(x)\,|\zeta'(x)| \int_0^x s(x)\,dx\right], \quad . \quad . \quad . \quad (7)$$

which includes equation (5) for the linear first term and satisfies equation (6) when $s'(x)$ and $\zeta'(x)$ are constant. It is admitted that there are several formulae which could be used to represent the non-linear term in equation (7), applying similar arguments to those given already. However, equation (7) satisfies one most necessary criterion for general usage, namely, that the load remains finite at the trailing edge if $s'(x)$ tends to zero there.

Since the accuracy of equation (7) is an unknown quantity, it will be assumed that the form of the aerodynamic loading may be written

$$l(x) = -\rho V^2 \frac{d}{dx}\left[l_1(x)\,\zeta'(x) + l_2(x)\,\zeta'(x)\,|\zeta'(x)|\right] \quad . \quad . \quad (8)$$

and the fundamental deformation equation will then be derived in terms of $l_1(x)$ and $l_2(x)$. As more information becomes available, accurate expressions may be substituted for $l_1(x)$ and $l_2(x)$ but, for the purposes of calculation in this paper, it will be assumed that

$$l_1(x) = \pi s^2(x) \quad . \quad . \quad . \quad . \quad . \quad (9)$$

$$\text{and} \quad l_2(x) = 4\int_0^x s(x)\,dx, \quad . \quad . \quad . \quad . \quad (10)$$

by comparison of equations (7) and (8).

It is assumed that the aircraft is trimmed for level flight by a trailing edge force P, which is induced by the inclination of the elevators.

In level flight the overall conditions that

$$\left.\begin{aligned} \text{lift} &= \text{weight} \\ \text{pitching moment} &= 0 \end{aligned}\right\} \quad . \quad . \quad . \quad . \quad (11)$$

must hold.

The first of these equations states that

$$-\rho V^2 [l_1(c)\,\zeta'(c)+l_2(c)\,\zeta'(c)\,|\zeta'(c)|]+P=W, \quad . \quad . \quad . \quad (12)$$

from equations (8) and (4), remembering that $l_1(0)=l_2(0)=0$. The second condition is

$$\int_0^c \left\{-\rho V^2 \frac{d}{dx}\left[l_1(x)\,\zeta'(x)+l_2(x)\,\zeta'(x)\,|\zeta'(x)|\right]-w(x)\right\}\{c-x\}\,dx=0, \quad . \quad (13)$$

by taking moments about the trailing edge, where $w(x)$ is defined in equation (3).

As explained in the Introduction, it is assumed that the structure may be treated as a beam, so the deformation equation is

$$\frac{d^2}{dx^2}\left(EI\zeta''(x)\right)+\rho V^2 \frac{d}{dx}\left[l_1(x)\,\zeta'(x)+l_2(x)\,\zeta'(x)\,|\zeta'(x)|\right]+w(x)=0, \quad . \quad (14)$$

together with the boundary conditions

$$EI\zeta''|_{x=0}=0 \quad . \quad . \quad . \quad . \quad . \quad . \quad (15)$$

$$EI\zeta''|_{x=c}=0 \quad . \quad . \quad . \quad . \quad . \quad . \quad (16)$$

$$\frac{d}{dx}(EI\zeta'')|_{x=0}=0 \quad . \quad . \quad . \quad . \quad . \quad . \quad (17)$$

$$\frac{d}{dx}(EI\zeta'')|_{x=c}=-P. \quad . \quad . \quad . \quad . \quad . \quad . \quad (18)$$

Equations (15) and (16) state that no bending moments are applied at the apex or the trailing edge. Equation (17) states that no shear force is exerted at the apex. Equation (18) states that the control force P acts at the trailing edge.

On integration, equation (14) gives

$$\frac{d}{dx}\left(EI\zeta''(x)\right)+\rho V^2 [l_1(x)\,\zeta'(x)+l_2(x)\,\zeta'(x)|\zeta'(x)|]+\int_0^x w(\bar{x})\,d\bar{x}=0. \quad . \quad (19)$$

Equation (19) satisfies the boundary equation (17), since the loading is zero at the leading apex. Equation (18) is also satisfied if equation (12) holds.

On further integration, equation (19) gives

$$EI\zeta''(x)+\rho V^2 \int_0^x [l_1(x)\,\zeta'(x)+l_2(x)\,\zeta'(x)\,|\zeta'(x)|]\,dx+\int_0^x dx_1 \int_0^{x_1} w(\bar{x})\,d\bar{x}=0. \quad . \quad . \quad (20)$$

Equation (20) satisfies the boundary condition (15). Using equation (20) it can be shown that boundary condition (16) is equivalent to equation (13).

If we now introduce the non-dimensional chordwise co-ordinate

$$\xi = x/c \ (i.e.\ 0 \leqslant \xi \leqslant 1) \quad . \quad . \quad . \quad . \quad (21)$$

and put $$\alpha(\xi) = -\zeta'(x), \quad . \quad . \quad . \quad . \quad . \quad . \quad . \quad (22)$$

then equation (20) becomes

$$EI\alpha'(\xi) = -\rho V^2 c^2 \int_0^{\xi} [l_1(\xi)\,\alpha(\xi) + l_2(\xi)\,\alpha(\xi)\,|\alpha(\xi)|]\,d\xi + c^3 \int_0^{\xi} d\xi_1 \int_0^{\xi_1} w(\xi)\,d\xi, \quad . \quad (23)$$

where the prime (′) now denotes differentiation with respect to ξ. The remaining boundary condition (*i.e.* equation (16)) to be satisfied by the solution of equation (23) is

$$\alpha'(1) = 0, \quad . \quad . \quad . \quad . \quad . \quad . \quad (24)$$

assuming that $EI(1) > 0$. Thus an integral-differential equation has been obtained for the incidence distribution $\alpha(\xi)$ of the flexible shape in terms of the known distributions $EI(\xi)$, $w(\xi)$, $l_1(\xi)$ and $l_2(\xi)$.

3. Slender Delta Plate Wing (Linear Aerodynamics)

We now consider the simple case of a slender delta plate wing, of constant thickness t and uniform weight distribution σ, trimmed for level flight by a control force P at the trailing edge, as explained in Section 2. In this case, from equations (1), (3), (9), and (10),

$$s(x) = Kx = Kc\xi \quad . \quad . \quad . \quad . \quad . \quad (25)$$

$$w(x) = 2\sigma s(x) = 2\sigma Kc\xi \quad . \quad . \quad . \quad . \quad (26)$$

$$EI(x) = \frac{2Et^3 s(x)}{12(1-\nu^2)} = \frac{2Et^3 Kc\xi}{12(1-\nu^2)} \quad . \quad . \quad . \quad (27)$$

$$\left.\begin{aligned} l_1(x) &= \pi s^2(x) = \pi c^2 K^2 \xi^2 \\ l_2(x) &= 4\int_0^x s(x)\,dx = 2Kc^2\xi^2 \end{aligned}\right\} \quad . \quad . \quad . \quad . \quad (28)$$

where K is a constant and equal to $\tan\gamma$, where γ is the semi-apex angle of the plate.

Substitution of equations (25), (26), (27) and (28) into equation (23) gives

$$\xi\alpha'(\xi) = -\Lambda \int_0^\xi \xi^2 \left(\alpha + \frac{2}{\pi K}\alpha|\alpha|\right) d\xi + \Lambda_1 \frac{\xi^3}{3}, \quad . \quad . \quad (29)$$

where Λ and Λ_1 are constants given by

$$\Lambda = 6\pi(1-\nu^2)\left(\frac{\rho V^2}{E}\right)\left(\frac{c}{t}\right)^3 K \quad . \quad . \quad . \quad . \quad (30)$$

$$\text{and} \quad \Lambda_1 = 6(1-\nu^2)\left(\frac{\sigma}{E}\right)\left(\frac{c}{t}\right)^3 . \quad . \quad . \quad . \quad . \quad . \quad (31)$$

The boundary condition for the differential equation (29) is, by equation (24),

$$\alpha'(1) = 0. \quad . \quad . \quad . \quad . \quad . \quad . \quad (32)$$

First the linear problem only is considered, so equation (29) becomes, on ignoring the non-linear terms,

$$\xi\alpha'(\xi) = -\Lambda \int_0^\xi \xi^2 \alpha \, d\xi + \Lambda_1 \frac{\xi^3}{3}. \quad . \quad . \quad . \quad (33)$$

It is seen immediately that one solution is

$$\alpha = \text{constant} = \frac{\Lambda_1}{\Lambda} = \frac{\sigma}{K\pi\rho V^2}. \quad . \quad . \quad (34)$$

This is due physically to the fact that the distribution of aerodynamic loading balances the weight distribution, so that no deformation exists. Also the trailing edge control force P is zero (from equation (18)). This problem is therefore similar to

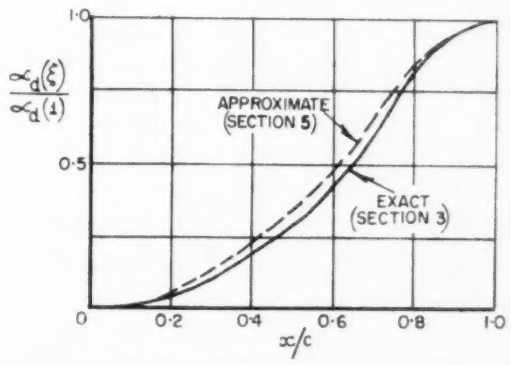

FIGURE 2. Deformation mode of delta plate (linear aerodynamics) at the maximum trim speed.

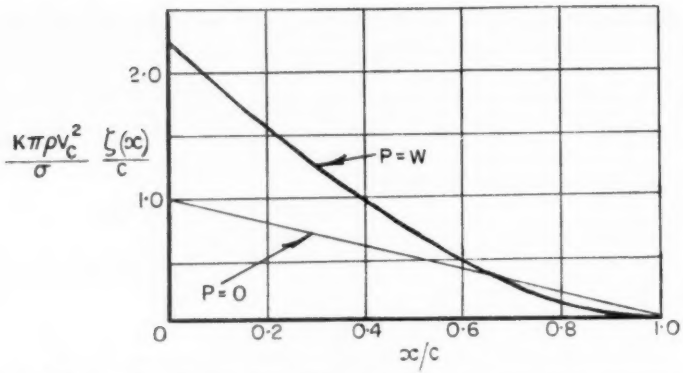

FIGURE 3. Two modes of equilibrium of delta plate (linear aerodynamics) at the maximum trim speed.

Model 4 discussed in Part I of this paper[1], in which it is also indicated that a speed may exist at which there are an infinite number of positions of equilibrium. Thus the solution given in equation (34) is not necessarily unique for all speeds.

The general solution of equation (33) may be obtained by the method of series, and it may be shown that

$$\alpha(\xi) = \alpha_0 - (\Lambda\alpha_0 - \Lambda_1)\left(\frac{\xi^3}{3^2} - \frac{\Lambda\xi^6}{3^2 \cdot 6^2} + \frac{\Lambda^2\xi^9}{3^2 \cdot 6^2 \cdot 9^2} - \ldots\ldots\right), \quad . \quad (35)$$

where α_0 is a constant and represents the incidence of the nose. The boundary condition, equation (32), gives

$$(\Lambda\alpha_0 - \Lambda_1)\left(\frac{1}{3} - \frac{\Lambda}{3^2 \cdot 6} + \frac{\Lambda^2}{3^2 \cdot 6^2 \cdot 9} - \ldots\ldots\right) = 0. \quad . \quad (36)$$

Therefore, either $\alpha_0 = \Lambda_1/\Lambda$,

which is the solution given by equation (34), or

$$\frac{1}{3} - \frac{\Lambda}{3^2 \cdot 6} + \frac{\Lambda^2}{3^2 \cdot 6^2 \cdot 9} - \ldots\ldots = 0. \quad . \quad . \quad . \quad (37)$$

When condition (37) is satisfied, α_0 is indeterminate, but the control force P is non-zero and depends on α_0. The value of Λ which satisfies equation (37) is

$$\Lambda = 33, \quad . \quad . \quad . \quad . \quad . \quad . \quad (38)$$

which gives, by reference to equation (30), a critical speed at which the deformation

amplitude is indeterminate. The angular mode of the deformation $\alpha_d(\xi)$, relative to the undistorted shape at this critical speed, is given by

$$\alpha_d(\xi) = \text{constant} \times \left(\frac{\xi^3}{3^2} - \frac{33\xi^6}{3^2 \cdot 6^2} + \frac{(33)^2 \xi^9}{3^2 \cdot 6^2 \cdot 9^2} - \cdots \right)$$

and this function is shown in Fig. 2. The amplitude of this mode is governed by the magnitude of the trailing edge force P by reference to equations (12) and (35). If $P < W$ (the all-up weight), then $\alpha(1) > 0$. If $P > W$, then $\alpha(1) < 0$, but this condition on the control force is impractical since it implies that all the lift is generated on the controls. However, for a sample calculation, for the sake of simplicity, we may take the case when $P = W$; then $\alpha(1)$ is zero, so that, from equation (35),

$$\alpha_0 = \frac{3{\cdot}43\sigma}{K\pi\rho V_c^2}$$

where V_c is the critical speed. This equilibrium position is shown in Fig. 3, together with the attitude when P is zero.

A more concise solution of equation (33) may be obtained directly in terms of Bessel functions; this is shown in Appendix I.

4. Slender Delta Plate Wing (Non-Linear Aerodynamics)

The case with the non-linear aerodynamic loading is now considered, that is, the full equation (29). Experience in the solution of the linear case (equation (33)) shows immediately that the non-linear case also has a similar trivial solution, that is,

$$\alpha\left(1 + \frac{2}{\pi K}|\alpha|\right) = \text{constant} = \frac{\Lambda_1}{\Lambda} = \frac{\sigma}{K\pi\rho V^2} . \quad . \quad . \quad . \quad (39)$$

There is only one positive attitude α_0 which satisfies equation (39). Physically there is again no deformation because the aerodynamic loading and weight distribution balance. The presence of the vortices does not alter the distribution of loading; only the intensity of loading is affected, so that the plate with the leading-edge vortices takes up a smaller incidence than the plate without leading-edge vortices.

The determination of an equivalent to the critical speed, including the effects of the leading-edge vortices, by the general solution of equation (29) is difficult and has not been fully solved. The difficulty arises because of the $|\alpha|$ term, when $\alpha(\xi)$ might be expected to change from a positive value at $\xi = 0$ to a negative value at $\xi = 1$, for large values of the control force P. However, if it is assumed that α does not change sign, the method of series can be applied and the solution will then only be valid when the control force P is less than W, which is not a severe practical imposition.

The series solution of equation (29), assuming that $\alpha(\xi)$ is positive, is

$$\alpha(\xi)=\alpha_0-\left[\Lambda\alpha_0\left(1+\frac{2}{\pi K}\alpha_0\right)-\Lambda_1\right]\left[\frac{\xi^3}{3^2}-\frac{\Lambda}{3^2\cdot 6^2}\left(1+\frac{4}{\pi K}\alpha_0\right)\xi^6+\right.$$

$$\left.+\frac{\Lambda^2}{3^2\cdot 6^2\cdot 9^2}\left(1+\frac{16}{\pi K}\alpha_0+\frac{32}{\pi^2K^2}\alpha_0^2-\frac{8\Lambda_1}{\pi K\Lambda}\right)\xi^9-\ldots\ldots\right] \quad . \quad (40)$$

and the boundary condition gives

$$\left[\Lambda\alpha_0\left(1+\frac{2}{\pi K}\alpha_0\right)-\Lambda_1\right]\left[\frac{1}{3}-\frac{\Lambda}{3^2\cdot 6}\left(1+\frac{4}{\pi K}\alpha_0\right)+\right.$$

$$\left.+\frac{\Lambda^2}{3^2\cdot 6^2\cdot 9}\left(1+\frac{16}{\pi K}\alpha_0+\frac{32}{\pi^2K^2}\alpha_0^2-\frac{8\Lambda_1}{\pi K\Lambda}\right)-\ldots\ldots\right]=0. \quad . \quad (41)$$

Obviously equation (39) represents one solution of equation (41), but equation (41) opens up many further interesting points. For example, it is now possible that for each value of Λ there are, at least, two values of α_0 which satisfy equation (41), obtained by equating both brackets separately to zero.

Now there is at least one value of Λ when both brackets are identically zero; this is given by the simultaneous conditions that

$$\alpha_0\left(1+\frac{2}{\pi K}\alpha_0\right)=\frac{\Lambda_1}{\Lambda}$$

and $$\frac{1}{3}-\frac{\Lambda\{1+4\alpha_0/(\pi K)\}}{3^2\cdot 6}+\frac{[\Lambda\{1+4\alpha_0/(\pi K)\}]^2}{3^2\cdot 6^2\cdot 9}-\ldots\ldots=0. \quad . \quad . \quad (42)$$

By reference to equation (37), and its solution in equation (38), these two conditions (42) become

$$\left.\begin{aligned}\alpha_0\left(1+\frac{2\alpha_0}{\pi K}\right)&=\frac{\Lambda_1}{\Lambda}\\ \text{and}\quad \Lambda\left(1+\frac{4\alpha_0}{\pi K}\right)&=33\end{aligned}\right\} \quad . \quad . \quad . \quad . \quad . \quad . \quad (43)$$

Thus, by solving these two equations, we obtain both the incidence $\alpha(\equiv\alpha_0)$ and the speed condition Λ at which the trailing edge boundary condition is "doubly" satisfied.

As an example, if we take $\Lambda_1=3{\cdot}6$ and $2/(\pi K)=2{\cdot}5$, then the unique solution of equations (43) is

$$\left.\begin{aligned}\Lambda&=19{\cdot}6\\ \alpha(\xi)=\alpha_0&=0{\cdot}137\end{aligned}\right\} \quad . \quad . \quad . \quad . \quad . \quad . \quad (44)$$

When $\Lambda < 19{\cdot}6$, two equilibrium positions may exist. If we take the speed given by $\Lambda = 16{\cdot}5$, the first bracket in equation (41) gives

$$\alpha_0 (1 + 2{\cdot}5\alpha_0) = 0{\cdot}22$$

with its associated deformation solution

$$\alpha(\xi) \equiv \alpha_0 = 0{\cdot}16. \quad . \quad . \quad . \quad . \quad . \quad (45)$$

The second bracket in equation (41) gives

$$\left\{1 - \frac{16{\cdot}5\,(1 + 5\alpha_0)}{3\,.\,6} + \frac{(16{\cdot}5)^2}{3\,.\,6^2\,.\,9}(1 + 20\alpha_0 + 50\alpha_0^2 - 2{\cdot}18) - \ldots\ldots\right\} = 0.$$

The solution of this equation is approximately

$$\alpha_0 = 0{\cdot}20 \quad . \quad . \quad . \quad . \quad . \quad . \quad (46)$$

so that, on substitution into equation (40), a second deformation solution is

$$\alpha(\xi) = 0{\cdot}20\,[1 - 0{\cdot}75\xi^3 + 0{\cdot}69\xi^6 - 0{\cdot}305\xi^9 + \ldots\ldots]. \quad . \quad . \quad (47)$$

This series is convergent and $\alpha(\xi) > 0$ for $0 \leqslant \xi \leqslant 1$, so that the solution is valid. Thus, equations (45) and (47) are the two equilibrium positions for the speed given by $\Lambda = 16{\cdot}5$.

It is also apparent that in a case where $\Lambda > 19{\cdot}1$ two finite solutions again may exist. For example if $\Lambda = 22$ then the two solutions are

$$\left.\begin{aligned} &\alpha(\xi) = 0{\cdot}125 \\ \text{and, approximately,} \quad &\alpha(\xi) = 0{\cdot}10\,[1 + 0{\cdot}97\xi^3 - 0{\cdot}89\xi^6 - 0{\cdot}36\xi^9 - \ldots\ldots] \end{aligned}\right\}. \quad (48)$$

Again, the series for the second solution is convergent and positive for $0 \leqslant \xi \leqslant 1$, so this solution is valid.

Thus it has been shown that a *delta plate* has two positions of equilibrium, at least over part of its speed range, when non-linear aerodynamics are assumed. The extreme values of Λ, either very small or very large, have not been considered, since their solution is not amenable to the technique applied here. It is established, however, that no reasonable speed exists at which an infinite number of equilibrium positions are possible, depending on the magnitude of the control force, as with linear aerodynamics.

The question which is now posed is whether both positions of equilibrium at any speed are stable. This can only be answered by reference to stability, which is outside the scope of the present paper.

5. A Numerical Method

We consider first the linear form of equation (23) which is

$$EI\alpha'(\xi) = -\rho V^2 c^2 \int_0^{\xi} l_1(\xi)\,\alpha(\xi)\,d\xi + c^3 \int_0^{\xi} d\xi_1 \int_0^{\xi_1} w(\bar{\xi})\,d\bar{\xi}. \quad . \quad . \quad (49)$$

Now, in principle, if the known functions $EI(\xi)$, $l_1(\xi)$ and $w(\xi)$ can be expanded as polynomials in ξ, then a solution can be obtained by the method of a series expansion. Some initial difficulty occurs if the polynomial for $[EI(\xi)]^{-1}$ has a radius of convergence less than unity, for then a transformation of variable is necessary. This occurs, for example, on an ogee plate (see Section 7). However, the convergence of the series for $\alpha(\xi)$ is extremely slow when $\xi = 1$ (where the boundary condition has to be applied), so the method becomes tedious. In a practical case it is possible that only discrete values of $EI(\xi)$ and $w(\xi)$ at particular points along the chord are available, so that the application of the series method becomes even more formidable. It is therefore desirable that a simple numerical technique should be introduced. Fortunately equation (49) is expressed in a suitable way for a simple step-by-step process. Starting at $\xi = 0$ with a value of $\alpha(0)$ then

$$EI(\varepsilon)\,\alpha'(\varepsilon) = -\rho V^2 c^2 \alpha(0) \int_0^{\varepsilon} l_1(\xi)\,d\xi + c^3 \int_0^{\varepsilon} d\xi_1 \int_0^{\xi_1} w(\bar{\xi})\,d\bar{\xi}. \quad . \quad . \quad (50)$$

where ε is a small value. Thus $\alpha'(\varepsilon)$ can be determined, since the other terms are calculable, and then it follows that

$$\alpha(\varepsilon) = \alpha(0) + \varepsilon\alpha'(\varepsilon). \quad . \quad . \quad . \quad . \quad . \quad (51)$$

The next step is the calculation of $\alpha'(2\varepsilon)$ from the equation

$$EI(2\varepsilon)\,\alpha'(2\varepsilon) = -\rho V^2 c^2 \left[\alpha(0) \int_0^{\varepsilon} l_1(\xi)\,d\xi + \alpha(\varepsilon) \int_{\varepsilon}^{2\varepsilon} l_1(\xi)\,d\xi\right] + c^3 \int_0^{2\varepsilon} d\xi_1 \int_0^{\xi_1} w(\bar{\xi})\,d\bar{\xi}. \quad . \quad (52)$$

This process can then be carried on until $\alpha'(1)$ is reached. This numerical method is easy to apply. The functions

$$EI(n\varepsilon), \quad \int_{n\varepsilon}^{(n+1)\varepsilon} l_1(\xi)\,d\xi \quad \text{and} \quad c^3 \int_0^{n\varepsilon} d\xi_1 \int_0^{\xi_1} w(\bar{\xi})\,d\bar{\xi}$$

are predetermined from the given distributions for all the points $n\varepsilon$, where $0 \leqslant n \leqslant N$ and $N\varepsilon = 1$. In the author's applications it is assumed that $\varepsilon = 0{\cdot}1$ and, as will be seen, this seems to give reasonable accuracy. The method described in equations (50), (51) and (52) can be applied rapidly, taking about 15 minutes to reach $\xi = 1$ on a desk machine.

The basis of the method is the determination of the initial value $\alpha(0)$ which ultimately satisfies boundary condition $\alpha'(1)=0$ after the application of the numerical technique. One could repeat the process for various values of $\alpha(0)$ and so find the correct $\alpha(0)$ which gives $\alpha'(1)=0$. However, since equation (49) is linear, the problem may be reduced to two independent problems, by noting that the complementary solution of the equation

$$EI\alpha'(\xi) = -\rho V^2 c^2 \int_0^{\xi} l_1(\xi)\,\alpha\, d\xi \quad . \quad . \quad . \quad . \quad (53)$$

may be added to any particular solution of equation (49). Thus, the numerical technique can be applied to equation (53) to find a function $\alpha_c(\xi)$, assuming initially

$$\alpha_c(0)=1 \quad . \quad . \quad . \quad . \quad . \quad . \quad (54)$$

and so determining $\alpha_c'(1)$. Then the technique can be applied to equation (49) to find a function $\alpha_p(\xi)$, assuming

$$\alpha_p(0)=0 \quad . \quad . \quad . \quad . \quad . \quad . \quad (55)$$

and so determining $\alpha_p'(1)$. Therefore, if the constant a_0 is determined from the condition

$$a_0\alpha_c'(1)+\alpha_p'(1)=0, \quad . \quad . \quad . \quad . \quad . \quad (56)$$

then the solution of equation (49) which satisfies the boundary condition $\alpha'(1)=0$ is

$$\alpha(\xi)=a_0\alpha_c(\xi)+\alpha_p(\xi). \quad . \quad . \quad . \quad . \quad (57)$$

One important point which arises directly from equation (56) is that, when

$$\alpha_c'(1)=0, \quad . \quad . \quad . \quad . \quad . \quad . \quad (58)$$

a_0 becomes infinite, assuming that $\alpha_p'(1)$ is non-zero. This, therefore, is the condition for the maximum trim speed at which a total loss of control power occurs. The deformation will tend to infinity as the speed approaches this critical condition. This is the phenomenon discussed in relation to Model 5 of Part I (Ref. 1). Thus the determination of the maximum trim speed in this linear case may be considered (equation (53)) independently of the overall deformation problem. Numerically the maximum trim speed is determined by applying the numerical method to equation (53) at increasing speeds until the boundary condition (equation (58)) is satisfied.

Although the delta plate wing is a special case, it illustrates the points already discussed. First, the accuracy of the numerical method can be assessed by comparison with the exact solution given in Section 2. The numerical method gives

$$\Lambda=32{\cdot}5 \quad . \quad . \quad . \quad . \quad . \quad . \quad (59)$$

for the maximum trim speed. This is approximately 2 per cent different from the

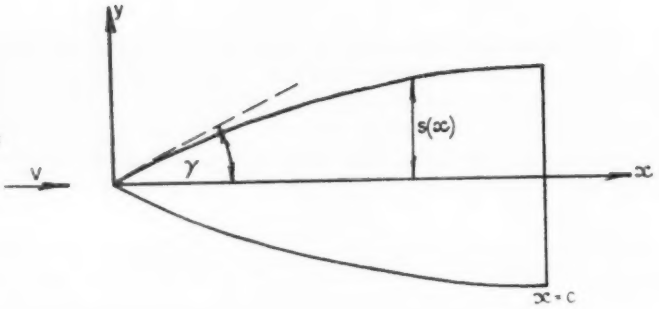

FIGURE 4. Gothic plate.

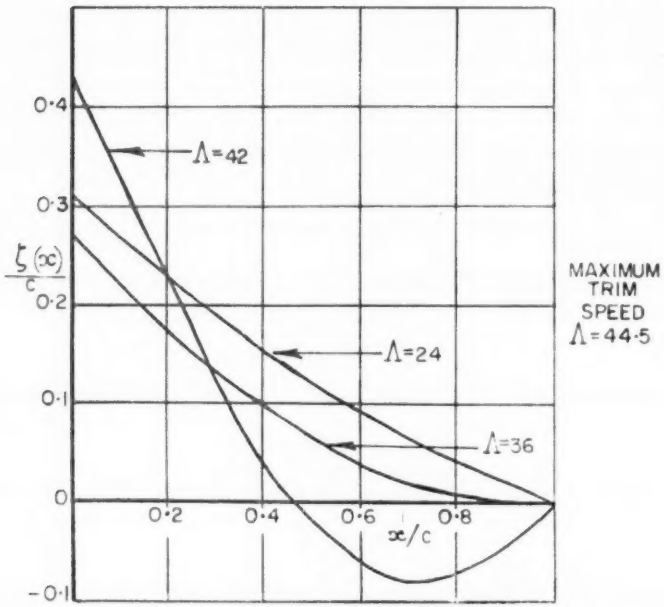

FIGURE 5. Equilibrium shapes for gothic plate (linear aerodynamics).

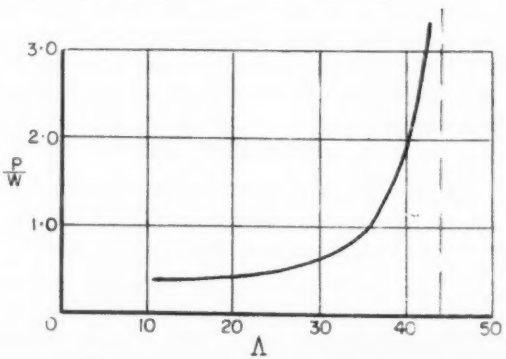

FIGURE 6. Variation of control force for gothic plate (linear aerodynamics).

exact value (equation (38)). A comparison of the approximate and exact deformation modes is given in Fig. 2, indicating reasonable agreement. At speeds below the maximum trim speed, the application of the numerical method, as described in the discussion of equations (54), (55) and (56), gives the result

$$\alpha'(n\varepsilon)\equiv 0 \qquad \text{for } 0\leqslant n\leqslant N. \quad . \quad . \quad . \quad . \quad (60)$$

Thus there is no deformation, which agrees with the exact solution.

The numerical technique described in equations (50), (51) and (52) may be extended to the case with non-linear aerodynamics (equation (23)), although the simplifications described in equations (53)–(56) for the linear case cannot now be applied. Thus, at a particular speed an initial value of $\alpha(0)$ has to be guessed and $\alpha'(1)$ calculated. By the variation of the values $\alpha(0)$, the correct value of $\alpha(0)$, together with its associated mode $\alpha(\xi)$, can be found which satisfies the boundary condition $\alpha'(1)=0$. A sample calculation is indicated in Appendix II.

6. Gothic Wing (Linear Aerodynamics)

The next case which is considered is that of a plate wing with a gothic plan form (Fig. 4) given by

$$s(x)=cK\xi\left(1-\frac{\xi}{2}\right). \quad . \quad . \quad . \quad . \quad . \quad (61)$$

In this case the differential equation is

$$\xi\left(1-\frac{\xi}{2}\right)\alpha'(\xi)=-\Lambda\int_0^{\xi}\xi^2\left(1-\frac{\xi}{2}\right)^2\alpha(\xi)\,d\xi+\Lambda_1\frac{\xi^3}{3}\left(1-\frac{\xi}{4}\right). \quad . \quad (62)$$

where Λ and Λ_1 are defined in equations (30) and (31). The application of the numerical technique gives the maximum trim speed as

$$\Lambda=44{\cdot}5. \quad . \quad . \quad . \quad . \quad . \quad . \quad (63)$$

The equilibrium shapes of the wing at various values of Λ below the maximum trim speed are shown in Fig. 5. It is seen that, as Λ tends to the critical value, the deformation increases. The value of the control force P as a function of Λ is shown in Fig. 6 and its divergence is indicated.

7. Ogee Wing (Linear Aerodynamics)

To investigate further the effects of plan form on deformation characteristics, a plate wing of ogee plan form, trimmed for level flight, is now considered.

The plan form (Fig 7) is given by

$$s(x)=Kc\xi(1+\xi-\xi^2). \quad . \quad . \quad . \quad . \quad . \quad (64)$$

This introduces a slight modification to the plan form of the delta plate investigated

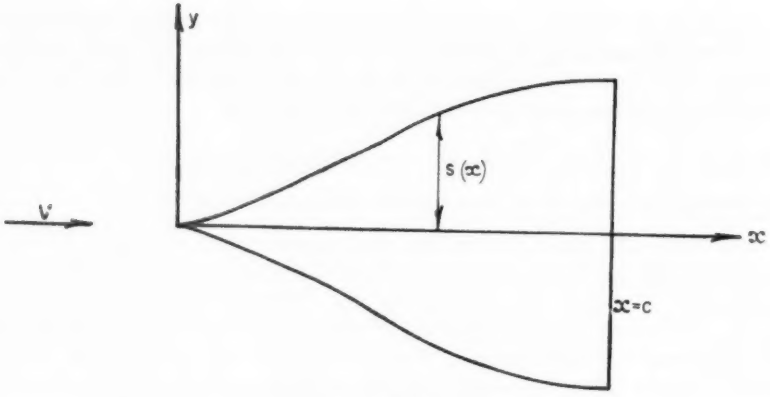

FIGURE 7. Ogee plate.

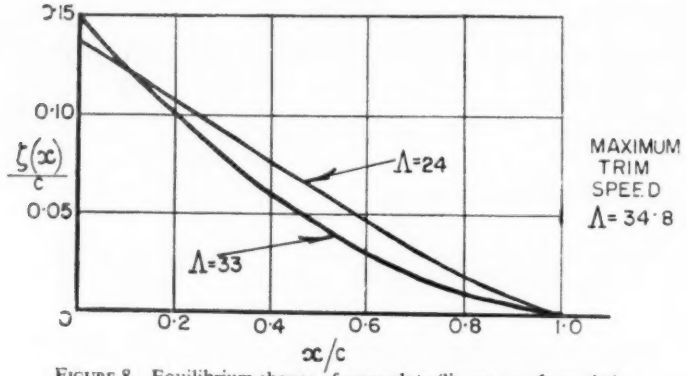

FIGURE 8. Equilibrium shapes of ogee plate (linear aerodynamics).

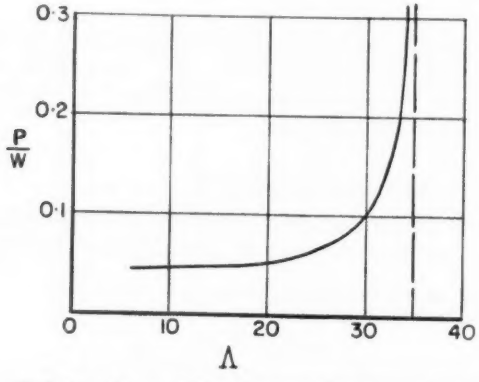

FIGURE 9. Variation of control force for ogee plate (linear aerodynamics).

in Section 3. For this case the differential equation is

$$\xi(1+\xi-\xi^2)\,\alpha'(\xi) = -\Lambda\int_0^{\xi}\xi^2(1+\xi-\xi^2)^2\alpha(\xi)\,d\xi+\Lambda_1\xi^3\left(\frac{1}{3}+\frac{\xi}{4}-\frac{\xi^2}{20}\right), \quad . \quad (65)$$

with the usual definitions of Λ and Λ_1. As mentioned previously, this equation cannot be solved as it stands by the method of series, since the term $(1+\xi-\xi^2)^{-1}$ has a radius of convergence less than unity. However, the numerical technique can be applied; this gives the maximum trim speed as

$$\Lambda = 34{\cdot}8. \quad . \quad . \quad . \quad . \quad . \quad . \quad (66)$$

The equilibrium shapes of the wing at various values of Λ below the critical values are shown in Fig. 8. The variation of the control force P as a function of Λ is shown in Fig. 9. It is seen that the rate of divergence of the control force P is rapid in the region of the critical condition. The loss of control effectiveness for trim has more significance for this ogee wing than for the gothic wing, in Section 6, where control would be lost in practice at speeds far below the critical.

8. Gothic Wing (Non-Linear Aerodynamics)

The case of the gothic wing considered in Section 5 is now extended to investigate the effects of assuming non-linear aerodynamics. The differential equation is, by reference to equations (62), (23) and (10),

$$\xi\left(1-\frac{\xi}{2}\right)\alpha'(\xi) = -\Lambda\int_0^{\xi}\xi^2(1-\xi/2)^2\alpha(\xi)\left\{1+\frac{2(1-\xi/3)}{\pi K(1-\xi/2)^2}|\alpha(\xi)|\right\}d\xi+\Lambda_1\xi^3/3(1-\xi/4).$$

$$. \quad . \quad . \quad (67)$$

It is seen from equation (67) that the shape of the wing must be further defined before any calculations may be carried out. It is now assumed that $K=\frac{1}{2}$. The procedure, as explained previously, is the calculation of the equilibrium position of the wing for low values of Λ, repeating the calculations for increasing values of Λ. This has been applied to equation (67) and the two important points which arise from these calculations are as follows:—

(*i*) For low values of Λ, two positions of equilibrium are found. This is similar to the delta wing (Section 4).

(*ii*) At a certain value of Λ there is only one position of equilibrium but, above this speed, *no position of equilibrium is possible.* This is essentially different from the delta plate case, where positions of equilibrium could always be found. There is really no resemblance to the case of the gothic wing with linear aerodynamic loading, where the deformation becomes infinite at a critical speed and there is divergence of the control force.

However, in this case with the non-linear loading, there is no divergence of the control force and the deformation is always finite but, above a certain speed, the aircraft cannot be trimmed.

The limiting speed for equation (67) is

$$\Lambda = 21{\cdot}6. \qquad (68)$$

The limiting distortion is shown in Fig. 10, together with the two positions of equilibrium at $\Lambda = 18$.

The limiting speed with linear aerodynamics is $\Lambda = 44{\cdot}5$ (equation (63)), so the limiting velocity is reduced by approximately 50 per cent by the introduction of non-linear aerodynamics. This may be significant for the aircraft which is designed to cruise without any appreciable leading-edge vorticity but will have to fly below its cruise conditions when the effects of leading-edge separations become more important.

9. Discussion

Deformation characteristics of slender plates have been discussed, assuming both linear and non-linear aerodynamics. Only the implications of these loadings have been discussed and there is no emphasis on which loading is the more practical. This is a matter for further work, but at least it is hoped that the difference between these loadings has been satisfactorily established.

With the assumption of linear aerodynamics a maximum trim condition occurs, with the aeroelastic deformation and the control force tending to infinity at the

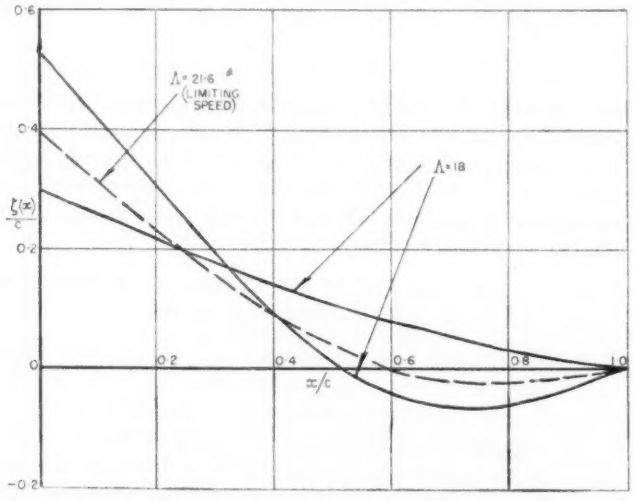

FIGURE 10. Equilibrium shapes for gothic plate (non-linear aerodynamics).

critical speed. The rate of loss of control effectiveness to trim at speeds approaching the maximum trim speed depends on the out-of-balance between the static inertia and aerodynamic loads. In the limit, when these two load distributions exactly balance, as for the delta plate, there is no deformation below a critical speed, but an infinite number of positions of equilibrium are possible at this critical speed, depending on the magnitude of the control force.

With the assumption of non-linear aerodynamics, a total loss of control effectiveness to trim apparently does not occur. Only two plate aerofoils have been investigated, a general delta (*i.e.* with variable aspect ratio) and a particular gothic (aspect ratio 3/4). Both plates have a "critical" speed at which there is only one equilibrium attitude, which is finite, and both plates have two positions of equilibrium at any speed below this "critical" speed. However, the delta plate also has two positions of equilibrium for each speed above the "critical" speed, while the gothic plate cannot be trimmed (*i.e.* no equilibrium state is possible) above its "critical" speed. Further work is needed to establish the relationship between the weight distribution and the aerodynamic loading when an upper limit on speed exists due to deformation. The study of the simple models used in this paper has enabled us to determine the trends and the fundamental aspects of the effects of the static aeroelasticity of slender configurations in level flight. The incentive to extend these ideas must come from the need to know the implications of more practical distributions of weight, bending stiffness, and so on, than are assumed in this note. The numerical method (Section 5) covers these more complicated distributions and their solution is a matter of routine calculation.

The significance of all these results is bound up with the relationship of static aeroelastic and dynamic aeroelastic effects as defined in Part I. We have only been concerned with the steady manoeuvre of trimmed flight of a slender configuration in this note. To complete our understanding of the overall picture, the distinct problem of the stability of this equilibrium solution is at present under consideration.

Appendix I

The solution of the equation (33), that is,

$$\xi\alpha' = -\Lambda \int_0^{\xi} \xi^2 \alpha \, d\xi + \frac{\xi^3}{3}\Lambda_1 \qquad . \quad . \quad . \quad . \quad . \quad (69)$$

may be expressed directly in terms of Bessel functions.

On differentiation with respect to ξ,

$$\xi\alpha'' + \alpha' + \Lambda\xi^2\alpha = \Lambda_1\xi^2. \qquad . \quad . \quad . \quad . \quad . \quad (70)$$

where the boundary conditions are

$$\alpha'(0) = \alpha'(1) = 0. \qquad . \quad . \quad . \quad . \quad . \quad (71)$$

The substitution $$\xi = u^2/3 \qquad (72)$$

in equation (70) gives

$$\alpha'' + \frac{1}{u}\alpha' + a_1\alpha = a_2 \qquad (73)$$

where $a_1 = 4\Lambda/9$, $a_2 = 4\Lambda_1/9$, and the prime (′) denotes differentiation with respect to u.

The solution of (73) which is finite for $0 \leqq u \leqq 1$ is

$$\alpha = A_1 J_0\{u\sqrt{(a_1)}\} + a_2/a_1 \qquad (74)$$

where A_1 is a constant.

The boundary conditions are

$$\frac{d\alpha}{du} = 0 \text{ where } u = 0 \text{ and } u = 1. \qquad (75)$$

Now $$\frac{d\alpha}{du} = -\sqrt{(a_1)}\, A_1 J_1\{u\sqrt{(a_1)}\}.$$

Therefore $d\alpha/du = 0$ as $u \longrightarrow 0$, since $J_1 \longrightarrow 0$. And, since $d\alpha/du = 0$ at $u = 1$, then either $A_1 = 0$ or $J_1\{\sqrt{(a_1)}\} = 0$. The solution $A_1 = 0$ in equation (74) gives the equivalent shape with no deformation. The fundamental solution of $J_1\{\sqrt{(a_1)}\} = 0$ is $\sqrt{(a_1)} = 3{\cdot}83$, which leads to $\Lambda = 33$. This agrees with the series solution (equation (38)). It is noted that higher mode solutions are available at approximately $\sqrt{(a_1)} = 7{\cdot}0$, $10{\cdot}2$, $13{\cdot}3$, etc.

Appendix II

Application of the Numerical Technique to the Gothic Plate with Non-Linear Aerodynamics

The equation to be solved is equation (67), namely

$$\alpha'(\xi) = \frac{1}{\xi(1-\xi/2)}\left\{-\Lambda\int_0^{\xi}\xi^2(1-\xi/2)^2\alpha\left[1+\frac{4}{\pi}\frac{(1-\xi/3)}{(1-\xi/2)^2}\,|\,\alpha\,|\right]d\xi + \Lambda_1\frac{\xi^3}{3}\left(1-\frac{\xi}{4}\right)\right\}$$

with the boundary condition

$$\alpha'(1) = 0.$$

The numerical technique which is to be applied to this equation is described in Section 5. This is a step-by-step process, from $\xi = 0$ to $\xi = 1$ and in steps of $\varepsilon = 0{\cdot}1$.

TABLE I

ξ	$\xi(1-\xi/2)$	$\frac{4}{\pi}\frac{(1-\xi/3)}{(1-\xi/2)^2}$	$\xi^3(1-\xi/4)$	$60\int_{(n-1)\epsilon}^{n\epsilon}\xi^2(1-\xi/2)^2 d\xi$
0·0	0·000	1·273236	0·0	
0·1	0·095	1·363762	0·000975	0·0185
0·2	0·180	1·467103	0·0076	0·1177
0·3	0·255	1·586038	0·024975	0·2845
0·4	0·320	1·724175	0·0576	0·4876
0·5	0·375	1·886274	0·109375	0·7011
0·6	0·420	2·078753	0·1836	0·9066
0·7	0·455	2·310409	0·282975	1·0954
0·8	0·480	2·593628	0·4096	1·2710
0·9	0·495	2·946330	0·564975	1·4504
1·0	0·500	3·395296	0·75	1·6672

To start with it is necessary to compute the functions

$$\left[\xi\left(1-\frac{\xi}{2}\right)\right]_{n\epsilon},\quad \left[\frac{4}{\pi}\frac{(1-\xi/3)}{(1-\xi/2)^2}\right]_{n\epsilon},\quad \int_{(n-1)\epsilon}^{n\epsilon}\xi^2\left(1-\frac{\xi}{2}\right)^2 d\xi,\quad \left[\frac{\xi^3}{3}\left(1-\frac{\xi}{4}\right)\right]_{n\epsilon}$$

where $0 \leqslant n \leqslant 10$. These are indicated in Table I.

A sample calculation for $\Lambda = 18$ and $\Lambda_1 = 3{\cdot}6$, assuming the initial value $\alpha(0) = 0{\cdot}4$, is as follows:—

$\alpha(0) = 0{\cdot}4$; $\quad \alpha'(0{\cdot}1) = \frac{1}{0{\cdot}095}\left[-\frac{18}{60}(0{\cdot}011169) + 1{\cdot}2\,(0{\cdot}000975)\right] = -0{\cdot}022955$

$\alpha(0{\cdot}1) = 0{\cdot}397705$; $\quad \alpha'(0{\cdot}2) = \frac{1}{0{\cdot}18}\,[-0{\cdot}3\,(0{\cdot}083367) + 1{\cdot}2\,(0{\cdot}0076)] = -0{\cdot}088273$

$\alpha(0{\cdot}2) = 0{\cdot}378878$; $\quad \alpha'(0{\cdot}3) = \frac{1}{0{\cdot}255}\,[-0{\cdot}3\,(0{\cdot}251073) + 1{\cdot}2\,(0{\cdot}024945)] = -0{\cdot}177851$

$\alpha(0{\cdot}3) = 0{\cdot}361093$; $\quad \alpha'(0{\cdot}4) = \frac{1}{0{\cdot}32}\,[-0{\cdot}3\,(0{\cdot}527978) + 1{\cdot}2\,(0{\cdot}0576)] = -0{\cdot}278979$

$\alpha(0{\cdot}4) = 0{\cdot}333195$; $\quad \alpha'(0{\cdot}5) = \frac{1}{0{\cdot}375}\,[-0{\cdot}3\,(0{\cdot}895782) + 1{\cdot}2\,(0{\cdot}109375)] = -0{\cdot}366625$

$\alpha(0{\cdot}5) = 0{\cdot}296533$; $\quad \alpha'(0{\cdot}6) = \frac{1}{0{\cdot}42}\,[-0{\cdot}3\,(1{\cdot}314990) + 1{\cdot}2\,(0{\cdot}1836)] = -0{\cdot}414707$

$\alpha(0{\cdot}6) = 0{\cdot}255052$; $\quad \alpha'(0{\cdot}7) = \frac{1}{0{\cdot}455}\,[-0{\cdot}3\,(1{\cdot}742001) + 1{\cdot}2\,(0{\cdot}282975)] = -0{\cdot}402594$

$\alpha(0{\cdot}7) = 0{\cdot}214793$; $\quad \alpha'(0{\cdot}8) = \frac{1}{0{\cdot}48}\,[-0{\cdot}3\,(2{\cdot}150483) + 1{\cdot}2\,(0{\cdot}4096)] = -0{\cdot}320051$

$\alpha(0{\cdot}8) = 0{\cdot}182783$; $\quad \alpha'(0{\cdot}9) = \frac{1}{0{\cdot}495}\,[-0{\cdot}3\,(2{\cdot}541274) + 1{\cdot}2\,(0{\cdot}564975)] = -0{\cdot}170529$

$\alpha(0{\cdot}9) = 0{\cdot}165730$; $\quad \alpha'(1{\cdot}0) = \frac{1}{0{\cdot}5}\,[-0{\cdot}3\,(2{\cdot}952497) + 1{\cdot}2\,(0{\cdot}75)] = +0{\cdot}285.$

This process can be written down as shown, with the aid of a desk machine, in about 15 minutes. By varying $\alpha(0)$, the associated value of $\alpha'(1)$ can be found. By plotting $\alpha(0)$ against $\alpha'(1)$, the values of $\alpha(0)$ for which $\alpha'(1)$ is zero can be determined, and so can the corresponding mode.

REFERENCES

1. HANCOCK, G. J. Static Aeroelastic Distortion of Slender Configurations. Part I. *Aeronautical Quarterly*, Vol. XII, p 293, August 1961.
2. JONES, R. T. Properties of Low Aspect Ratio Pointed Wings at Speeds Below and Above the Speed of Sound. N.A.C.A. Report 835, 1946.
3. MANGLER, L. W. and SMITH, J. H. A Theory of Flow past a Slender Delta Wing with Leading Edge Separation. *Proc. Roy. Soc.* A, 251, May 1959.
4. MASKELL, E. C. and WEBER, J. On the Aerodynamic Design of Slender Wings. *Journal of the Royal Aeronautical Society*, December 1959.

The Correlation of Unstable Crack Length Data for Sheet Materials

E. R. WELBOURNE

(Technical Department, Royal Aeronautical Society)

SUMMARY: A semi-empirical analysis of unstable crack propagation in thin sheets is given. An effective value of the crack tip strain concentration factor is used as the criterion for instability. Good correlation is achieved with experimental results from unreinforced sheets of aluminium and titanium alloys and high-strength steels. The interdependence of geometry and stress-strain curve properties in determining the unstable crack propagation characteristics of sheet materials is illustrated in an appendix.

1. Introduction

Fracture mechanics has been a subject of some interest to the aircraft structures engineer for a number of years past. However, the problem of predicting the relationship between unstable crack length and stress for a fatigue crack in a structure is still far from solution in any general case. All theoretical analyses of the basic problem depend on at least one empirically determined parameter[1, 2, 3] and many purely empirical methods are in use. The mechanism of stable crack propagation is not properly understood although a tentative model has been proposed[4].

Deficiencies in the basic theory and reliance on purely empirical representation have tended to obscure certain important features of the experimental data which have been collected. This is particularly so in regard to unstable crack length results obtained from unreinforced sheets. In this note an attempt is made to show how such results can be correlated with a simple semi-empirical analysis, and to indicate the factors influencing the unstable crack propagation characteristics of various materials.

2. Basic Theoretical Considerations

In order to be quite clear about the initial assumptions of the analysis method proposed, brief consideration of basic principles is necessary.

For unstable propagation of a crack in any material two conditions must be satisfied.

(*a*) The strain at the crack tip must be high enough to cause fracture of the material.

(*b*) The energy released during an incremental advance of the crack tip must just exceed the energy absorbed in this advance.

Received October 1961.

In a material which fails elastically, *i.e.* without experiencing plastic deformation, these conditions are satisfied simultaneously; in a real material condition, (*a*) is satisfied before condition (*b*), in general, giving rise to a period of stable crack growth. However, if the stable crack growth period is neglected, then the two conditions are assumed to be satisfied simultaneously. By this assumption either one is then a sufficient condition for instability. Existing analyses invariably disregard the slow growth period and, in view of this, it is perhaps surprising that so much work has been based on theoretical analysis of condition (*b*). Approximate theoretical analysis of condition (*a*) is considerably simpler and less restricted in application. Furthermore, such an analysis requires only the normal engineering concepts of stress and strain, avoiding the obscurity of some of the material properties encountered in an energy analysis. For these reasons an approximate theoretical analysis of condition (*a*) is used in correlating the experimental results.

NOTATION

a length of sheet in direction of applied load (in.)

b width of sheet (in.)

t thickness of sheet (in.)

E modulus of elasticity of sheet material (lb./in.^{2})

f_t tensile strength of sheet material (lb./in.^{2})

f_p 0·2 per cent proof strength of sheet material (lb./in.^{2})

ε_{max} nominal elongation of sheet material

m material characteristic

r effective radius of crack tip (in.)

f average stress on net area of sheet (lb./in.^{2})

f_0 average stress on gross area of sheet (lb./in.^{2})

ε average strain corresponding with stress f

k effective strain concentration factor for crack

x_u unstable crack length (in.)

3. Analysis

3.1. BASIC EQUATION

Unstable propagation of the crack is assumed to occur when

$$k\varepsilon = \frac{f_t}{E} + \varepsilon_{max}, \qquad . \quad . \quad . \quad . \quad (1)$$

i.e. when the crack tip strain reaches the maximum elastic-plus-plastic strain of which the sheet material is capable. For convenience in calculation, maximum stress and maximum strain are taken to be coincident on the stress-strain curve. It

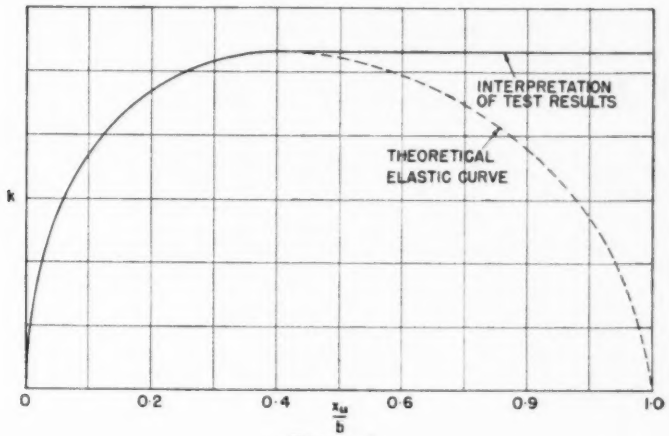

FIGURE 1.

is further assumed that nominal material properties can be applied when considering the highly localised region around the crack tip. This is possible since k values are determined empirically.

3.2. DETERMINATION OF k

In calculating values of the effective strain concentration factor k, two preliminary assumptions are made.

(*i*) The effective radius of the fatigue crack r is a constant for the material.

(*ii*) The expression for k found by elastic analysis is valid for large plastic strains.

On this basis, for a central crack in a sheet of finite width subject to a uniform tensile stress normal to the line of the crack,

$$k = \left\{1 + 2\left(\frac{x_u}{2r}\right)^{1/2}\right\} \cdot \left\{\frac{1-(x_u/b)}{1+(x_u/b)}\right\}^{1/2} \quad . \quad . \quad . \quad . \quad (2)$$

using the well-known expression for the infinite sheet modified for finite width, as in Ref. 5. Fig. 1 shows k as a function of x_u/b for some arbitrary values of b and r. For values of x_u/b less than about 0·4, equation (2) agrees closely with the strain concentration factor derived from actual tests on cracked sheets by using equation (1). For values of x_u/b greater than this, however, the decrease in k predicted by elastic theory is not in agreement with k values derived from actual test results, which remain approximately constant, as indicated in the figure. As far as is known, no independent evidence of this effect exists and its interpretation in terms of a constant value of strain concentration is open to question. However, within the framework of this analysis, it can be accepted insofar as it must give the right answer.

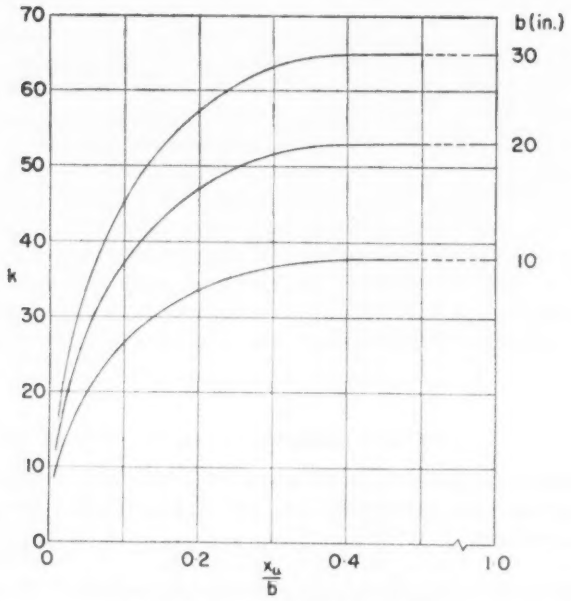

FIGURE 2. k for aluminium alloys.

Figures 2, 3 and 4 give values of k for three materials computed on the basis given in the previous paragraph, using a value of r for each material chosen empirically to fit the available unstable crack length results. Some limitations on the application of these curves must be noted.

No allowance is made for the variation of strength of centrally cracked plates with thickness, which arises from buckling of the crack edges. The curves given correspond with a sheet thickness of about 0·064 in. and predictions of unstable crack length in thinner sheets based on these k values may be slightly unconservative. Conversely, conservative results will be obtained for thicker sheets.

The effect of sheet aspect ratio has been neglected by assuming uniformity of the stress field to be achieved between the ends of the sheet and the crack region. This implies a value of a/b of about 2 or greater. Results obtained from square sheets tend to be influenced by the end conditions.

Values of k are quoted for sheets up to 30 in. wide. Data for sheets wider than this are scarce for aluminium alloys and virtually non-existent for steel and titanium. Figures 3 and 4 are based on results from 10 in. wide sheets only. Extrapolation of the analysis to sheet widths over about 30 in. leads to substantially conservative results when the unstable length exceeds about 12 in. in aluminium alloy materials. For short cracks in very wide sheets, values of k calculated by equation (2) must still be valid.

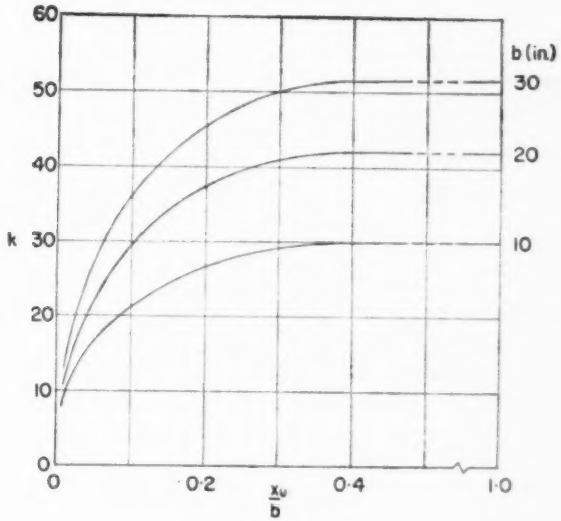

FIGURE 3. k for titanium alloys.

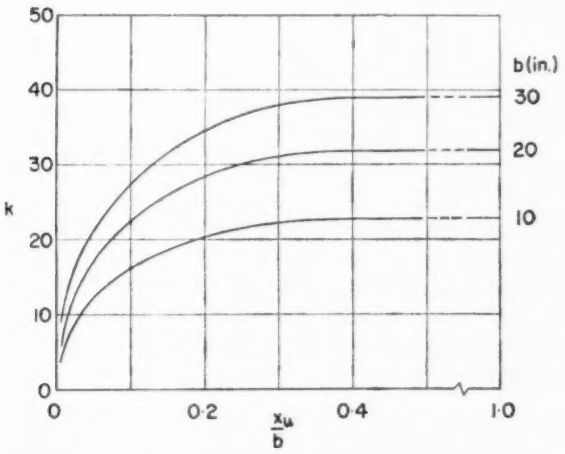

FIGURE 4. k for high-strength steels.

3.3. SOLUTION OF BASIC EQUATION

It is clear from equation (1) that, in order to derive a relationship between stress and crack length, knowledge of the material stress-strain curve is required. If the complete curve is available, having found the appropriate value of k, equation (1) can be solved for ε and the corresponding stress f read from the curve.

If the curve is not available, as is generally the case, and only normal material properties are known, use can be made of the generalised stress-strain relationship given in R.Ae.S. Structures Data Sheet 00.02.04.

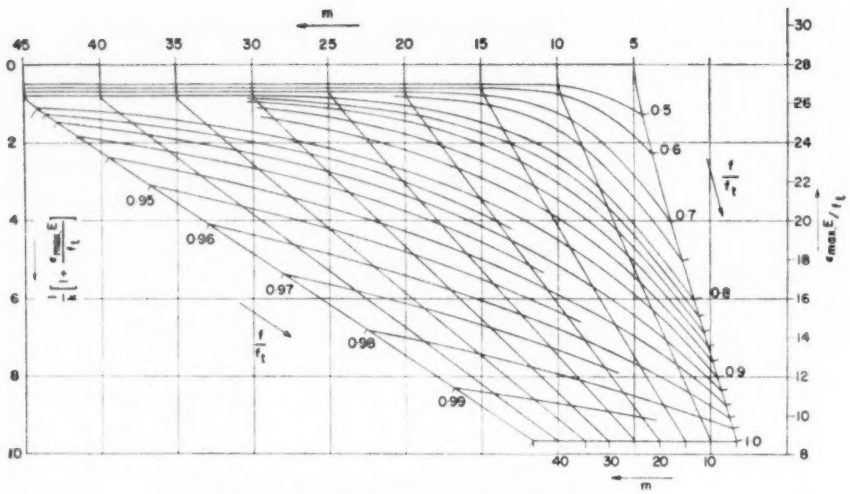

FIGURE 5. Nomogram solution of equation (4).

This relationship is

$$\varepsilon = \frac{f}{E} + \varepsilon_{max}\left(\frac{f}{f_t}\right)^m \quad . \quad . \quad . \quad . \quad . \quad (3)$$

Substitution into equation (1) with some transposition gives

$$\frac{f}{f_t} + \frac{\varepsilon_{max} E}{f_t}\left(\frac{f}{f_t}\right)^m = \frac{1}{k}\left(1 + \frac{\varepsilon_{max} E}{f_t}\right). \quad . \quad . \quad (4)$$

Figure 5 is a nomogram solution of this equation. When values of f_t, ε_{max}, E and m are known for the material and k has been found from the appropriate figure, the net area stress f can be determined from the nomogram. This figure is reproduced from R.Ae.S. Structures Data Sheet 00.02.05 with the notation suitably modified. Reference should be made to this sheet and to Data Sheet 00.02.04 for detailed information on this method of solution.

3.4. CORRELATION WITH EXPERIMENTAL RESULTS

Figures 6 to 11 show curves of gross area stress against unstable crack length for several materials and sheet sizes. All curves were derived using values of k obtained from Figs. 2, 3 and 4 and stress-strain properties from control tests on the material from which the experimental results were obtained. Within the limitations of the available experimental data these figures show materials of markedly different characteristics. It is important to realise that differences in the relationship between stress and unstable crack length for different alloys of the same basic group result entirely from differences in their stress-strain curves. The effect of the stress-strain curve parameters and sheet size is illustrated in the Appendix by a detailed analysis of some experimental data.

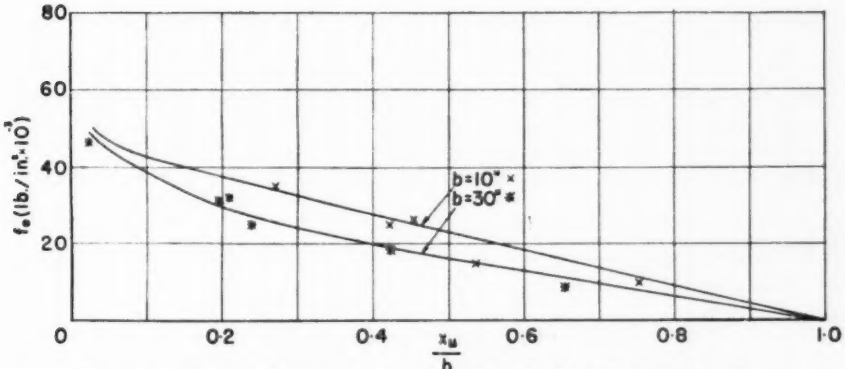

FIGURE 6. Theoretical curves and experimental results for L.72 aluminium alloy.

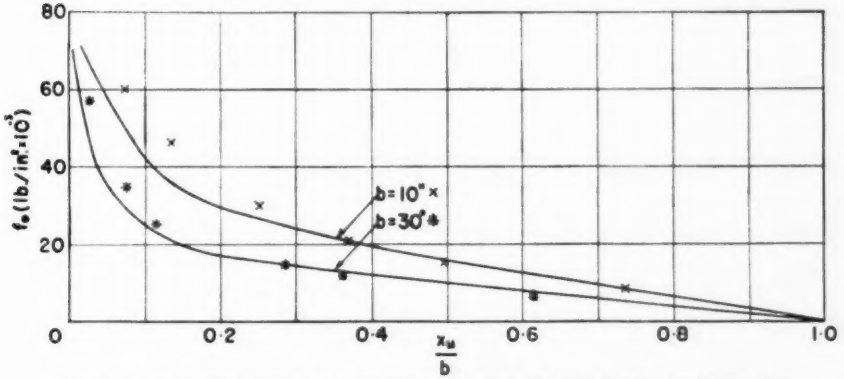

FIGURE 7. Theoretical curves and experimental results for D.T.D.687 aluminium alloy.

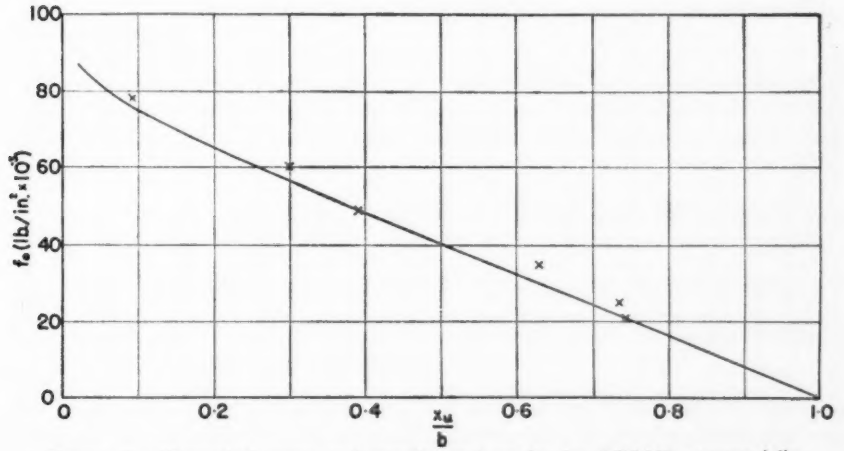

FIGURE 8. Theoretical curve and experimental results for I.C.I.160 commercially pure titanium (b=10 in.).

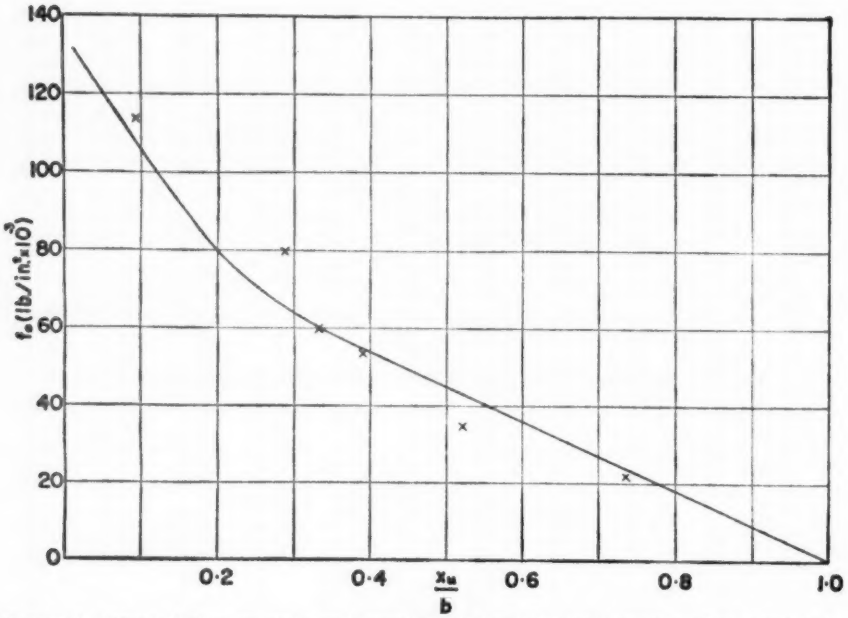

FIGURE 9. Theoretical curve and experimental results for I.C.I.318A titanium alloy ($b = 10$ in.).

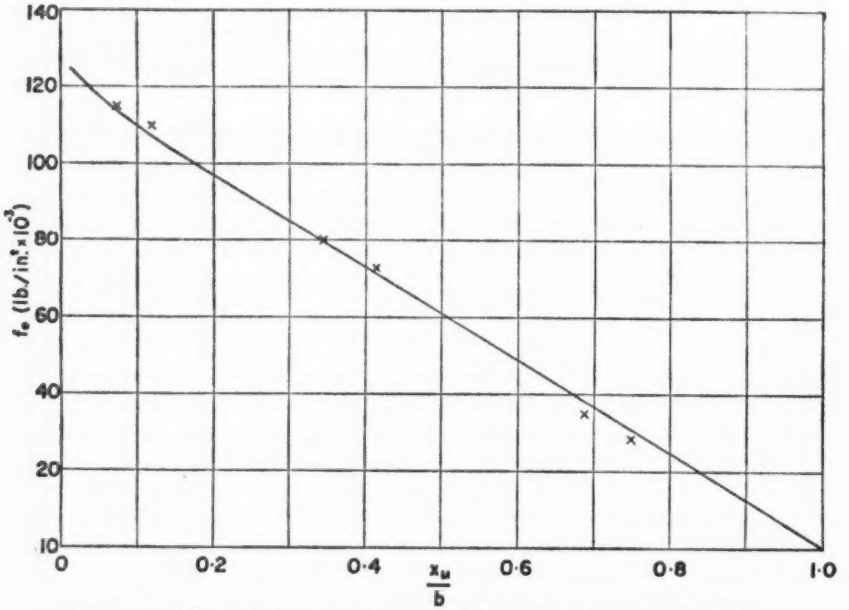

FIGURE 10. Theoretical curve and experimental results for S.520 steel ($b = 10$ in.).

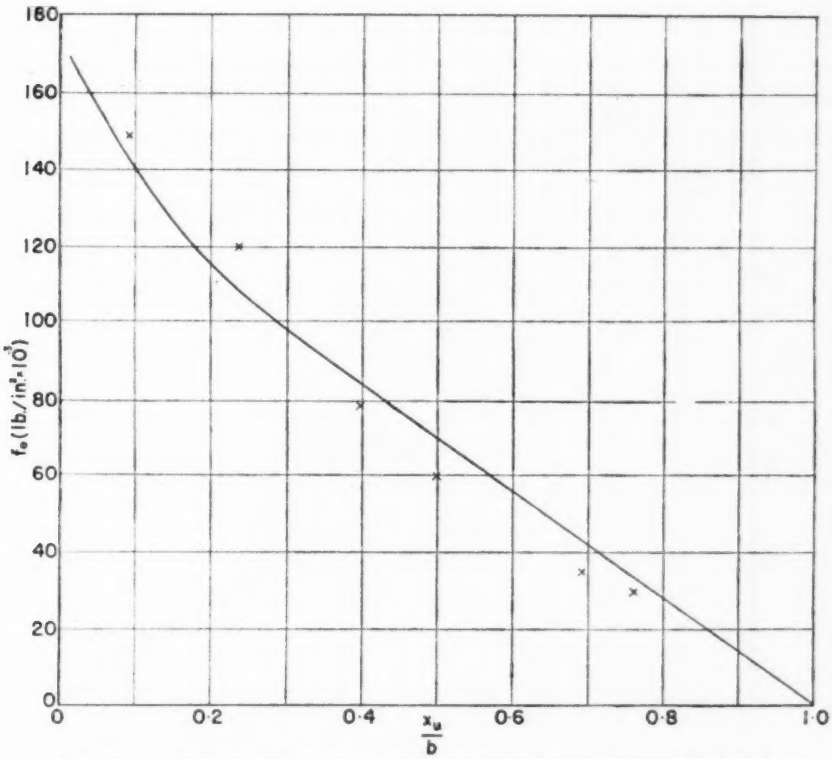

FIGURE 11. Theoretical curve and experimental results for F.V.520 steel ($b=10$ in.).

4. Discussion

In spite of the approximate nature of the analysis it is seen to agree remarkably well with experimental data from a range of typical aircraft structural materials. This shows that the relationship between unstable crack length and stress in sheet materials depends on three factors.

(1) The inherent "sharpness" of the fatigue crack—essentially a property of the material

(2) The geometry of the sheet as it affects the strain distribution

(3) The material stress-strain curve properties, principally elongation and proof/ultimate ratio.

The basic principle may be applied to more complex two-dimensional stress systems, such as that in a sheet structure with discrete reinforcement, the only fundamental requirement being sufficient knowledge of the stress system to estimate

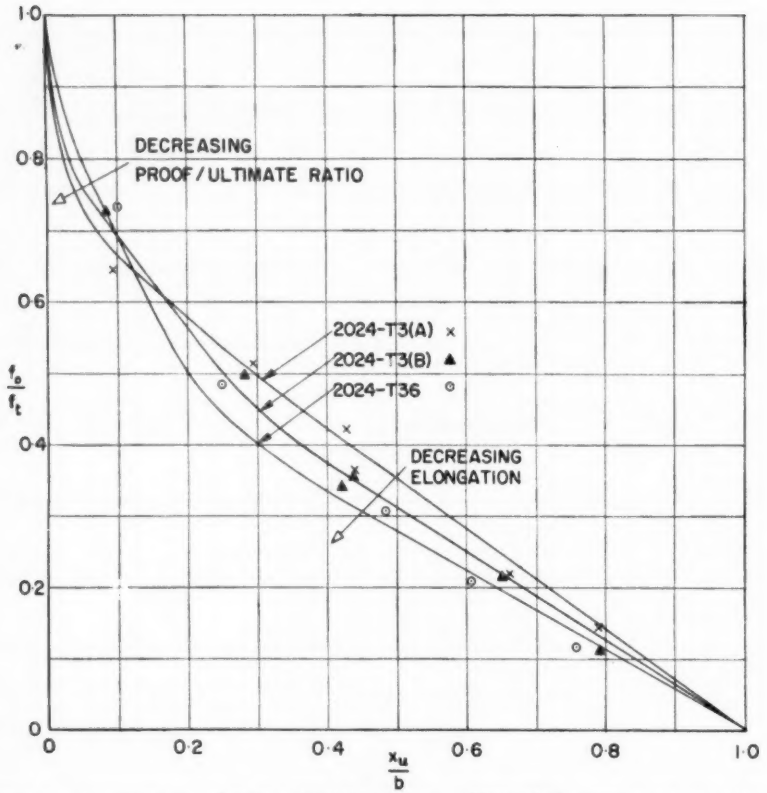

FIGURE 12. Comparison of three aluminium alloys. Theoretical curves and experimental results for 10 in. wide sheets.

k values. References 8 and 9 give this information for reinforced sheet structure. For thick plates and solid sections the influence of biaxiality on the failure condition must be considered[10].

While it is realised that this analysis is in no sense an advance on the more usual Griffith-Irwin analysis, it affords a much clearer picture of the parameters which influence the unstable crack propagation characteristics of materials. As indicated earlier, the introduction of an energy condition at instability is unnecessary if no preceding stable crack growth is considered. The present analysis has an additional slight advantage in being applicable over the whole stress range where the usual method is restricted to net area stresses below about 1·1 times the yield stress.

ACKNOWLEDGMENT

The author wishes to acknowledge the assistance given by Dr. A. J. Barrett, Head of the Technical Department, Royal Aeronautical Society, in the initial stages of the work and during preparation of this note.

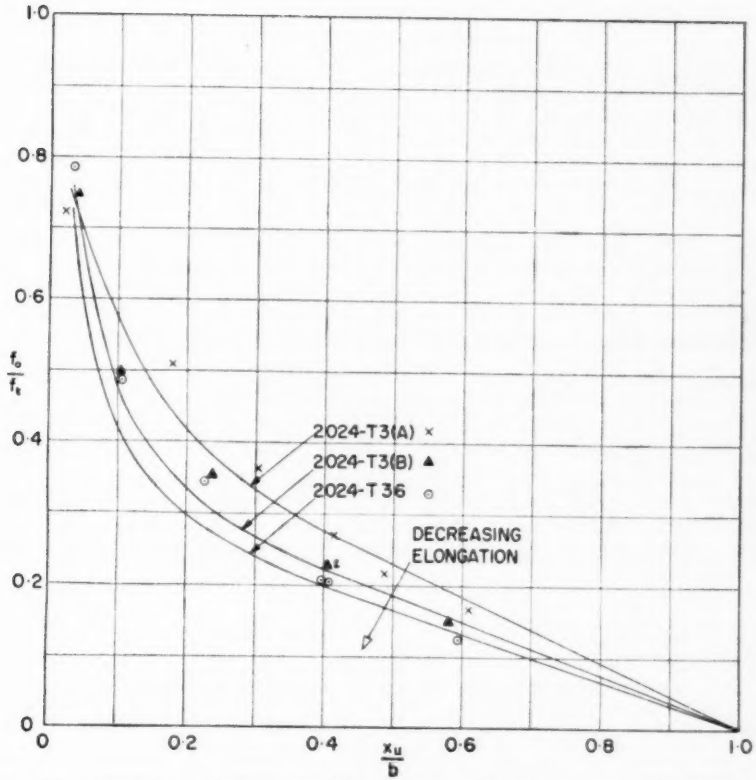

FIGURE 13. Comparison of three aluminium alloys. Theoretical curves and experimental results for 30 in. wide sheets.

Appendix

INFLUENCE OF SHEET SIZE AND STRESS-STRAIN CURVE PROPERTIES ON UNSTABLE CRACK LENGTH BEHAVIOUR

The effect of sheet size and stress-strain curve properties can be shown by detailed analysis of the data given in Ref. 7 for the alloys 2024-T3(A), 2024-T3(B) and 2024-T36. The data were obtained from tests on sheets $30\times10\times0{\cdot}064$ in. and $90\times30\times0{\cdot}064$ in. Both 2024-T3 materials were within specification but were obtained from different suppliers.

The relevant mean material properties obtained from three control tests on each material are quoted in Table I. In Table II the curve of theoretical stress against crack length is calculated for 10 in. wide sheets of each material and in Table III for 30 in. wide sheets. In these tables k values are obtained from Fig. 2 and the stress-strain relation from the mean of control test curves. Conversion from net area stress f to gross area stress f_0 is accomplished in plotting Figs. 12 and 13 which give the theoretical curves and experimental results for 10 in. and 30 in. wide sheets respectively. (A straight line

TABLE I*

STRESS-STRAIN CURVE PROPERTIES

Material	2024-T3 (A)	2024-T3 (B)	2024-T36
E (lb./in.$^2 \times 10^{-6}$)	10·6	10·2	10·3
f_t	68·2	69·9	71·7
ϵ_{max}	0·19	0·16	0·14
$f_t/E + \epsilon_{max}$	0·1964	0·1669	0·1470
f_p/f_t	0·75	0·79	0·83

TABLE II*

RELATION BETWEEN STRESS AND CRACK LENGTH FOR 10 IN. WIDE SHEETS

Material		2024-T3 (A)			2024-T3 (B)			2024-T36		
x_a/b	k	ϵ	f	f/f_t	ϵ	f	f/f_t	ϵ	f	f/f_t
0·05	19·8	0·00992	52·8	0·774	0·00843	55·7	0·797	0·00742	59·4	0·835
0·1	26·5	0·00742	51·3	0·741	0·00630	54·3	0·776	0·00555	55·4	0·771
0·2	33·6	0·00585	50·2	0·725	0·00497	49·2	0·704	0·00437	44·7	0·624
0·3	36·7	0·00536	49·2	0·711	0·00455	45·0	0·644	0·00400	41·1	0·573
0·4	37·8	0·00520	48·8	0·705	0·00441	43·8	0·626	0·00389	40·0	0·558

TABLE III*

RELATION BETWEEN STRESS AND CRACK LENGTH FOR 30 IN. WIDE SHEETS

Material		2024-T3 (A)			2024-T3 (B)			2024-T36		
x_a/b	k	ϵ	f	f/f_t	ϵ	f	f/f_t	ϵ	f	f/f_t
0·05	33·5	0·00587	50·3	0·736	0·00498	49·2	0·704	0·00439	44·7	0·623
0·1	45·2	0·00434	43·7	0·641	0·00369	37·0	0·529	0·00325	33·6	0·468
0·2	57·2	0·00343	35·5	0·520	0·00292	29·3	0·419	0·00257	26·8	0·374
0·3	63·2	0·00311	32·2	0·472	0·00264	26·6	0·381	0·00232	24·6	0·343
0·4	64·9	0·00303	31·4	0·460	0·00257	25·9	0·371	0·00226	23·7	0·330

TABLE IV*

RELATION BETWEEN STRESS AND CRACK LENGTH FOR 2 IN. WIDE SPECIMENS

Material		2024-T3 (A)			2024-T3 (B)			2024-T36		
x_a/b	k	ϵ	f	f/f_t	ϵ	f	f/f_t	ϵ	f	f/f_t
0·05	9·5	0·02067	56·0	0·821	0·01757	59·1	0·845	0·01547	64·0	0·893
0·1	12·4	0·01584	54·2	0·795	0·01346	57·7	0·825	0·01185	62·6	0·873
0·2	15·4	0·01275	53·4	0·783	0·01084	56·5	0·808	0·00955	61·0	0·851
0·3	16·8	0·01169	52·8	0·774	0·00993	56·2	0·804	0·00875	60·4	0·842
0·4	17·2	0·01142	52·7	0·773	0·00970	56·0	0·801	0·00855	60·2	0·840

*Values of f are in lb./in.$^2 \times 10^{-3}$.

joining some value of f_0 on the vertical axis to $x_u/b=1{\cdot}0$ on the horizontal axis is a line of constant net area stress, $f=f_0$.)

Considering Fig. 12, it can be seen that there are two quite distinct regions of the curves of stress against crack length. For short crack lengths and correspondingly low k values, general yielding occurs before failure in all three materials and their relative strengths are determined by their proof/ultimate ratios. For longer cracks, the value of k has increased such that the net area stresses are still below the yield region at failure; consequently the relative strengths of the materials are determined by their respective elongations.

In Fig. 13 the basic result is the same except that the general yielding region is reduced in size. Even so, the reversal of order of the three highest experimental points with respect to the elastic region confirms its effect. It is apparent that the increase in k values by a factor of approximately $\sqrt{3}$ caused by the 3:1 increase in sheet width keeps net area stress at failure substantially elastic except for cracks less than about $1\frac{1}{2}$ in. long.

It follows from the previous paragraph that, if much narrower specimens, say 2 in. wide, were tested, k values would be sufficiently low that general yielding would occur before failure, whatever the crack length. Thus, the relative strengths of the three

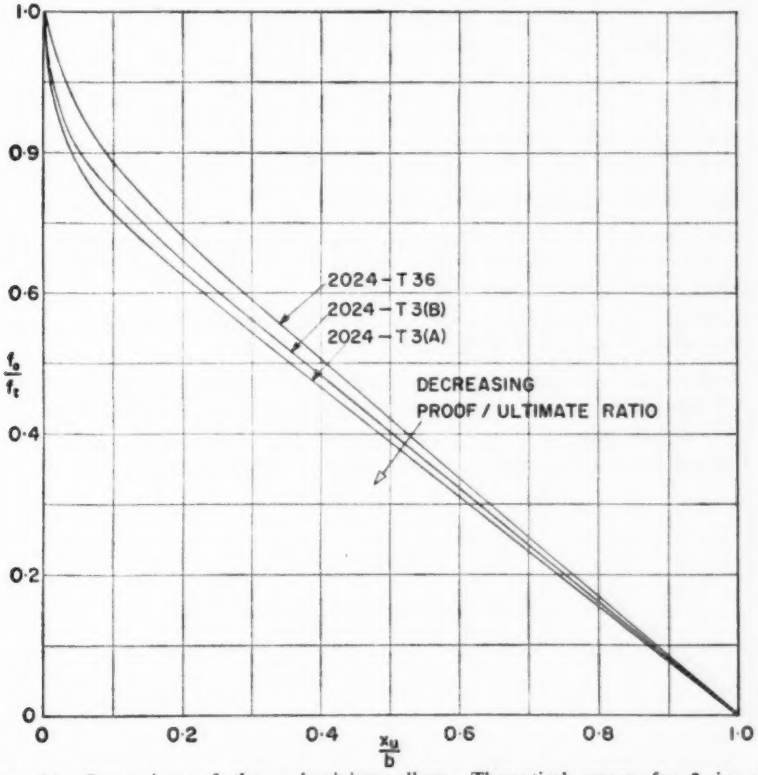

FIGURE 14. Comparison of three aluminium alloys. Theoretical curves for 2 in. wide specimens.

materials would be determined entirely by their proof/ultimate ratios, so that their apparent order of merit for crack resistance would be completely reversed to that which is observed in specimens of more practical dimensions. In Table IV, the theoretical curve of stress against crack length is calculated for 2 in. wide specimens of each material, k values being computed as in Section 3.2. The curves are plotted in Fig. 14 and show the anticipated effect.

The general conclusion from this is that comparisons of the unstable crack propagation characteristics of materials are incomplete without reference to specimen geometry and size or the amount of yielding of the uncracked section. The simple analysis proposed in this note shows the influence of these factors for the particular case of an unreinforced thin sheet.

REFERENCES

1. IRWIN, G. R. and KIES, J. A. Fracturing and Fracture Dynamics. *Welding Journal*, Vol. 31, Research Supplement, February 1952.
2. MCEVILY, A. J., ILLG, W. and HARDRATH, H. F. Static Strength of Aluminum Alloy Specimens Containing Fatigue Cracks. N.A.C.A. T.N. 3816, 1956.
3. WILLIAMS, D. Crack Propagation Properties of Thin Sheet—Some Recent Results and Their Impact on Design. A.R.C. Current Paper 564, 1961.
4. Fracture Testing of High-Strength Sheet Materials. Report of A.S.T.M. Committee, *Bulletin of the American Society for Testing Materials*, January and February 1960.
5. DIXON, J. R. Stress Distribution Around a Central Crack in a Plate Loaded in Tension; Effect of Finite Width of Plate. *Journal of the Royal Aeronautical Society*, March 1960.
6. Royal Aeronautical Society Structures Data Sheets, Vol. 1.
7. Bristol Aircraft Ltd. An Experimental Investigation into the Crack Propagation Characteristics of Sheet Materials used in Aircraft Construction. Engineering Laboratory Report 2/335/1 (Unpublished, 1959).
8. SANDERS, J. L. Effect of a Stringer on the Stress Concentration Due to a Crack in a Thin Sheet. N.A.C.A. T.N. 4207, 1957.
9. ROMUALDI, J. P., FRASIER, J. T. and IRWIN, G. R. Crack Extension Force Near a Riveted Stiffener. Naval Research Laboratory (Washington) Memorandum Report 4956, 1957.
10. ILLG, W. and MCEVILY, A. J. Static Strength of Cross-Grain 7075-T6 Aluminum Alloy Extruded Bar Containing Fatigue Cracks. N.A.C.A. T.N. 3994, 1957.

The Aeronautical Quarterly

A Journal devoted to Aeronautics and the Allied Sciences

Editorial Board

Dr. A. M. BALLANTYNE, T.D., B.Sc., Ph.D., F.R.Ae.S., Hon.F.C.A.I., F.I.A.S. (*Chairman*)

Mr. HAYNE CONSTANT, C.B., C.B.E., M.A., F.R.S., F.R.Ae.S.

Sir HAROLD ROXBEE COX, D.Sc., D.I.C., Ph.D., F.R.Ae.S., F.I.A.S.

Sir WILLIAM FARREN, C.B., M.B.E., M.A., D.Sc., F.R.S., Hon.F.R.Ae.S., Hon.F.I.A.S.

Sir ARNOLD HALL, M.A., F.R.S., F.R.Ae.S.

Sir ALFRED PUGSLEY, O.B.E., D.Sc., F.R.S., F.R.Ae.S.

Sir GEOFFREY TAYLOR, M.A., D.Sc., F.R.S., Hon.F.R.Ae.S.

Dr. P. B. WALKER, C.B.E., M.A., F.R.Ae.S.

Editor—E. C. PIKE, M.A., A.F.R.Ae.S.

VOLUME XII

FEBRUARY 1961—NOVEMBER 1961

PRINTED BY THE LEWES PRESS, WIGHTMAN & CO. LTD., FRIARS WALK, LEWES, AND PUBLISHED BY THE ROYAL AERONAUTICAL SOCIETY, 4 HAMILTON PLACE, LONDON, W.1.

NOTICE TO CONTRIBUTORS

1. All communications should be addressed to the Editor, The Aeronautical Quarterly, 4 Hamilton Place, London, W.1.

2. Papers for consideration should be typewritten with double spacing and be accompanied by a summary of not more than 250-300 words. *Papers must be as short as possible*, otherwise considerable delay in publication will result, and in any case they should not be longer than twenty foolscap pages. Full descriptions and complete results of work, as written for an internal report, are not suitable for publication in *The Aeronautical Quarterly*, and such reports need to be rewritten in concise form. Only necessary equations should be included in the text; routine mathematics should be omitted or given as an Appendix to the paper. Illustrations should be reduced to a minimum. The titles of papers should be kept short—with sub-titles if necessary.

3. Only simple symbols and formulae should be typewritten. All others should be written clearly in ink. Greek letters should be indicated and a clear distinction drawn between capital and small letters. Particular attention should be paid to the use of alpha and *a*, kappa and *k*, mu and *u*, nu and *v*, eta and *n*. The letter *l* must be distinguished from the numeral 1, and the letter *O* from the zero 0.

   The use of dots, bars, and so on, over letters, or the use of dots as multiplication signs and bars for brackets should be avoided as far as possible.

   Suffixes and prefixes must be indicated clearly and complicated suffixes and prefixes should be avoided.

4. A list of *all* symbols used, both in the illustrations and text, *must* be given whether they are standard or not.

5. *Clear* diagrams or sketches must be submitted for redrawing by the Society's draughtsman.

   Photographs must be not less than half plate size and must be clear black and white glossy prints.

6. References should be given in the form:—
   WARD, G. N. Calculation of Downwash Behind a Supersonic Wing. *The Aeronautical Quarterly*, Vol. I, p. 35, May 1949.

7. The copyright of every paper printed in *The Aeronautical Quarterly* is the property of The Royal Aeronautical Society. Permission to reprint or to use any paper will not be unreasonably refused.

8. It is a condition of publication that the author shall have obtained consent where necessary to use any material in his paper which is copyright or the property of any other person or his employers.

9. Authors will be entitled to 20 reprints of their papers free of charge. This number will be shared between joint authors.

The Aeronautical Quarterly is published at the Offices of The Royal Aeronautical Society, 4 Hamilton Place, Piccadilly, London, W.1, at 15s. 0d. net for a single number to non-members and 7s. 6d. net for a single number to members of The Royal Aeronautical Society. Instructions for Contributors are given above. None of the papers must be taken as expressing the opinion of the Council of The Royal Aeronautical Society unless such is definitely stated to be the case. All communications for publication or advertisement in The Quarterly should be addressed to—The Editor, The Aeronautical Quarterly, 4 Hamilton Place, W.1.

Telephone: Grosvenor 3515. Telegraphic Address: Didaskalos, London W.1.

THE AERONAUTICAL QUARTERLY

It is the aim of *The Aeronautical Quarterly* to attract not only original papers contributing to aeronautical science and engineering, and papers developing new or improved methods of analysis and experimental techniques, but also papers on allied sciences which have a bearing on aeronautical problems. *The Aeronautical Quarterly* is open to authors of any nationality and is not restricted to members of the Society. Most papers can be published within nine months of receipt. Short papers, of not more than 2,000 words, are published much more quickly.

VOLUME XIII

Volume XIII of *The Aeronautical Quarterly* will be published in February, May, August and November 1962.

The price of *The Aeronautical Quarterly* has remained unchanged since 1953, but it has now been found necessary, because of increases in printing and general costs, to make a slight increase in price. The new prices, which take effect from Volume XIII, are, *including postage and packing*:—

	To Members of the Society		*To Non-Members*	
	£ s. d.		£ s. d.	
Per Part	9 0	($1.50)	18 0	($2.60)
Subscription (4 parts)	1 16 0	($5.50)	3 12 0	($10.30)

Prices for Volumes I-XII remain unchanged.

Papers to be published in future issues include:—

J. C. Cooke—Boundary Layer Flow between the Attachment Lines on a Flat Plate Delta Wing at Incidence.

I. T. Cook and K. C. Rockey—Shear Buckling of Clamped and Simply-Supported Infinitely Long Plates Reinforced by Transverse Stiffeners.

D. S. Dosanjh, E. P. Gasparek and S. Eskinazi—Decay of a Viscous Trailing Vortex.

R. H. Gallagher and I. Rattinger—The Deformational Behaviour of Low Aspect Ratio Multi-Web Wings. Parts II and III.

T. H. Lambert and R. J. Brailey—The Influence of the Coefficient of Friction between the Pin and the Plate on the Stress Concentration Factor for a Pin-Jointed Connection with Load Applied through an Interference-Fit Pin.

R. D. Milne—On the Use of Linearised Unsteady Aerofoil Theory in Arbitrarily Moving Axis Systems.

W. H. Wittrick—Stress Concentrations for a Family of Reinforced Square Holes with Rounded Corners.

PRINTED BY THE LEWES PRESS WIGHTMAN & CO. LTD., LEWES, SUSSEX, ENGLAND, AND PUBLISHED BY THE ROYAL AERONAUTICAL SOCIETY, 4 HAMILTON PLACE, LONDON W.1, ENGLAND.